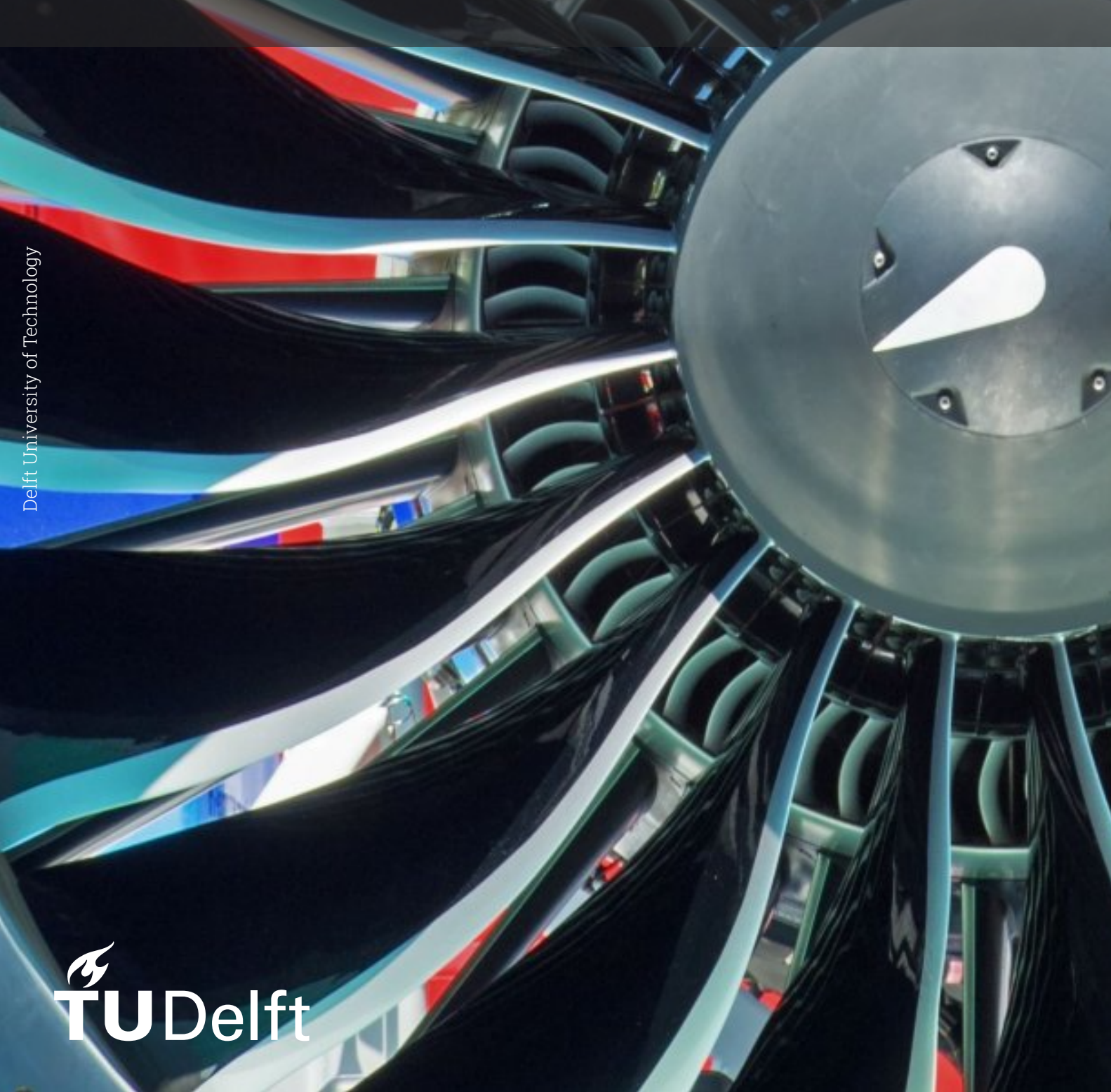


MSc Aerospace Engineering: Propulsion and Power Eliisabet Jahilo



MSc Thesis

Simulating a Steam Injection and Water Recovery Gas Turbine Cycle fuelled by Hydrogen

by

Eliisabet Jahilo

Student number: 4679024

GKN Supervisor: A. Lundbladh
TU Delft Supervisor: A. Gangoli Rao

Project Duration: Oct, 2024 - Dec, 2024

Faculty: Faculty of Aerospace Engineering, Delft

Cover: P. J. Richards/Agence France-Presse/Getty Images

Style: TU Delft Report Style, with modifications by Daan Zwaneveld



Preface

It is a privilege to write a thesis on a topic that truly fascinated me, challenged my skills and kept me inquisitive throughout the whole process. I hope that gas turbine design continues to innovate and seek out novel solutions to improve fuel consumption and reduce negative environmental impacts.

This work would not have been possible without the guidance and support of Anders Lundbladh and GKN, who I was glad to work with for the last nine months. A deep thank you to the two people who believed in me through the years, Arvind Gangoli Rao and Georg Eitelberg. I owe a lot to my family, partner and friends for their support, care and inspiration.

Eliisabet Jahilo Delft, June 2025

Executive Summary

Aviation is facing a potential transformative change due to increasing air traffic demand and new environmental sustainability requirements. With the industry constituting 2% of global CO₂ emissions and 13% of transport emissions [1], and air traffic expected to more than double [2] in the next two decades, aviation faces mounting pressure to develop technologies that both increase fuel efficiency and reduce emissions [3]. Incremental developments in engine efficiencies can lead to a fuel consumption decrease in the coming decades, but returns may be diminishing [4]. Disruptive technologies, including novel cycles or the use of alternative fuels such as hydrogen can provide the accelerated reduction in fuel consumption and emissions needed to match emission reduction goals, as well as increase profits.

The steam injection cycle

Water and steam injection are used in ground-based gas turbines to improve specific power, reduce fuel consumption, and lower emissions by integrating a simplified combined cycle that merges a Rankine cycle with a Brayton cycle. Injecting steam helps lower turbine inlet temperatures, decreasing NO_X emissions and allowing higher fuel flow and thrust. The process's efficiency benefits from using exhaust heat for water evaporation, but a supply of water is required for producing steam. In aircraft, this necessitates carrying water and adds weight, offsetting gains. Recovering not just heat but also water from the exhaust stream is thus needed for aircraft applications. Ways to achieve this, like condensers, have been proposed such systems are complex and costly, limiting their widespread adoption outside laboratory experiments.

Hydrogen-fuelled engines

Noting the uncertainty of affordable future supply and the environmental impacts of currently used hydrocarbon fuels, there is great momentum to explore alternative energy sources in the aviation industry. Industry giants such as Airbus have launched projects investigating hydrogen aircraft [5], with further research incentivised by collective programmes such as the European *Clean Aviation Joint Undertaking* [6]. For the foreseeable future, the only alternative energy source able to compete with kerosene for missions of all ranges is liquid hydrogen [7]. A comparison of the storage and thermochemical properties of liquid hydrogen and kerosene is given in Table 1.

Hydrogen is an attractive fuel due to its lack of CO_2 emissions as well as its wide flammability range allowing for leaner combustion, reducing NO_X emissions [8]. While providing a significantly higher mass-specific energy, the challenge of using liquid hydrogen arises from its low volumetric energy density and cryogenic storage conditions, complicating tank design and impacting aircraft configuration.

	Liquid hydrogen	Kerosene
Storage temperature [K]	20	298
Storage pressure [bar]	1.5	1
Density [kg/m ³]	71	804
Mass-specific energy (LHV) (MJ/kg)	120	43.2
Volume-specific energy (GJ/m ³)	8.25	34.7
Adiabatic combustion temperature (⊕=1) [K]	2400	2300
Heat capacity at constant pressure (1400 < T < 1800) [J/kg/K]	1285-1400	1235-1310
Combustor	0.2-0.65	0.58-1.1

Table 1: Comparison of storage properties and energy densities of liquid hydrogen and Kerosene [9] [10]

Using hydrogen as a fuel also has impacts on the aircraft level, both positive and negative. These are summarised in Table 2.

Positives	Negatives
Lower fuel mass	Higher tank volume
Smaller wing possible	Lower L/D
Reduced maintenance cost	No wing load alleviation
	Configuration complexity

Table 2: Impacts of hydrogen fuel on aircraft design

The Hydrogen-fuelled Steam Injection Cycle

The use of steam injection and water recovery with a hydrogen-fuelled gas turbines shows a promising synergy, as:

- Hydrogen combustion exhaust is highly humid, positively affecting water condensation.
- Liquid hydrogen is a good heat sink, which can be utilised to support condensation.
- The energy consumption of hydrogen aircraft is lower than for kerosene. Steam injection reduces the fuel consumption, helping offset this difference.
- Hydrogen combustion can have high NO_X emissions. Steam injection reduces NO_X emissions, offsetting this effect.

The challenges of integrating steam injection into a hydrogen-fuelled engine stem largely from challenges specific to hydrogen, but some specific concerns exist also for the combination:

- The higher exhaust temperature of hydrogen negatively impacts water condensation.
- Stacking two complex technologies leads to a high level of risk and increased complexity.
- Hydrogen combustors are at a lower technological readiness level than conventional kerosene combustors.
- Hydrogen heat exchangers have a high risk of icing and embrittlement, increasing design complexity.

This engine cycle is identified as providing significant fuel consumption improvement and emission reduction and is also being investigated by Pratt & Whitney's Hydrogen Steam-Injected, Intercooled Turbine Engine, or HySIITE concept, promising "up to 35% improvement in mission energy over today's geared turbofan engines" (M. Winters) [11]. Combining two novel technologies introduces an added level of uncertainty in the interaction of the two technologies, as well as increasing complexity and risk. However, the potential benefits of the cycle as well as an identified gap in published research motivate further study on the concept.

Research objective

The research objective is outlined as follows:

The research objective is to determine the on-design and off-design performance of a hydrogen-fuelled engine with steam injection and water recovery for a short-to-medium range aircraft

With the research objective defined, two research questions are developed and presented below.

- 1. How can we model a hydrogen-fuelled engine with steam injection and water recovery?
 - (a) What is an efficient architecture for the engine?
 - (b) How can the engine be accurately modelled in a cycle evaluation tool?
- 2. What is the on-design and off-design performance of the engine?
 - (a) At which operating points can the engine be self-sufficient on water?
 - (b) What is the change in TSFC of the engine compared to a hydrogen-fuelled engine without steam injection?

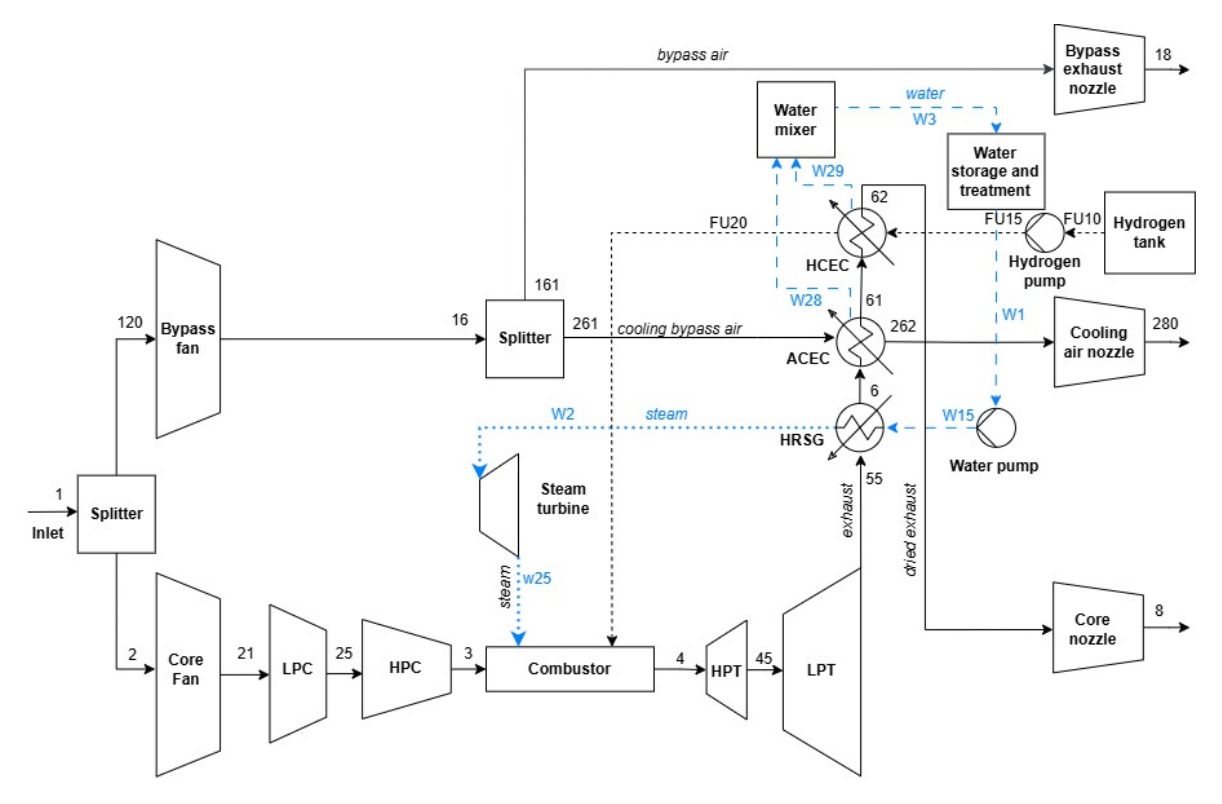


Figure 1: Overview of the steam injection and water recovery cycle

Modelling

In order to answer the research questions, a modelling approach in the NPSS software is developed, building upon a previously developed engine cycle model. Custom elements are developed to model the heat exchangers in the cycle, and the solver setup and design parameters are outlined in detail. An overview of the cycle is presented in Figure 6.1.

The critical components to the steam injection and water recovery cycle are the *heat recovery steam generator* HRSG, the *air-cooled exhaust condenser* ACEC and the *hydrogen-cooled exhaust condenser* HCEC. The core exhaust flow passes through the HRSG where its energy is harnessed to generate steam. After the HRSG, the exhaust passes through the ACEC and HCEC, where water from the humid exhaust is condensed. The ACEC is cooled by a fraction of the bypass flow, while the HCEC is cooled by the hydrogen flow, functioning also as a fuel pre-heater. The condensed water is separated from the flow and pumped through the HRSG, evaporating before injection into the combustor. The steam is also expanded through a turbine to provide additional shaft power.

Predicting the accurate performance of the HRSG, ACEC and HCEC is done by developing a separate model of the three heat exchangers. While in the general model the heat exchangers are treated as single components with only inlet and outlet conditions calculated, this ignores the pinch point and the varying heat transfer along the heat exchangers, specifically in the streams with two-phase flow. The detailed model individually considers the sections of the heat exchangers in order to capture the changing flow properties and rates of heat transfer in the components. Some general assumptions made in the detailed model are summarised below.

- The HRSG, ACEC and HCEC are modelled as counter-flow heat exchangers.
- The heat exchangers are modelled as tube-and-shell type.
- Boiling effects are neglected in the estimation of heat transfer in the evaporator.
- Constant and equal pressure drops are assumed over each of the HRSG, ACEC and HCEC.
- Heat transfer coefficients are calculated based on mean flow conditions calculated from the inlet and outlet values.

In Figure 2, an overview of the HRSG in the detailed model is given.

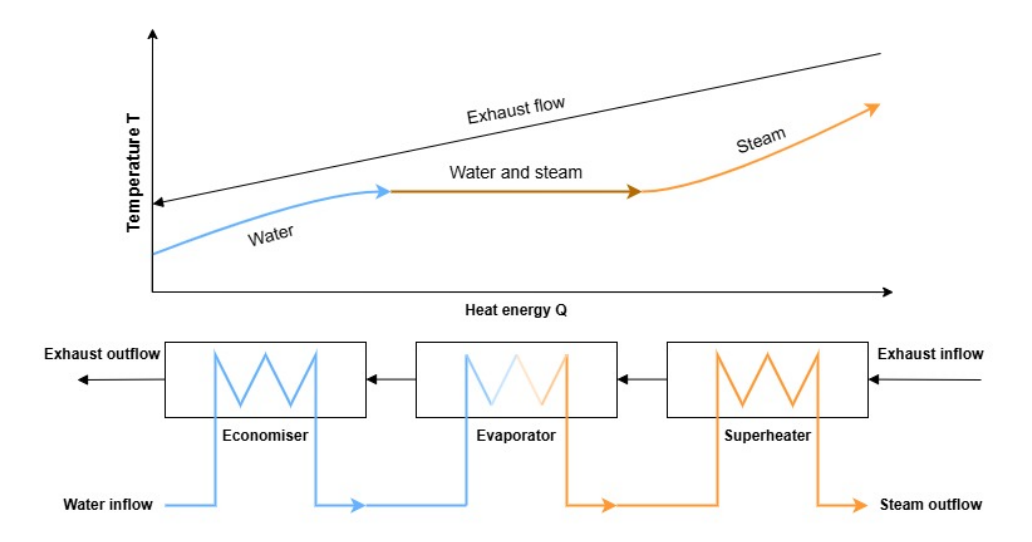


Figure 2: Detailed HRSG model

In Figure 3, an overview of the ACEC and HCEC in the detailed model is given. The detailed model is integrated into the general model. The inlet conditions to the heat exchanger are obtainted from the general model simulation, and accurate condenser performance is determined by running the detailed model.

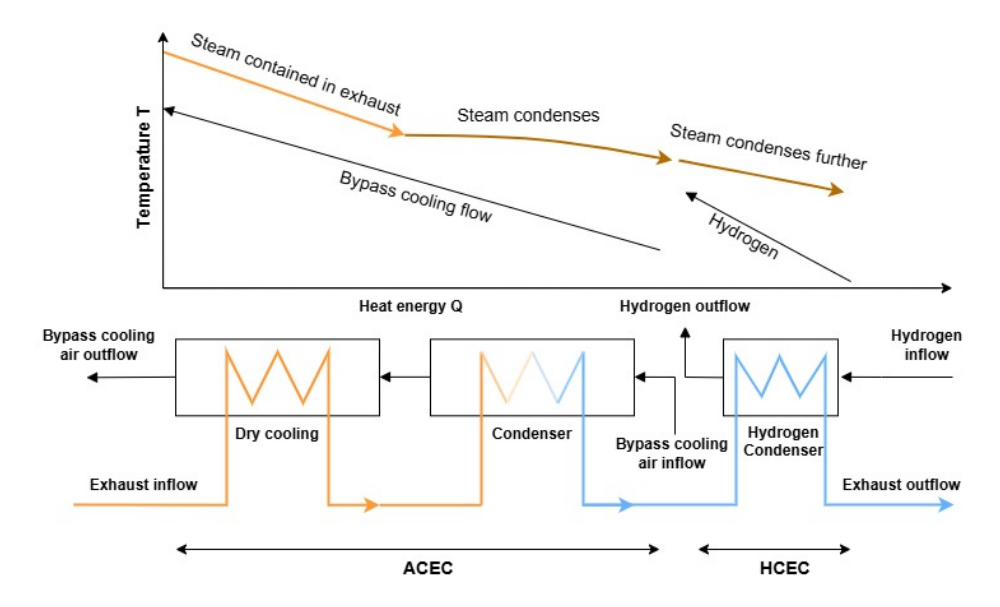


Figure 3: Overview of the section ACEC and HCEC in the detailed heat exchanger model model

Estimating the heat transfer coefficients of the fluids in the condenser and evaporator is complicated by their varying chemical composition as well as changing state in the components. Thus, considering the behaviour of two-phase flow is crucial, with existing correlations providing some basis for estimating heat transfer in these components [12].

The modelling is completed using *Numerical Propulsion System Simulation* (NPSS), a cycle simulator designed to perform cycle design, steady-state and transient off-design performance prediction, among other tasks [13]. While being a powerful tool, difficulties are faced with convergence of the model due to the rudimentary nature of the solver. Lack of debugging and the termination of the solver sequence on many errors leads to further complications in achieving a converged solution.

Solver setup

In order to solve the system of equations introduced by the definition of a cycle model, dependent and independent parameters need to be introduced. Independent parameters will be those that the NPSS solver iteratively changes, seeking a value which matches target performance, expressed as a dependent variable of fixed required value. In design mode, engine geometry and scale factors are calculated in order to achieve a specified performance, in this case including net thrust, inlet corrected mass flow and BPR, among other parameters. In off-design, the geometry and scale factors are fixed and the design calculations are used instead to calculate a resulting performance. A target is still set in off-design performance - in this model, net thrust is still targeted. However, the independent and dependent variables change from the ones set for design.

Results

A number of design parameters are investigated to reach a design point which is water self-sufficient and minimises SFC at the top of climb operating point, summarized in Table 6.1.

Water-to-air ratio WAR [-]	0.33
Cooling flow ratio W_{cool}/W_{core} [-]	11.3
Ideal exhaust jet velocity ratio ζ [-]	1.3
Overall pressure ratio OPR [-]	40
Steam pressure [MPa]	4

Table 3: Final values of parameters for the top of climb design point determined in the study

In addition to the cycle model, a detailed heat exchanger model is developed to model the HRSG, ACEC and HCEC in detail, allowing for sizing estimation to be completed at the design point. Various configurations are explored, after which the design of heat exchangers is fixed and off-design conditions simulated. The detailed heat exchanger model is used to augment the overall cycle model by correcting the assumed effectiveness values by more accurately estimated ones, as well as fixing the cooling flow rate to ensure water self-sufficiency at the design point.

Parameter	Value
F_n [kN]	38.178
SFC [g/(kNs)]	5.215

Table 4: Overview of baseline hydrogen engine performance at top of climb

In Table 6.2, the performance of the baseline hydrogen engine without steam injection are presented. The results of simulating the steam injection and water recovery hydrogen cycle, integrating the overall model with the detailed heat exchanger model, are provided in Table 6.3.

Point	Top of climb (Design)	Mid-cruise	Take off
F_n [kN]	38.178	28.686	138.194
SFC [g/(kNs)]	4.645 (-18%)	4.269	2.974
Injected steam \dot{m}_{inj} [kg/s]	2.94	2.48	6.95
Total condensed water \dot{m}_{cond} [kg/s]	3.09	3.43	2.26
ACEC condensed water [kg/s]	2.92 (94.4%)	3.43 (97.9%)	1.92 (84.7%)
HCEC condensed water [kg/s]	0.17 (5.5%)	0.070 (2.1%)	0.35 (15.3%)
Condensation margin [%]	+5%	+38%	-67.5%
Steam turbine power [kW]	134	0	4156
Turbine power fraction [%]	1.2%	0%	9.8%

Table 5: Overview of engine performance

Water self-sufficiency is reached for both the top of climb design point and the cruise off-design point. At top of climb, a condensation margin of 5% excess of the required flow for steam injection is achieved,

which accounts for an assumed 95% separation efficiency of condensed water from the flow. In cruise, a significantly higher excess of 38% is condensed. while a significant deficit in condensed water is seen for take-off, necessitating the inclusion of a water tank to provide additional water during take-off and part of the climb. The inclusion of a water tank together with the high rate of condensation in cruise could allow for solutions such as condensing and storing water at cruise during one mission for use during the descent and even the take off and climb segment of the following mission. Alternatively, redesigning the ACEC completely would be necessary to ensure water sufficiency at all operating points.

The ACEC provides nearly all of the condensed water flow for both top of climb and cruise, which is due to the small relative size of the HCEC. While hydrogen has a high heat capacity and provides a high maximum temperature difference due to its low storage temperature, the small fuel flow rate compared to the core mass flow rate limits the heat transfer by the total stream capacity of the hydrogen flow. In take off, the HCEC provides a notably larger fraction of total condensation at 15%, but this is a result of the drop in heat transfer and signficant reduction of condensation in the ACEC for this operating point.

Conversely to condensation, water evaporation is not successful in cruise, with the HRSG unable to raise pure steam. This impacts the steam turbine included in the cycle model, which must be bypassed at this operating point. The inclusion of a steam turbine is shown to generate nearly 10% of the total engine shaft power in take off while having a small impact at top of climb. With the expanded power largely limited by the quality of steam at the turbine exit, removing the turbine from the cycle entirely relaxes that design constraint and also slightly reduces the complexity of the engine. With steam injection not strictly requiring saturated steam, a cycle without a steam turbine can be a wiser choice to avoid redesign or heat transfer enhancements in the HRSG.

A significant 18% improvement in thrust-specific fuel consumption is achieved compared to the baseline hydrogen engine, but this is with the caveat of weight estimation missing from detailed analysis. The heat exchangers, specifically the ACEC, will add a significant amount of weight, complexity and maintenance cost to the engine, the effect of which has not been quantified and may outweigh the improvement in SFC.

Results of the detailed heat exchanger areas and effectivness are given in Table 6.4. The ACEC is infeasibly large for all operating points and significant redesign is required to reduce the required heat transfer area and the resulting engine weight. This could be achieved by adding fins on tubes in order to increase the total heat transfer area or by considering other configurations such as a plate heat exchanger. The HRSG and HCEC sizes are reasonable and show promise for the steam injection and water recovery cycle if the ACEC design is resolved.

Point	Top of climb (Design)	Mid-cruise	Take-off
Total HRSG $(A_h)_{HRSG}$ [m ²]	28	37	
HRSG effectiveness [%]	82.1%	79.7%	84.7%
Total ACEC $(A_h)_{ACEC}$ [m ²]	29	56	
ACEC effectiveness [%]	93.5%	98.9%	72.3%
$HCEC\ (A_h)_{HCEC}\ [m^2]$	52	2.7	
HCEC effectiveness [%]	95%	95%	95%

Table 6: Overview of total heat transfer areas and effectiveness in design and off-design

The cycle benefit of steam injection and water recovery is shown to be large, improving the specific fuel consumption from 5.215 g/s.kN without steam injection to 4.645 g/s.kN with steam injection, as shown in Table 5.1 and Table 5.3. The cycle has a smaller core than a conventional engine, with a high BPR. Despite the improvements in fuel consumption, uncertainties remain about the weight of the added heat exchangers, the pressure drop across them and the design of the exhaust condenser, which is identified as a critical point for the success of this engine. If a suitable configuration is found for the ACEC to reduce its size to feasible limits, the cycle shows an interesting possibility for harnessing two complex and novel technologies in order to improve fuel consumption and reduce emissions. The specific synergy with hydrogen is notable as steam injection has not proven as successful in kerosene engines [14], whereas it can help alleviate some of the problems faced by hydrogen-fuelled engines and encourage a transition to the carbon-free fuel.

Contents

Pre	eface	•
Su	mma	ary i
No	men	clature
1	Intro	oduction
2		kground and Theory
		Motivation
	2.2	The steam injection cycle
		2.2.1 History and applications
		2.2.2 Description of the steam injection cycle
	2.3	steam injection cycle components
		2.3.1 Heat exchangers
		2.3.2 Design of heat exchangers
		2.3.3 Steam cycle components
	2.4	Hydrogen-fuelled engines
		2.4.1 Application in aircraft
		2.4.2 Evaluating the use of hydrogen
		2.4.3 Combustion emissions
		2.4.4 Hydrogen combustor
		2.4.5 Hydrogen evaporator
		2.4.6 Hydrogen tank and feed system
		2.4.7 Impacts on aircraft design
		2.4.8 Safety
		2.4.9 Infrastructure
	2.5	The hydrogen-fuelled steam injection cycle
	2.6	Numerical Propulsion System Simulation (NPSS)
	0	2.6.1 Input files
		2.6.2 Previous model development
		·
3	Prol	blem definition 39
	3.1	Research objective
	3.2	Research questions
	3.3	Thesis project scope
	3.4	Engine operating point performance
4	Moti	hods 4
•		Modelling in NPSS
	7.1	4.1.1 Model definition
		4.1.2 The solver
		4.1.3 Problem setup
		4.1.4 Output files
	4.2	Model setup
	4.2	·
		,
		3
		4.2.3 Heat exchanger elements
		4.2.4 Estimating condensation
		4.2.5 Water separation
		4.2.6 Hydrogen components
		4.2.7 Water/steam loop components 4

Contents ix

Re	ferer		
6	Con	clusion 8	32
	5.5	Recommendations for future work	
	5.4	Heat exchanger sizing	
	5.3	Design and off-design performance	
	E 2	5.2.7 Steam pressure	-
		5.2.6 Overall pressure ratio	
		5.2.5 Jet exhaust velocity ratio	
		5.2.4 Cooling flow rate correction	
		5.2.3 WAR and W_{cool}	
		5.2.2 Cooling flow rate	
		5.2.1 Water self-sufficiency	
	5.2	Parameter studies	
	5.1	Baseline engine results	4
5	Res	ults and Discussions 6	4
	4.8	Verification and validation	3
	4.7	Integration of detailed model into overall model	
		4.6.10 Off-design heat exchanger calculations	
		4.6.9 Pressure drops	
		4.6.8 Heat transfer enhancements	
		4.6.7 Flow configuration	
		4.6.6 Exhaust Condensers	
		4.6.5 Heat Recovery Steam Generator	
		4.6.4 General assumptions	
		4.6.3 Heat exchanger geometry	
		4.6.2 Heat exchanger type choice	
		4.6.1 Pinch analysis	6
	4.6	Detailed heat exchanger model	
		4.5.5 Cooling flow rate	
		4.5.4 Water-to-air ratio WAR	
		4.5.3 Steam pressure	
		4.5.1 Ideal exhaust jet velocity ratio	
	4.5	Parameter studies	
	4.4	Baseline engine simulation	
	4.4	4.3.3 Simulation limitations and challenges	
		4.3.2 Solver variables	
		4.3.1 Fixed parameters	_
	4.3	Solver setup	_
		4.2.8 Compressor scaling effects	_

Nomenclature

Acronyms

Acronym	Definition
ACEC	Air-Cooled Exhaust Condenser
CCA	Cooled Cooling Air
EC	Exhaust Cooling
FPR	Fan pressure ratio
HCEC	Hydrogen-Cooled Exhaust Condenser
HPC	High-Pressure Compressor
HPT	High-Pressure turbine
HRSG	Heat Recovery Steam Generator
HySIITE	Hydrogen Steam-Injected, Intercooled Turbine En-
	gine
IC	Inter-Compressor Cooling
LPC	Low-Pressure Compressor
LPT	Low-Pressure Turbine
NPSS	Numerical Propulsion System Simmulation
NTU	Number of Transfer Units
OPR	Overall Pressure Ratio
PC	Precooling
PR	Pressure Ratio
TIT	Turbine Inlet Temperature
TSEC	Thrust-Specific Energy Consumption
TO	Take Off
ToC	Top of Climb
SFC	(Thrust-)Specific Fuel Consumption
WAR	Water-to-air ratio
WET	Water-Enhanced Turbofan
WGR	Water-to-Gas Ratio
WRR	Water Recovery Ratio

Symbols

Symbol	Definition	Unit
\overline{A}	Area	[m ²]
a	Non-dimensional coefficient	[-]
Bo	Nucleate boiling number	[-]
C	Total stream capacity	[W/kg]
C_f	Skin friction coefficient	[-]
c_p	Heat capacity at constant pressure	[J/kg/K]
C_{rat}	Ratio of heat capacities	[-]
Co	Convection number	[-]
D	Drag	[N]
d	Diameter	[m]
F	Thrust	[N]
F	Correction factor	[-]

Contents xi

Symbol	Definition	Unit
\overline{Fr}	Froude number	[-]
f_D	Darcy-Weisbach friction factor	[-]
f_2	Froude number factor	[-]
g	Gravitational acceleration	$[m/s^2]$
h	Heat transfer coefficient	[W/m ² /K]
h	Specific enthalpy	[J/kg]
k	Thermal conductivity	[W/m/K]
L	Lift	[N]
LHV	Lower Heating Value	[J/kg]
l	(Characteristic) length	[m]
m	Mass	[kg]
\dot{m}	Mass flow	[kg/s]
Nu	Nusselt number	[-]
P	Pressure	[Pa]
Pr	Prandtl number	[-]
Q	Total volumetric flow	[m³/s]
$egin{array}{c} Q \ \hat{Q} \ \hat{Q} \end{array}$	Rate of heat transfer	[W]
	Maximum possible rate of heat transfer	[W]
R	Thermal resistance	[K/W]
Re	Reynolds number	[-]
r	Radius	[m]
S	Spacing	[m]
T	Temperature	[K]
V	Velocity	[m/s]
W	Mass flow	[kg/s]
Δ	Difference	[-]
ϵ	Effectiveness	[-]
ζ	Pressure loss coefficient	[-]
ζ	Ideal exhaust jet velocity ratio	[-]
η	Efficiency	[-]
μ	Dynamic viscosity	[kg/s]
ho	Density	[kg/m³]
$ u_s$	Superficial velocity	[m/s]
au	Shear stress	$[N/m^2]$
Φ	Stoichiometric equivalence ratio	[-]
χ	Vapour quality	[-]

Subscripts

Definition
Stream 1
Station 18 (secondary nozzle exit)
Stream 2
Station 25 (engine core)
Station 261 (cooling bypass flow)
Station 280 (tertiary nozzle exit)
Station 8 (core nozzle exit)
Acceleration
Bend
Cross-sectional
Cold (fluid)
Condensation

Contents xii

Subscript	Definition
cool	Bypass cooling flow
core	Engine core flow
cr	Critical
cr	Cruise
f	Final
fan	Fan
fl	Fluid
fr	Friction
g	Gas
gr	Gravitational
H_2	Hydrogen
h	Hydraulic
h	Heat transfer
hot	Hot (fluid)
I	Ideal (expansion)
i	Initial
ISA	International Standard Atmosphere
in	Inflow
inj	Injection
is	Isentropic
L	Longitudinal
l	Liquid
lm	Logarithmic mean
lo	Single-phase liquid
m	Mean
max	Maximum
min	Minimum
p	Polytropic
pmp	Pump
opt	Optimum
out	Outflow
rec	Recovery
sat	Saturation
st	Steam
steam	Steam turbine
T	Transverse
t	Total
tank	Tank
tot	Total
vap	Vaporisation
vapour	Vapour
w	Wall
wat	Water
∞	Free stream

1

Introduction

The aviation sector is facing a potential transformative change, driven by the dual pressures of increasing air traffic demand and environmental sustainability requirements. With air traffic expected to more than double [2] in the next two decades, the industry faces mounting pressure to develop technologies that both increase fuel efficiency and reduce emissions [3].

Engine fuel consumption has decreased over the years and will continue to do so with incremental developments in components, but conventional Brayton cycle gas turbines appear to be approaching their limits [4]. Disruptive technologies, including novel cycles or the use of alternative fuels such as hydrogen can provide the reduction in fuel consumption needed to match current emission reduction goals, as well as increase profits.

Two technologies will be considered in this thesis: steam injection, and the use of hydrogen as fuel. The injection of steam into gas turbines has been shown to increase Brayton cycle efficiency, reducing thrust-specific fuel consumption as well as lowering NO_X emissions [15]. For the foreseeable future, the only alternative energy source able to compete with kerosene for missions of all ranges is liquid hydrogen [7], an attractive fuel due to its lack of CO_2 emissions, high specific energy and wide flammability range resulting in lower NO_X emissions [8].

The combination of the two technologies is shown to have synergy, as their combined effects have a greater impact than either technology alone. This can lead to significant improvements in fuel consumption and emission reduction [11],[16]. The goal of this thesis is to develop a cycle model for a hydrogen-fueled steam injection and water recovery turbofan engine and simulate its design and off-design performance, investigating the capability of the cycle to be water self-sufficient and quantifying the fuel consumption benefits that may be realised with the novel cycle.

In the cycle modelling software NPSS, a detailed model of the cycle is constructed and designed for the top of climb operating point of a short-to-medium-range aircraft engine. Modelling the steam injection and water recovery cycle requires accurate modelling of the heat exchangers which are integral to the cycle operation. The *heat recovery steam generator* (HRSG) is introduced to produce the steam required for injection, while the *air-cooled exhaust condenser* (ACEC) and *hydrogen-cooled exhaust condenser* (HCEC) in turn supply the required water flow rate by condensing water out of the core exhaust. The development of accurate models for heat exchangers and integrating these with the overall cycle model is undertaken, with a focus on estimating heat transfer coefficient in the various flow streams and determining estimated sizes of the HRSG, ACEC and HCEC.

The relevant theory and background are covered in Chapter 2, starting with the motivating factors driving the undertaken work. The technology of steam injection and its application is introduced in Section 2.2, leading to an overview of relevant cycle components in Section 2.3. The use of hydrogen as a fuel for aircraft is covered in Section 2.4, which evaluates its potential and challenges, outlines critical components for hydrogen-fuelled engines, and considers the broader implications of hydrogen adoption. Finally, the combination of steam injection and hydrogen in an engine is evaluated in Section 2.5.

In Chapter 3, the research plan is outlined. First, a research objective is introduced in Section 3.1, followed by specific research questions in Section 3.2. Finally, the thesis is bounded by a scope and

the baseline desired engine performance is defined in Section 3.4.

In order to answer the posed research questions, the required methods and tools are outlined in Chapter 4. An overview of the NPSS software is given in Section 2.6 and the modelling approach introduced in Section 4.1. The setup of the numerical simulation is outlined in Section 4.3, and the design parameters that will be investigated defined in Section 4.5. Finally, a detailed model for sizing the cycle heat exchangers is presented in Section 4.6 and its integration with the overall cycle simulation described in Section 4.7.

Chapter 5 presents the results of the work together with discussions on parameter choices, engine design and off-design performance. Some recommendations for future work are given in Section 5.5 and conclusions are drawn in Chapter 6.

Background and Theory

In this chapter, the motivation and theory relevant to the thesis work will be outlined. In Section 2.1, the key trends in turbofan engine development and their drivers are identified to motivate the research. Two promising technologies of steam injection and hydrogen as fuel are identified and their theoretical background covered subsequently. In Section 2.2, the steam injection cycle is outlined, followed by a discussion on heat exchangers, their design and relevance to the cycle in Section 2.3. An evaluation of hydrogen as a fuel, its application in aircraft and relevant design considerations is then given in Section 2.4. The section concludes with a discussion on the combination of the steam injection and hydrogen in Section 2.5.

2.1. Motivation

Aviation is an essential sector of the worldwide transportation network, providing mobility, creating jobs, and supporting international trade and tourism. The civil aviation sector employs 1.2 million people worldwide, with a further 5.6 million people working in other on-airport positions and another 55.3 million indirect jobs are supported by aviation [2]. Both passenger and air freight traffic are expected to more than double in the next two decades [2], highlighting the significance of considering the impacts and effects of this sector.

The key driver in the aviation sector is cost. The global airline industry operates on thin profit margins and aviation is considered a strongly volatile market [17] due to rapidly fluctuating demand, fuel cost uncertainty and the effect of global events such as pandemics or international conflicts. Lowering operating costs is desirable both to lower volatility and improve competitiveness in the market.

To meet rising global demand and increase profits, the aviation industry is driven to develop technologies that contribute to an increase in fuel efficiency. Performance improvements to existing engines are thus key for research and development, with fuel efficiency being driven primarily by thermal efficiency and propulsive efficiency [3].

Beyond being crucial to the global economy, aviation industry also has a notable climate footprint. With the entire world facing the effects of global warming, aviation is also pushed to focus on sustainable development, with various bodies and agencies setting environmental agreements and goals for the industry. Following their inaugral meeting at the 26th Conference of the Parties (COP26) to the United Nations Framework Convention on Climate Change, the International Aviation Climate Ambition Coalition (ICAO) published a declaration, with signatories committing to working on reducing the CO_2 emissions of aviation towards limiting the global average temperature increase to 1.5°C and achieve net zero CO_2 emissions by 2050 [18].

Air traffic in 2022 constituted around 2% of global CO_2 emissions and 13.9% of transport emissions [1], with advances in technology promising improvements in energy efficiency. Still, with aviation emissions predicted to triple by 2050 [19], there is no certainty that these advances will be sufficient to balance the growth in air traffic nor that aviation will be exempt from the general drive to reduce CO_2 emissions.

2.1. Motivation 4

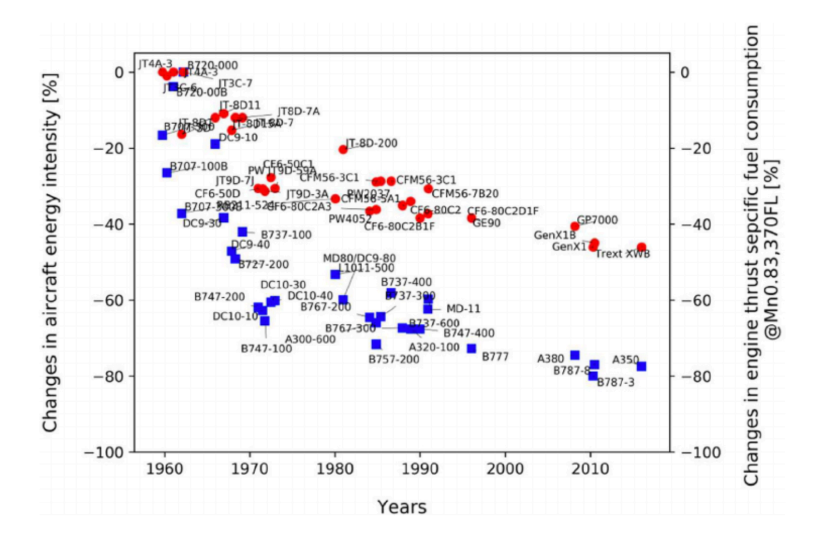


Figure 2.1: The percentage change in aircraft energy intensity and thrust-specific fuel consumption in cruise from 1960 to 2020 [20]

The change in thrust-specific fuel consumption (SFC) in the past 60 years is shown in Figure 2.1. A large improvement is seen in the early days of jet engines owing largely to the adoption of the turbofan, a disruptive technology that significantly improved engine efficiency compared to the previous turbojet engines. Technological advances such as modern geared turbofans, new materials and further improvement of current technologies are a feasible way forward to improve fuel consumption but their impact is smaller with each iteration.

In Figure 2.2, the thrust-specific fuel consumption SFC as a function of thermal and propulsive efficiency of an aircraft engine is shown. Thermal efficiency is primarily a function of the *turbine inlet temperature* (TIT) and the *overall pressure ratio* (OPR) [21]. Advances in increasing both of these can allow for a theoretical limit of around 0.6, but higher TIT leads to significantly higher NO_X emissions, so a practical limit of 0.55 is reached earlier and indicated by the dashed line. Propulsive efficiency is driven primarily by the *bypass ratio* (BPR) [21], with a limit reached for an open rotor configuration. However, increasing BPR will increase engine diameter, leading to higher drag and weight which offsets the improvement in propulsive efficiency. Gas turbines with conventional cycles are arguably approaching their performance and capacity limits [4] and in order to meet proposed environmental goals, long-term solutions may require more radical innovations, such as novel cycles.

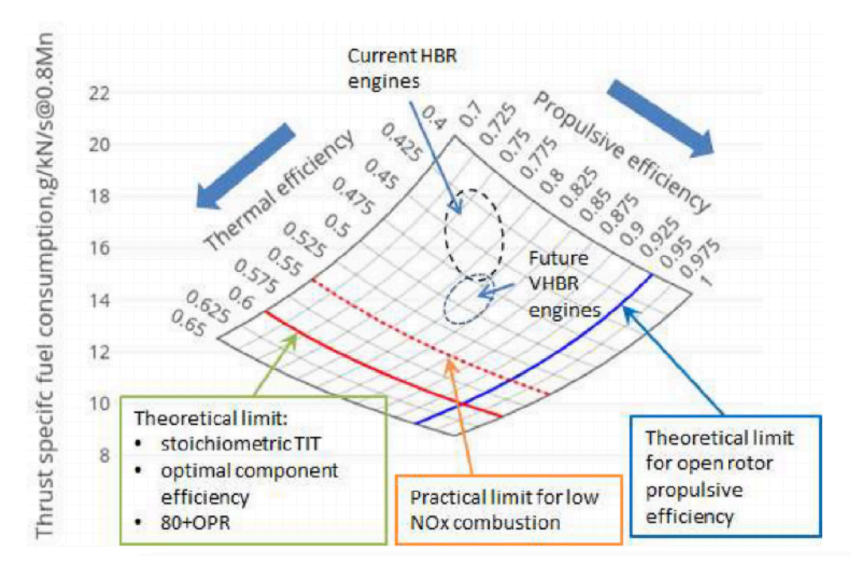


Figure 2.2: Thrust-specific fuel consumption as a function of propulsive and thermal efficiencies of an aircraft engine, with future predictions and theoretical limits [20]

Another disruptive concept is the investigation of new energy sources for aircraft. While fuel cells or hybrid-electric solutions are being researched, currently the gas turbine is almost unbeatable in its power-to-weight ratio. Moving away from hydrocarbon-based fuels, hydrogen is a promising carrier offering a very high mass-specific heating value at the drawback of low density, necessitating cryogenic or pressurised storage. Current studies on hydrogen combustion predict a 1.9% to 4.6% improvement in *thrust-specific energy consumption* (TSEC) for a hydrogen-fuelled gas turbine compared to kerosene [10]. Direct combustion emissions of CO₂ are reduced to zero, however the climate impact must be considered as a whole, taking into account NO_X emissions and contrail formation, as well as the production of hydrogen. Still, Hydrogen is currently the most viable alternative to kerosene, providing sufficient energy at significantly reduced direct emissions, and as such is a key fuel to investigate.

2.2. The steam injection cycle

Turbofan engines operate on the Brayton cycle [22], a thermodynamic cycle characterized by adiabatic compression and expansion, and isobaric heat addition and rejection. Improving the cycle efficiency to reduce fuel consumption can be achieved in many ways - one of these is by injecting steam into the cycle. In this section, the development of steam injection as a technology is explored and an overview of the steam injection cycle presented.

2.2.1. History and applications

Historically, water has been injected into aircraft engines for thrust augmentation. More commonly, water and steam have been injected into ground-based gas turbines for improved power output, efficiency and lowered emissions, a practice that continues today. A chronological history of the development of steam and water technology is provided.

Water injection

While the present work addresses steam injection, it is significant to consider water injection in the history of steam injection. The injection of water in its liquid form has been historically employed in both aircraft and industrial engines with varying objectives, both to boost thrust and reduce emissions.

Use in aircraft served the primary purpose of increasing take-off thrust, especially on hot days requiring higher thrust [22]. Water was generally injected into the compressor, increasing engine mass flow but more importantly intercooling within the compressor. As an example the early Boeing 707-120 Stratoliner featured four water-injected Pratt & Whitney JT3C-6 engines and the practice continued until early Boeing 747 aircraft using Pratt & Whitney JT9D-3AW and JT9D-7AW engines [23].

In industrial gas turbines, water injection is primarily employed to reduce NO_X emissions. By injecting water into the combustor, local temperature peaks in the primary zone can be reduced, discouraging the dissociation of nitrogen and oxygen and thus formation of thermal NO_x [22]. There is an added benefit of increased power output with a penalty of possibly increased CO emissions due to lower temperature and mechanical problems due to uneven combustion. Common water-to-fuel ratios are between 1 and 2 [22] and additional pumps and tanks are required for the water, leading to a high weight penalty. As such, stationary applications are better able to harness the emission reduction benefits than mobile ones. However, the idea of water injection for emission reduction has recently been revisited in aircraft [23], investigating injecting water before the low-pressure compressor (LPC), before the high-pressure compressor (HPC) or directly into the combustor. Injection before the low-pressure compressor was found to offer the highest performance benefits, reducing NO_x emissions by 47% with a 3.5% fuel efficiency benefit and a 200 K reduction in turbine inlet temperature [23]. While a weight penalty for the water and feed system components is introduced, the system cost increase per takeoff is estimated as \$41 per takeoff without including the added benefit of engine lifetime extension [23], giving an attractive NO_X emissions reduction cost-to-benefit ratio and showing that water injection could still serve some benefit for aircraft applications.

Steam injection and heat recovery

Injecting steam, rather than water, into the combustor provides the same benefit in terms of NO_X reductions while providing a possible SFC reduction because the steam can be raised using exhaust heat in a *Heat Recovery Steam Generator* (HRSG) [22], improving the cycle efficiency. Furthermore, more uniform cooling leads to little or no increase in CO emissions or combustion noise with a small complexity penalty due to the addition of a heat exchanger. Many industrial processes also have steam as a byproduct, making use of it for injection an attractive prospect.

Larson and Williams [24] provide a comprehensive overview of early steam-injection technology for natural gas turbines, including preliminary performance improvement calculations for power station applications. Steam injection is shown to increase power output by up to 70%, efficiency by up to 45% and reduce power-specific fuel consumption by up to 31.4% for the Allison 501-KH turbine. The technology is identified as an attractive one to transition to the "Post-Petroleum Era" [24].

An example of a cycle using steam injection is the Cheng Cycle. This is a simplified form of the combined cycle, integrating a Rankine cycle in parallel with a Brayton cycle [25]. In the Cheng cycle, steam is produced using heat recovered from the gas turbine exhaust in an HRSG, improving the thermal efficiency while steam injection boosts the specific power of the gas turbine. For sample gas turbines ranging in output power from 20 MW to 314 MW, the Cheng cycle has around 40% higher efficiency and up to twice as high output power compared to a simple cycle [25]. Cheng cycle gas turbines are commonplace around the world, being in use since the 1980s [25].

Early potential of steam injection cycles was largely focused on improving power output and efficiency, while water injection was a known and proven technique for NO_X control. In 1988, the Cheng cycle's potential for reducing NO_X emissions was discussed by Kelleher and Haselgrübler, with 24% greater emission reduction resulting from combining steam injection and water injection when compared to simply water injection in the Allison 501-KH turbine [26]. Today, water and steam injection are both common strategies for reducing NO_X emissions in land-based gas turbines. As the concern with NO_X emissions has grown in the past few decades, the importance of steam injection from an emission reduction perspective increases.

As discussed above, water and steam injection require a considerable supply of purified water, necessitating water tanks, pumps and an evaporator in the case of steam. For mobile application such as aircraft, this imposes a weight penalty that might outweigh the performance improvement and emission reduction provided. For land-based applications, even though weight is not a significant design limiter almost all steam systems are *total loss*, with the injected steam being ejected in the exhaust stack [22]. This has two main drawbacks: a considerable water consumption and a large thermal loss owing to the heat required to vaporise water.

Steam injection, water and heat recovery

While the steam injection cycle allows for steam injection at a higher thermal efficiency, the concern of water supply remains, especially for aircraft applications. Given that the combustion of hydrocarbon fuels produces some amount of steam in the exhaust, a system to recover not only heat, but also water itself can be considered. The original patent of the Cheng cycle introduced a condenser into the cycle, recovering water out of the exhaust of the gas turbine and vaporising it in the HRSG for injection into the combustor [27]. However, no mention of design or sizing methods for the condenser was given.

The feasibility of water recovery was further tested at Gent University, with both a finned tube type condenser and a direct contact condenser being built and tested with natural gas combustion exhaust mixture, but without the use of an actual gas turbine [28]. Full recovery was reached for both. A spiral type condenser and shell-and-tube type condenser were built and tested at the Harbin Marine Boiler and Turbine Research Institute [29], achieving full water recovery. In 1992, NOVA Corporation, noting the lack of a field installation of a steam injection and water recovery cycle, described the installation of a shell-and-tube condenser to be implemented on a natural gas-fuelled turbine, predicted to give full recovery in colder periods [30]. The feasibility of recovering water from a gas turbine exhaust has been demonstrated and various condenser designs explored, but functional field applications are not yet common [28].

Steam injection, water and heat recovery in aircraft

As covered above, current applications of steam injection are limited to ground-based gas turbines. Water recovery has also been investigated for ground-based systems, but not realised in non-laboratory applications, which could be due to the complexity and cost of the added condenser as well as less constraining weight and volume constraints. For aircraft applications, water recovery becomes an integral factor in maximising the performance benefits of the steam injection cycle, as water supply, storage and treatment systems apply a great weight penalty.

Two current projects are noted when considering steam injection in aircraft. The *Water-Enhanced Turbofan* (WET) project is an engine concept proposed by MTU Aero Engines [15]. The concept is expected to lead to a 15% reduction in fuel consumption and CO_2 emissions, promising near-zero NO_X emissions and potential to reduce or avoid contrail formation, further reducing environmental impact. A schematic of the proposed cycle is given in Figure 2.3, highlighting the addition of a condenser and water recovery system, from which liquid water is pumped to, and vaporised to steam in, an HRSG before injection into the combustion chamber.

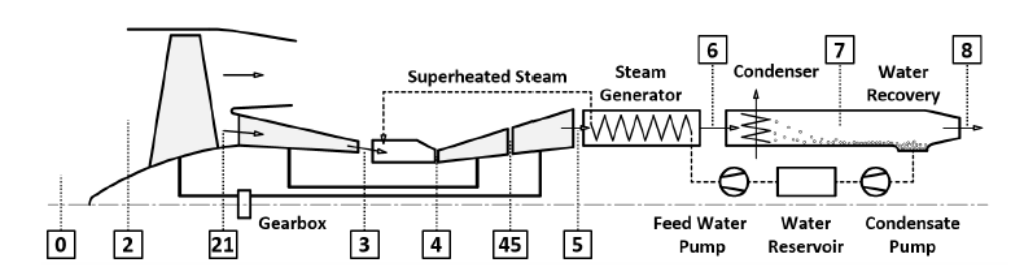


Figure 2.3: Scheme of a half side arrangement of the WET engine applying steam injection and water recovery [15]

In the US, Pratt & Whitney has been awarded \$3.8 million in funding from the Department of Energy for the development of the *Hydrogen Steam-Injected, Intercooled Turbine Engine* (HySIITE) concept. A simple overview of the engine is given in Figure 2.4, highlighting the proposed cycle with steam injection into the combustor as well as at the high-pressure compressor inlet. A condenser is added in the core exhaust of the gas turbine to recover water, with that water passing through a heat exchanger to vaporise the liquid hydrogen fuel before combustion. A second heat exchanger is added to raise the steam required for steam injection.

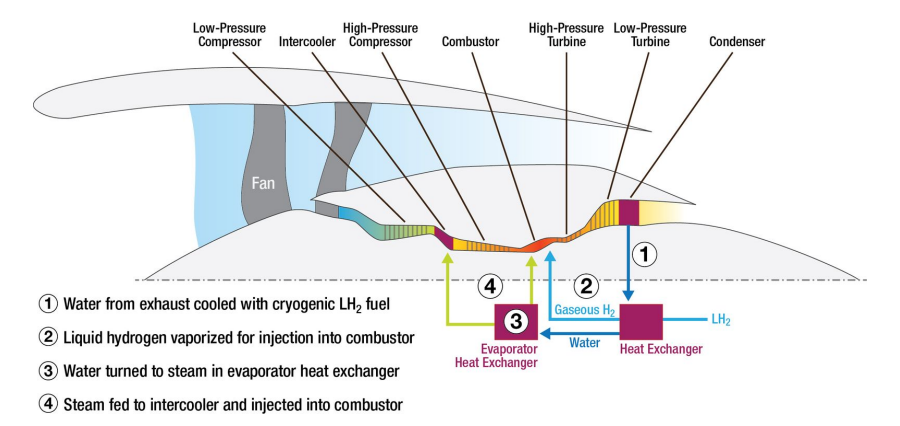


Figure 2.4: Overview of the HySIITE engine, adapted from [31]

While little has been published on the project, the concept promises "up to 35% improvement in mission energy over today's geared turbofan engines" (M. Winters) [11]. In addition to the performance and emission benefits of steam injection, the use of hydrogen instead of kerosene is introduced in the context of emissions reduction as well as its synergy with steam injection technology, as will be further discussed in Section 2.5. In addition, RTX Corporation has filed patents for a conceived hydrogen steam injection and recovery cycle and relevant cycle components such as the condenser, water separator and heat exchanger, which will be covered subsequently in Section 2.3.

2.2.2. Description of the steam injection cycle

A history of the development of the steam injection, heat recovery and water recovery cycle has been presented. Moving forward, the cycle will be referred to as the steam injection cycle, while still encompassing the aspects of water and heat recovery. The cycle can be considered as a combined Rankine (steam) and Brayton (turbofan) cycle. A simplified overview of the cycle and its relevant components is given in Figure 2.5.

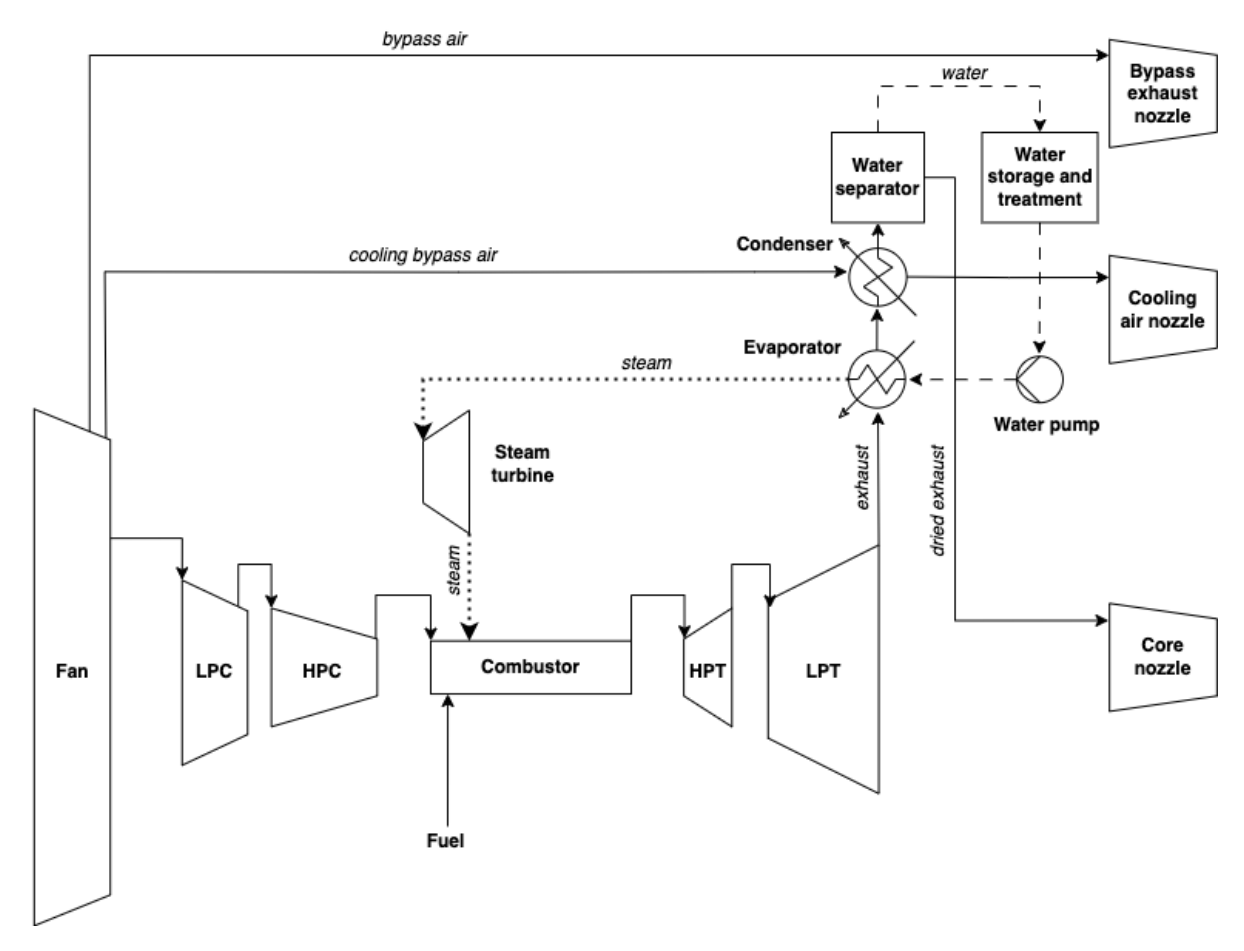


Figure 2.5: Overview of the steam injection cycle

This example schematic features a simplified turbofan engine with an added steam cycle comprising an evaporator, a condenser, water storage and treatment, and a steam turbine. Shafts are not included in the schematic as the integration of the steam turbine is a variable to consider and the main objective of the graphic is to highlight the added cycle components as well as visualise the exhaust, water and steam flows.

As a notable change from the standard turbofan, all of the core exhaust is fed through the evaporator or HRSG. The exhaust then passes through a condenser where water vapour condenses, followed by a separator to remove the condensed water from the now *dried* exhaust. The liquid water is then treated to remove any undesirable impurities and stored in a reservoir. From there, the water is pumped through the evaporator, expanded through a steam turbine to generate power and finally injected into the combustor. The rest of the dried exhaust is accelerated through the core nozzle. Cooling for the condenser is provided by a segment of the bypass air which is accelerated through a nozzle after passing through the condenser, but it is noted that alternative sources of cooling could be considered, such as ram air, or fuel, which also provides pre-heating of the fuel. The mixing of any of the three exhaust streams can also be considered in further design.

2.3. steam injection cycle components

As seen in Figure 2.5, various new components are added to the gas turbine to facilitate steam injection, heat recovery and water recovery. The condenser, water separator and evaporator are the most critical components, with no existing aircraft engine solutions in operation. Of relevance are also the components needed for the storage and treatment of recovered water, water pump(s) and the steam turbine. As such, the operation, requirements and complexities of these components will be covered in the following subsections.

2.3.1. Heat exchangers

A heat exchanger is a device that can be used to *exchange heat* - transfer enthalpy between two or more media, such as two (or more) fluids, at differing temperatures and in thermal contact, usually without external heat or work addition [32]. When simulating the steam injection cycle, the condenser to extract water from the exhaust and evaporator in order to produce steam to be injected into the gas turbine core need to be modelled. Both of these are examples of heat exchangers and the design of both is critical for cycle performance.

Heat exchangers come in varying forms and can be classified by numerous different characteristics [32], which are outlined shortly.

- Classification by transfer process: For indirect-contact exchangers the flows are separated by a surface through which transient heat transfer occurs. The two fluid streams do not mix and heat transfer is continuous through a dividing wall or transient into and out of a wall. Indirect contact type exchangers are further broken down into direct transfer type, storage type or fluidized bed type. In a direct transfer type exchanger, also called a recuperator, heat transfers continuously from the hot to the cold fluid through a wall. For a storage type the heat transfer is intermittent by energy storage and release through the exchanger surface, being referred to as a regenerator. In a fluidized bed type one side of a two-fluid exchanger is immersed in a bed of fine solid material that floats in the upward flow of fluid and behaves as a liquid, allowing for very high rates of heat transfer. For direct-contact exchangers the two fluids come into contact, heat exchange occurs and the streams are then separated commonly these exchangers also include mass transfer in addition to heat transfer. They are further classified into immiscible fluid exchangers, gas-liquid exchangers and liquid-vapour exchangers.
- Classification by the number of fluids: At least two fluids are required for an exchange and
 most heat exchangers do function to transfer heat between two fluid streams. However, heat
 exchangers for three or more fluids do exist with three-fluid heat exchangers widely used in cryogenics and some chemical processes.
- Classification by surface compactness: Compactness refers to the ratio of heat transfer surface area to volume of the heat exchanger. For gas-to-fluid exchanger a ratio of 700 m²/m³ and above is considered *compact* and exchangers with ratios below that *noncompact*. For liquid-to-liquid and phase-change exchangers, the limit is lower at 400 m²/m³.
- Classification by construction type: The major exchanger constructions types are tubular, plate-type, extended surface and regenerative. *Tubular* exchangers are built of circular or rarely elliptical or rectangular tubes and are commonly used for liquid-to-liquid and liquid-to-phase transfer processes. *Plate-type* exchangers are usually constructed of thin plates, smooth or with some form of corrugation, being placed flat or wound in the exchanger. *Extended surface* heat exchangers feature fins on one or both fluid sides to increase the surface area for heat transfer. *Regenerators* are storage-type exchangers where the heat transfer occurs through a matrix that is either stationary for fixed-matrix regenerators or moves periodically into and out of the fluid streams for a rotary regenerator.
- Classification by flow configuration: First, exchangers are classed as single-pass if both fluids pass through the exchanger length once, or multi-pass at least one fluid reverses and passes (a part of) the length, of the exchanger once or multiple times more. For single-pass exchangers, the relative flow direction and orientation of the fluids determines a further classification into counterflow, parallel flow, crossflow, split-flow and divided flow exchangers. For multi-pass exchangers, depending on the construction type the exchanger can be classed similarly according to the flow direction and orientation as well as the number of passes.

Classification by heat transfer mechanism: Heat transfer can be single-phase (free or forced) convection or two-phase convection (condensation or evaporation). A two-fluid exchanger can be classed as having single-phase convection on both sides, two-phase convection on both sides, single-phase on one side and two-phase on the other side or combined convection and radiative heat transfer.

For this work, the components to be designed are the condenser and evaporator which are both examples of *two-fluid* and *indirect-contact* heat exchangers or *recuperators*. Furthermore, both are *direct transfer* type. Considering that condensation and evaporation involve a phase change in water, the heat exchangers will have sections of a *two-phase* convection on one side and *single-phase* convection on the other, as well as sections with single-phase convection on both sides. As will be discussed, both the condenser and evaporator are required to be *compact*. When considering construction and flow arrangements, multiple configurations are possible and the design is left for further stages. For modelling purposes, a simple *tubular* construction can be chosen to determine the heat transfer and size the heat exchangers.

2.3.2. Design of heat exchangers

The objective in the design of a heat exchanger is to determine the required surface area for the specified rate of heat transfer, known as the *duty*, knowing the overall heat coefficient and temperature differences available. An overview of the theory behind heat transfer in heat exchangers is introduced, after which techniques to estimate the temperature difference and overall heat coefficients to solve the heat balance are introduced.

The Reynolds analogy

The fundamental relations correlating convective heat transfer are derived based on the *Reynolds analogy*, stating that the heat transfer coefficient in specific classes of fluid flow is a simple multiple of the skin friction coefficient [33]. Considering two fluid layers of temperature T_1 and T_2 adjacent to a wall of temperature T_w in a boundary layer with mass flow \dot{m} and heat capacity c_p , the rate of heat transfer \dot{Q} can be expressed as:

$$\dot{Q} = \dot{m}c_p[(T_1 - T_w) - (T_2 - T_w)] \tag{2.1}$$

The Reynolds analogy finds that the ratio of heat transfer to fluid tangential stress is the same throughout the laminar and turbulent parts of a boundary layer for a Prandtl number Pr=1. This dimensionless number is a ratio of the momentum diffusivity to thermal diffusivity given by Equation 2.2, with k the thermal conductivity.

$$Pr = \frac{\mu/\rho}{k/(c_p\rho)} = \frac{c_p\mu}{k} \tag{2.2}$$

Gases have Prandtl numbers sufficiently close to unity (for example, 0.7 for air [33]) for the analogy to be an acceptable approximation. This can be utilised by placing layers 1 and 2 at the wall and free-stream, respectively, giving for the ratio of heat transfer to shear stress τ_w in a flow of free stream temperature T_∞ and velocity V_∞ :

$$\frac{\dot{Q}/A}{\tau_w} = \frac{c_p(T_\infty - T_w)}{V_\infty} \tag{2.3}$$

The heat transfer coefficient h and the non-dimensional heat transfer coefficient or Nusselt number Nu for a characteristic length l are defined as:

$$h = \frac{\dot{Q}}{A(T_{\infty} - T_w)}, \quad Nu = \frac{hl}{k}$$
 (2.4)

Finally, together with the non-dimensional skin friction coefficient C_f , the Nusselt number can be expressed as:

$$Nu = Pr \times Re\frac{C_f}{2} \tag{2.5}$$

Estimating heat transfer in heat exchangers

For a heat exchanger, Equation 2.4 is often simplified to Equation 2.6, introducing the overall heat transfer coefficient U, mean heat transfer area A_h and mean temperature difference ΔT_m . As real heat exchangers feature fluid flows with varying chemical composition, temperature profiles, and flow dynamics, all of these overall terms need to be estimated.

$$\dot{Q} = U A_h \Delta T_m \tag{2.6}$$

The logarithmic mean temperature difference

The temperatures in the fluid streams vary, and as such an appropriate mean temperature difference to evaluate this equation is to be determined. For a single-pass heat exchanger operating with parallel or counterflow, the mean temperature difference can be estimated with the *logarithmic mean temperature difference*(LMTD) defined as ΔT_{lm} in Equation 2.7 [34]. In Figure 2.6, a tubular single-pass parallel-flow and counterflow heat exchanger are shown together with the temperature plot of the hot and cold streams.

$$\Delta T_{lm} = \frac{(T_{hot,in} - T_{cold,out}) - (T_{hot,out} - T_{cold,in})}{\ln \frac{(T_{hot,in} - T_{cold,out})}{(T_{hot,out} - T_{cold,in})}} = \frac{\Delta T_a - \Delta T_b}{\ln \left(\frac{\Delta T_a}{\Delta T_b}\right)}$$
(2.7)

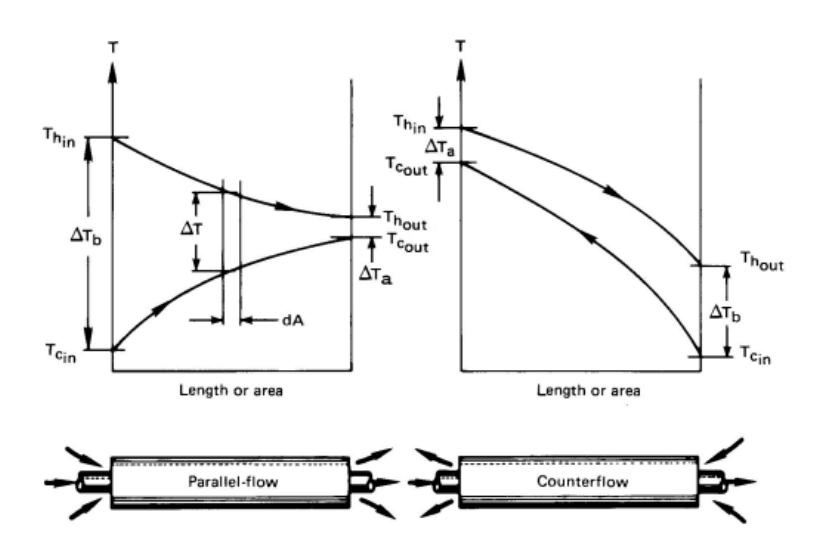


Figure 2.6: Temperature plots for two tubular two-fluid single-pass parallel-flow and counterflow heat exchangers [34]

In many cases, the overall heat transfer coefficient can be taken as roughly constant, but flow configurations may vary widely, including multiple passes and/or cross-flow. In these cases, a correction factor F_{lm} can be applied to the LMTD with $\dot{Q}=UA_hF_{lm}\Delta T_{lm}$, with the factor dependent on the temperature, effectiveness, heat capacity ratio, and flow arrangement [12].

The ϵ -NTU method

The determination of the LMTD assumes knowledge of the inlet and outlet temperatures of both fluid streams, which is in practice not always the case. In order to solve such cases, the effectiveness-NTU or ϵ -NTU method is introduced [33]. The method works well if the overall heat transfer coefficient is fairly uniform, which is more likely in a compact heat exchanger [34], which the modelled heat exchangers in the steam injection cycle preferably are.

The performance of a heat exchanger can be measured by its *effectiveness* ϵ , defined in Equation 2.8, with \dot{Q} the ratio of actual heat transferred and $\dot{\hat{Q}}$ the maximum possible heat that could be transferred.

$$\epsilon = \frac{\dot{Q}}{\dot{\hat{Q}}} = \frac{UA_h}{(\dot{m}c_p)_{min}} \left(\frac{\Delta T_m}{\Delta T_{max}}\right) \tag{2.8}$$

The maximum possible heat transfer is found when the fluid with a smaller heat capacity, $(\dot{m}c_p)_{min}$ reaches the inlet temperature of the other fluid. The maximum heat difference ΔT_{max} is the difference between the inlet temperatures of the two streams.

The dimensionless heat exchanger size $UA_h(\dot{m}c_p)_{min}$ is termed the *number of transfer units* NTU, thus giving:

$$\epsilon = \mathsf{NTU}\left(\frac{\Delta T_m}{\Delta T_{max}}\right) \tag{2.9}$$

The temperature difference ratio is a function of flow arrangement and NTU or effectiveness, and the ratio of stream capacities of the two fluids, C_{rat} . There are published charts of effectiveness versus NTU, with C_{rat} as a parameter, for common heat-exchanger flow arrangements. The ϵ -NTU method highly simplifies the design of heat exchangers, linking size (expressed in NTU) to the performance (effectiveness) of a heat exchanger, depending on the flow arrangement and composition. The design of heat exchangers is still complex, however, one reason being a high degree of freedom [33].

The overall heat transfer coefficient

The other parameter needing to be estimated is the overall heat transfer coefficient U. This can be done by considering the thermal circuit model of a simplified cross-flow heat exchanger as shown in Figure 2.7. Scale or fouling deposit layers are shown on each side of the wall, which often have low thermal conductivity and are thus undesirable as they increase thermal resistance.

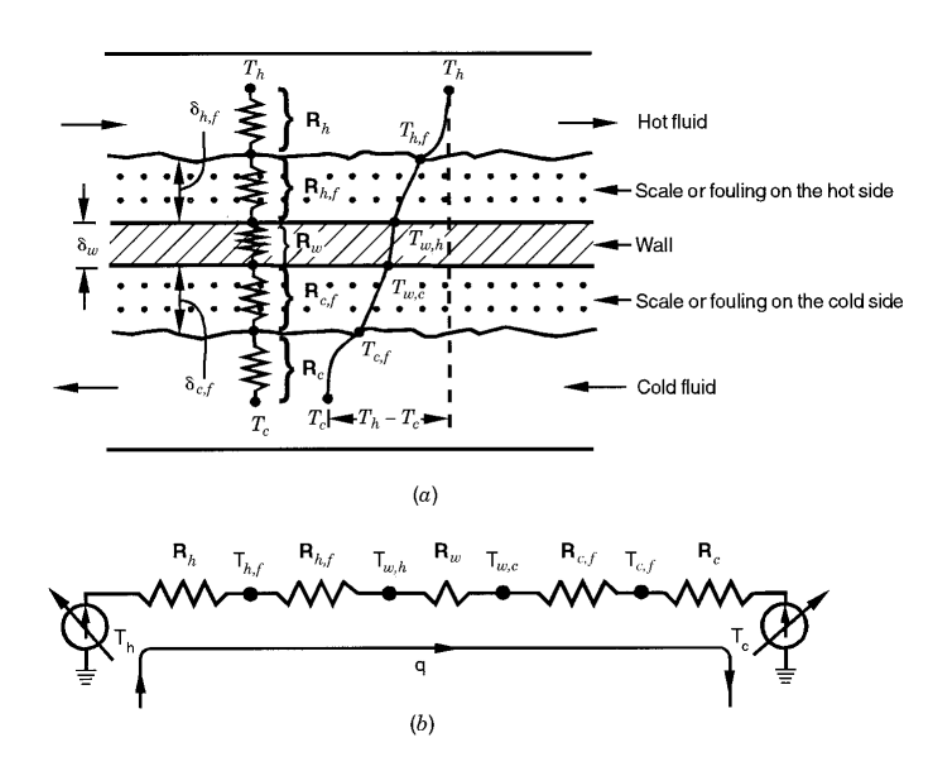


Figure 2.7: Illustration of the (a) thermal resistances and (b) thermal circuit for a heat exchanger [12]

First, the thermal resistance is defined as:

$$UA_h = \frac{1}{R} \tag{2.10}$$

With the assumption of heat transfer surface area being distributed uniformly on each fluid side, the overall heat transfer coefficient can be expressed as a sum of the individual resistances of heat transfer processes in the thermal circuit. The wall resistance R_w is determined based on the wall geometry, number of tubes and number of wall layers.

$$\frac{1}{UA_h} = R_{hot} + R_{hot,f} + R_w + R_{cold} + R_{cold,f} = \frac{1}{(hA)_h} + \frac{1}{(h_fA)_h} + R_w + \frac{1}{(hA)_{cold}} + \frac{1}{(h_fA)_{cold}} \tag{2.11}$$

The model above includes the effect of fouling layers on both sides of the wall, but the effect of fouling is far greater for liquid-to-liquid heat exchangers than liquid-to-vapour or vapour-to-vapour heat exchangers due to the far larger heat transfer coefficients in the liquid-to-liquid case. For the heat exchangers in the steam injection cycle, the relevant cases will be vapour-to-vapour or liquid-to-vapour. The only pure liquid stream is water entering the evaporator, and this will be treated before entering the heat exchanger, so fouling is can be expected to be small. If the engine is to run on hydrogen at least one additional heat exchanger will be required for the pre-heating of the fuel, but the purity of cryogenic hydrogen can be assumed to be high enough to neglect fouling [35]. Considering these facts and to limit modelling complexity, the thermal resistance provided by fouling layers can be neglected, simplifying the overall heat transfer coefficient to:

$$\frac{1}{UA_h} = R_{hot} + R_w + R_{cold} = \frac{1}{(hA)_{hot}} + R_w + \frac{1}{(hA)_{cold}}$$
(2.12)

The overall heat transfer coefficient is not always uniform across the length of the heat exchanger due to changes in phase, composition and flow speed, so accurately modelling the component may require breaking it into separate sections where individual heat transfer coefficients for the hot and cold fluid can be defined. This will then allow for the determination of an overall heat transfer coefficient in the section, which together with the LMTD or ϵ -NTU method allows for the sizing and performance estimation of the heat exchanger.

For the work at hand, the heat exchangers will be modelled as shell-and-tube type. For the thermal modelling, this means a thermal balance can be set up for individual tubes, with the heat transfer coefficients for the outer (shell) and inner (tube) flow needing to be estimated.

Heat transfer coefficient for single-phase outer flow

The outer flow for all considered heat exchangers will be single-phase. The heat transfer coefficient can be estimated by flow across tube banks, with a possible correlation for a staggered tube arrangement proposed by Zukauskas [34] as a function of the ratio of S_T , the transverse spacing between two tube centres and S_L , the longitudinal spacing between two centres. The relationship, given in Equation 2.13, holds for $1000 \le Re \le 2 \cdot 10^5$ and $\frac{S_T}{S_L} \le 2$.

$$Nu = 0.35 \cdot Re^{0.6} \cdot Pr^{0.36} \cdot \left(\frac{S_T}{S_L}\right)^{0.2} \tag{2.13}$$

Heat transfer coefficient for single-phase inner flow

The inner tube flow in the condenser and evaporator will include sections of single-phase (liquid water or gaseous steam) flow, as well as sections of two-phase (condensing or evaporating) flow. The heat transfer coefficient for single-phase flow in a tube can be estimated by Gnieliski's correlation [12] for turbulent flow, valid for $2300 \le Re \le 5.10^6$ and $0.5 \le Pr \le 2000$.

$$Nu = \frac{(f/2)(Re - 1000)Pr}{1 + 12.7(f/2)^{1/2}(Pr^{2/3} - 1)}$$
 (2.14)

where f, the friction factor for smooth pipes, can be determined by Filonenko's equation [34]:

$$f_D = \frac{1}{(1.82\log(Re_D) - 1.64)^2}$$
 (2.15)

Interlude: Two-phase inner flow

Estimating the heat transfer coefficient for two-phase flow is more complex. In two-phase flow, the fluid exists in two phases, with mass transfer in phase change resulting in variable flow rates and properties of each phase. The two-phase flow relevant to the discussed heat exchangers is gas-liquid flow. To visualise the flow composition the *quality*, or *vapour fraction*, χ is introduced, with χ =0 signifying a saturated liquid and χ =1 signifying a saturated vapour.

$$\chi = \frac{m_{vapour}}{m_{tot}} \tag{2.16}$$

The quality alone is not sufficient to describe the flow, as the distribution of liquid and vapour is able to take on an infinite number of possible forms. However, these forms can be classed into types of distributions called *flow regimes*. In [36], flow regime diagrams are produced for the possible flow regimes in two-phase gas-liquid flow inside tubes, presented for vertical flows in Figure 2.9 and horizonal flows in Figure 2.11. The regime domain is discretised by the superficial liquid velocity $\nu_{s,liquid}$ and superficial gas velocity $\nu_{s,gas}$, defined as the velocity of liquid/gas as if it was flowing in the tube without gas/liquid. It is to be noted that these regime diagrams are qualitative illustrations of a possible regime diagram for a given tube, as transitions between flow regimes are a function of the pipe diameter, interfacial tension and density of the phases.

$$u_{s,g} = \frac{Q_g}{A}, \quad \nu_{s,l} = \frac{Q_l}{A}$$
(2.17)

The superficial velocities are calculated by Equation 2.17, where ${\it Q}$ is the total volumetric flow and ${\it A}$ is the cross-sectional area of the tube.



Figure 2.8: Flow regimes in vertical gas-liquid flow in a tube [37]

In Figure 2.8, five flow regimes for gas-liquid flow in a vertical tube are identified. In *bubble* flow, gas bubbles are dispersed inside the liquid flow. In *slug* or *plug* flow, the bubbles have coalesced and form larger bubbles, up to the diameter of the tube. For *churn* flow, those bubbles break down and an oscillating churn regime emerges. In *annular* flow, liquid flows along the wall as a film with some drops in the central gas core flow. Finally, in *wispy annular* flow the increasing concentration of bubbles in the gas core leads to large streaks of liquid forming.

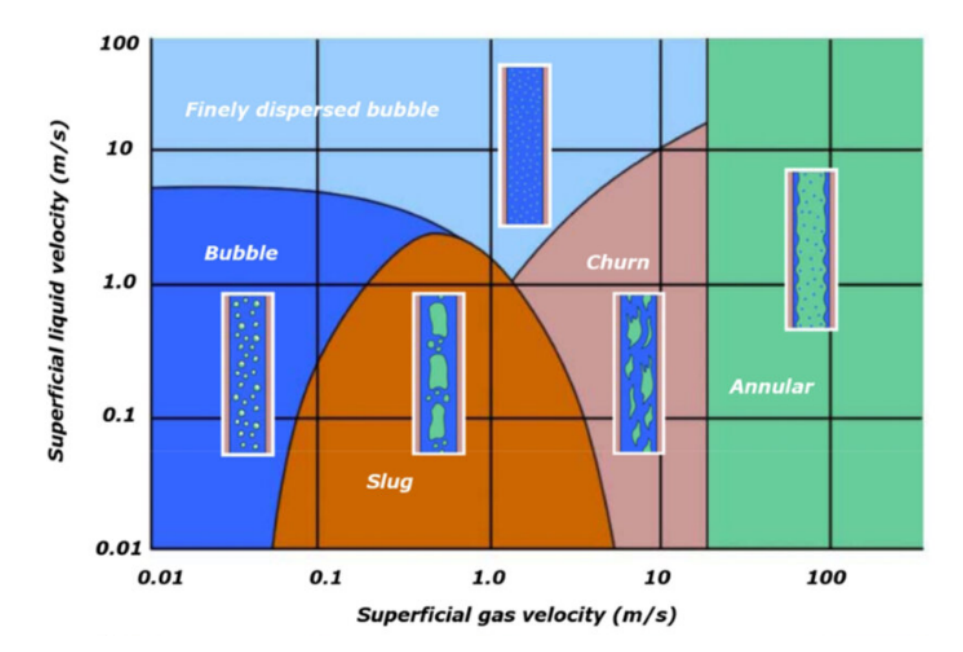


Figure 2.9: Example flow regime diagram for vertical gas-liquid flow in a tube [36]

Figure 2.9 shows an example of a regime diagram showing when flow regimes develop and transition. For low superficial gas velocities, the gas remains as bubbles inside the liquid flow. For a constant superficial liquid velocity, the flow develops from bubble, to slug, churn, and finally annular flow with increasing superficial gas velocity. However, there is also a superficial liquid velocity above which the flow remains in a separate, finely dispersed bubble regime, until transition to annular. In the finely dispersed bubble regime, small gas bubbles are dispersed in a continuous rapid fluid flow.

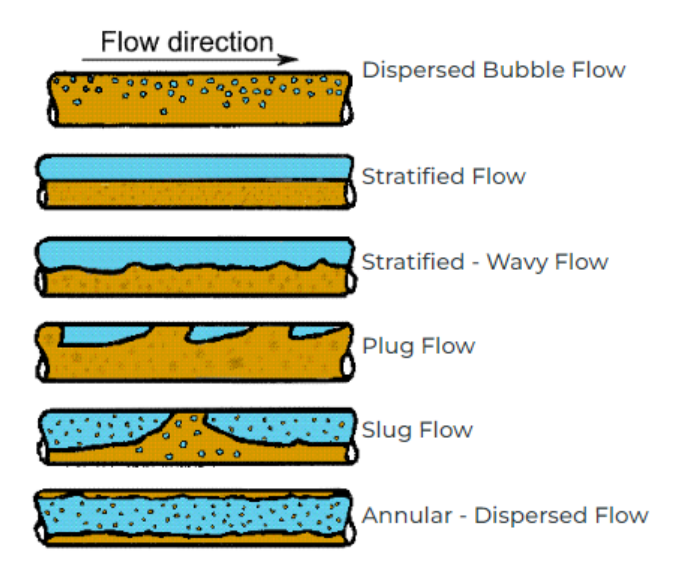


Figure 2.10: Flow regimes in vertical gas-liquid flow in a tube [37]

In Figure 2.10, flow regimes for horizontal flow are given. As gravity now acts normal to the flow direction, separation of the flow occurs due to the difference in density between gas and liquid. The dispersed bubble flow is similar to the vertical case, but there is some separation due to gravity. In stratified flow, the flow is fully separated and in stratified-wavy flow the flow is separated, but waves form at the interface due to increasing gas flow. In plug flow, large bubbles form near the top of the tube. Slug flow emerges when waves grow high enough to touch the top tube wall, forming a liquid slug that passes along the wall. Annular-dispersed flow is also similar to the vertical case, but now there is asymmetry in the thickness of the film layer due to gravity.

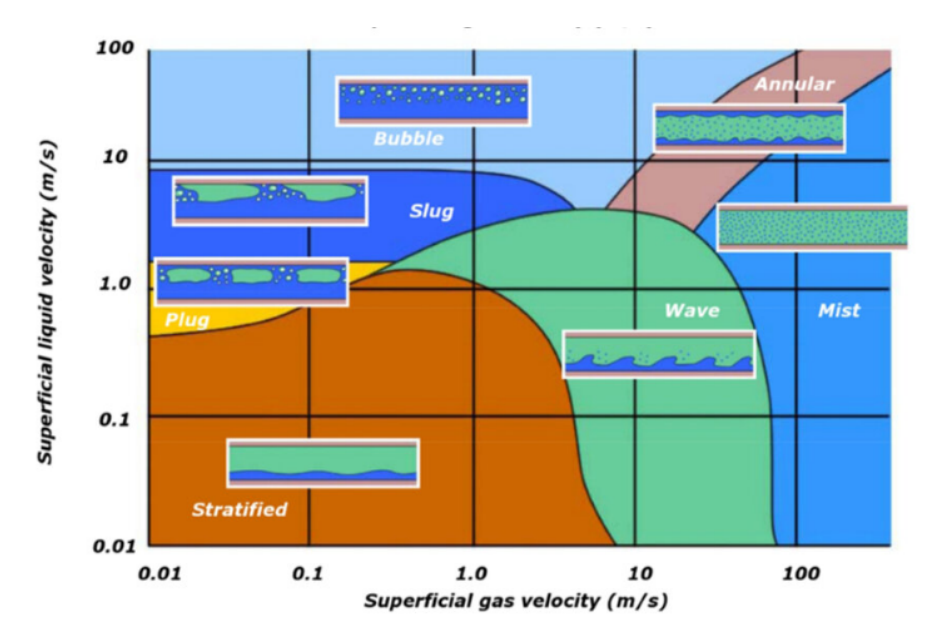


Figure 2.11: Example flow regime diagram for horizontal gas-liquid flow in a tube [36]

The flow regime diagram in Figure 2.11 shows that determining the regime and transition is somewhat more complex for horizontal flows as compared to vertical. For low superficial gas and liquid velocities, the flow remains stratified, as gravity is the primary force at play. If the superficial gas velocity is increased, waves begin to form, and increasing turbulence begins to rip liquid from the waves, finally resulting in an annular-dispersed flow or mist flow where liquid droplets travel in a gaseous flow stream and a liquid film forms at the tube walls. If instead the superificial liquid velocity is increased at a low superficial gas velocity, large bubbles form and float to the top of the flow as seen in plug and slug flow. Finally, for a high superficial liquid velocity turbulence is high and any gas in the flow tends to be dispersed as fine bubbles.

Heat transfer coefficient for two-phase evaporating flow

Vaporisation phenomena have been reported extensively in literature with empirical relations for the heat transfer coefficient developed, such as a general forced convective boiling correlation for tube flow proposed by Kandlikar, described in detail in [12]. The correlation relates the two-phase vaporisation heat transfer coefficient h_{vap} to h_{lo} , the single-phase heat transfer coefficient for the entire flow as liquid flow.

$$\frac{h_{vap}}{h_{lo}} = \text{larger of} \begin{cases} [0.6683Co^{-0.2} \cdot f_2(Fr_{lo}) + 1058Bo^{0.7} \cdot F_{fl}](1-\chi)^{0.8} \\ [1.136Co^{-0.9} \cdot f_2(Fr_{lo}) + 667.2Bo^{0.7} \cdot F_{fl}](1-\chi)^{0.8} \end{cases}$$

where $h_{lo} \sim f(Re_{lo}, Pr_l, Pr, k_l, d_i)$. Co is the convection number that is a function of the quality and the ratio of vapour to liquid density. Bo is the nucleate boiling number and Fr the Froude number which characterises the strength of the flow's inertia to the gravitational forces that drive separation of the two flow phases. The factor f_2 depends on the single-phase liquid Froude number as:

$$f_2(Fr_{lo}) = \begin{cases} f_2(Fr_{lo})^{0.3} & \text{for } Fr_{lo} < 0.04 \text{ in horizontal tubes} \\ f_2(Fr_{lo})^{0.3} & \text{for vertical tubes and for } Fr_{lo} \geq 0.04 \text{ in horizontal tubes} \end{cases}$$

 F_{fl} is a fluid-surface parameter that depends on the fluid and the heat transfer surface, with some suggested values given in [12].

Heat transfer coefficient for two-phase condensing flow

The two most common flow regimes for convective condensation are annular film flow in horizontal and vertical tubes and stratified flow in horizontal tubes [12]. A correlation for the condensation heat transfer coefficient h_{con} for annular flow, valid for horizontal, vertical or inclined tubes, is proposed by Shah and outlined in [12].

$$h_{con} \text{ (annular flow)} = 0.023 \frac{k_l}{d_i} \cdot Re_l^{0.8} \cdot Pr_l^{0.4} \left[(1 - \chi)^{0.8} + \frac{3.8\chi^{0.76}(1 - \chi)^{0.04}}{(p_{sat}/p_{cr})^{0.38}} \right]$$
 (2.18)

Carey proposes a correlation for the heat transfer coefficient in stratified flow in horizontal tubes of diameter d, also outlined in [12].

$$h_{con} \text{ (stratified flow)} = 0.728 \left[1 + \frac{1 - \chi}{\chi} \left(\frac{\rho_g}{\rho_l} \right)^{2/3} \right]^{-3/4} \left[\frac{k_l^3 \rho_l(\rho_l - \rho_g) g h'_{lg}}{\mu_l(T_{sat} - T_w) d} \right]^{1/4} \tag{2.19}$$

where:

$$h'_{lg} = h_{lg} + 0.68c_{p,l}(T_{sat} - T_w)$$
(2.20)

The above equations refer to the situation in which the condensing flow is the inner flow of a tubeand-shell heat exchanger. This is generally preferred as the condensing flow is expected to have a higher coefficient of heat transfer and also as collecting water may be easier with such a configuration. However, this may not always be the best design choice and the choice of flow configuration will be explored further in Subsection 4.6.7. For condensation outside a cylinder, Shekriladze and Gomelauri [34] suggest the following equation for Nusselt number:

$$Nu = 0.64 \left\{ Re_D \left[1 + (1 + 1.69 \frac{g h_{fg}^{'} \mu_f D}{V_{\infty}^2 k_f (T_{sat} - T_w)}) \right]^{1/2} \right\}^{1/2}$$
 (2.21)

Under appropriate flow conditions, such as large values of the shell-side flow velocity V_{∞} , gravity becomes unimportant and the equation simplifies to:

$$Nu_D = 0.64\sqrt{2Re_D}$$
 (2.22)

Pressure drop

The heat exchangers in the steam injection cycle experience liquid water flow, condensing and evaporating water flow, a steam flow and bypass and core exhaust gas flows. Estimating the pressure drop inside the heat exchanger is more important for the gaseous flows, as the pressure drop for liquid water is small. Detailed estimation of the pressure drop is not within the scope of the work. Despite this, an overview of the sources of pressure loss in heat exchangers is given and detailed estimation of the pressure drop is recommended for future work.

The total pressure loss is expressed in Equation 2.23 as a sum of the friction loss Δp_{fr} , the acceleration loss Δp_a , the gravitational pressure loss Δp_{gr} and the loss due to bends in the tubes Δp_{bend} [38]. For the shell-side flow, the bend loss does not apply, the acceleration term can be neglected as there is no phase change, and the gravitational term can be neglected if the flow is perpendicular to the direction of gravitational acceleration.

$$\Delta p = \Delta p_{fr} + \Delta p_a + \Delta p_{ar} + \Delta p_{bend} \tag{2.23}$$

The frictional pressure loss can be predicted for any kind of flow by Equation 2.24 [39], where the pressure loss coefficient ζ can be obtained from various correlations dependent on Re and the nondimensional coefficient a depends on the flow type.

$$\Delta p_{fr} = \zeta a \frac{\rho V^2}{2} \tag{2.24}$$

For the shell-side, Gaddis and Gnielinski [40] present a correlation where u is taken at the smallest cross-section of the tube bundle and a is set equal to the number of tubes. The pressure loss coefficient ζ is calculated with Re at the smallest cross-section, the number of tube rows in the bundle, wall

temperature and tube arrangement. For parallel flow, [39] presents a model with $a = l/d_h$ for tubes of length l and hydraulic diameter d_h .

For the tube-side pressure drop, Equation 2.24 simplifies to the Darcy-Weisbach equation [12], where V_m is the mean flow velocity inside the tube. The Darcy-Weisbach friction factor f_D depends on Re, cross-section geometry and surface roughness and can be obtained from the Moody diagram [12].

$$\Delta p = f_D \frac{l}{d_b} \frac{\rho V_m^2}{2} \tag{2.25}$$

Estimating the pressure loss for two-phase flow is complex and for this the acceleration term Δp_a is introduced, accounting for the acceleration of the fluid due to changes in density during evaporation or condensation. A_c is the tube cross-sectional area.

$$\Delta p_a = \frac{\dot{m}}{A_c} \left(\frac{1}{\rho''} - \frac{1}{\rho'} \right) \tag{2.26}$$

The pressure drop can be calculated by a number of empirical correlations for different tube diameters, pressures and fluids. Schmelcher et al. [38] recommend the correlation of Friedel presented in [41] for the preliminary design of heat exchangers in aircraft engines.

The gravitational pressure loss can be determined by Equation 2.27, where ρ is the density of the fluid, g is the gravitational acceleration and Δh the vertical height difference, defined as positive when flowing against the direction of gravitational acceleration.

$$\Delta p_{gr} = \rho g \Delta h \tag{2.27}$$

Finally, the bend pressure loss term accounts for the bends in tube bundles, which are needed in a compact heat exchanger to achieve a highly packed bundle. The small bending radius for narrow bends might lead to a significant pressure drop. The pressure loss is a function of flow velocity, density, ratio of bend radius to tube diameter r_{bend}/d and the bending angle. Schmelcher et al. [38] suggest the correlation of Chisholm [42], which models the flow assuming a single-phase flow and scales the results with a term dependent on the steam quality χ .

Heat exchangers in aicraft

The design of heat exchangers for aircraft applications poses some specific challenges as highlighted in [43], with an overview of the primary ones given below.

- A large range of heat transfer duties: As commercial aircraft engines operate in a wide range of operating conditions, heat exchangers need to be designed for a range of duties, with the maximum duty being approximately five times the minimum [43].
- **High specific duties:** Minimising weight is a primary design requirement for aircraft, encouraging the use of light-weight materials and thin-walled components, which can be seen as competing requirements since thermodynamic cycles are advantageous to run at higher pressure ratios [21], imposing requirements on part thickness and strength.
- High desired compactness: Due to weight and drag penalties as well as integration of the heat exchanger with other engine components, a heat exchanger as compact as possible is preferred. A two-phase heat exchanger is referred to as compact if the surface ares density is greater than about 400 m²/m³ [12].
- High required lifetime: Modern turbofan engines can be expected to last 10 000 hours between
 overhauls [44], giving an estimate for the minimum hours of operation without servicing for the
 heat exchanger.
- Corrosive environment: Combustors on modern turbofans run lean or oxygen-rich, meaning
 there will be excess oxygen in the core exhaust stream of the engine. Any heat exchangers that
 include the core exhaust must choose corrosion-resistant materials, use protective coatings or
 other corrosion prevention measures in order to limit heat exchanger material degradation and
 reduced heat transfer efficiency.

- Low desired pressure drop: Limiting the pressure drop for the exhaust stream over both the evaporator and condenser is desirable as it reduces the temperature difference required for sufficient water recovery in condenser. For the water stream, limiting pressure drop over the evaporator also reduces the required pump power, although this is not as critical given the required power for pumping liquid water is relatively low.
- Thermal gradients: The above mentioned requirements of compactness and high specific duties result in large temperature gradients over small distances, posing thermomechanical design challenges.

Condenser and water separator

A condenser is a heat exchanger designed to facilitate condensation, with a gaseous stream changing phase to vapour and transferring latent heat to another fluid stream. A condenser offers effective heat rejection owing to the high efficiency of heat transfer by latent heat compared to sensible heat. **Latent heat** refers to the energy emitted or absorbed during a phase change, in this case condensation, at constant temperature, whereas *sensible heat* is the energy which leads a temperature change without a change in phase. For the steam injection cycle the objective is to ensure sufficient condensation of the water in the exhaust of the gas turbine, providing a water supply for steam injection. While Figure 2.5 shows a fraction of the bypass airflow being used for cooling, alternative choices of the cooling fluid stream can provide an additional thermodynamic benefit. In the case of liquid hydrogen incorporating the fuel flow in the condenser could provide additional cooling for the water as well as be pre-heating for the fuel.

An overview of the condenser and water separator, represented as a counter-flow heat exchanger, is given in Figure 2.12. The condenser has two sections: a dry cooling phase where steam is brought to its saturation temperature, followed by the condenser where steam changes phase from vapour to liquid. The temperature change of the exhaust is shown as linear for simplicity when in reality the changing humidity and temperature of the exhaust leads to non-linear heat transfer. As the outflow consists of liquid water droplets suspended in a gas mixture, a separator is added to separate the water from the rest of the dried exhaust.

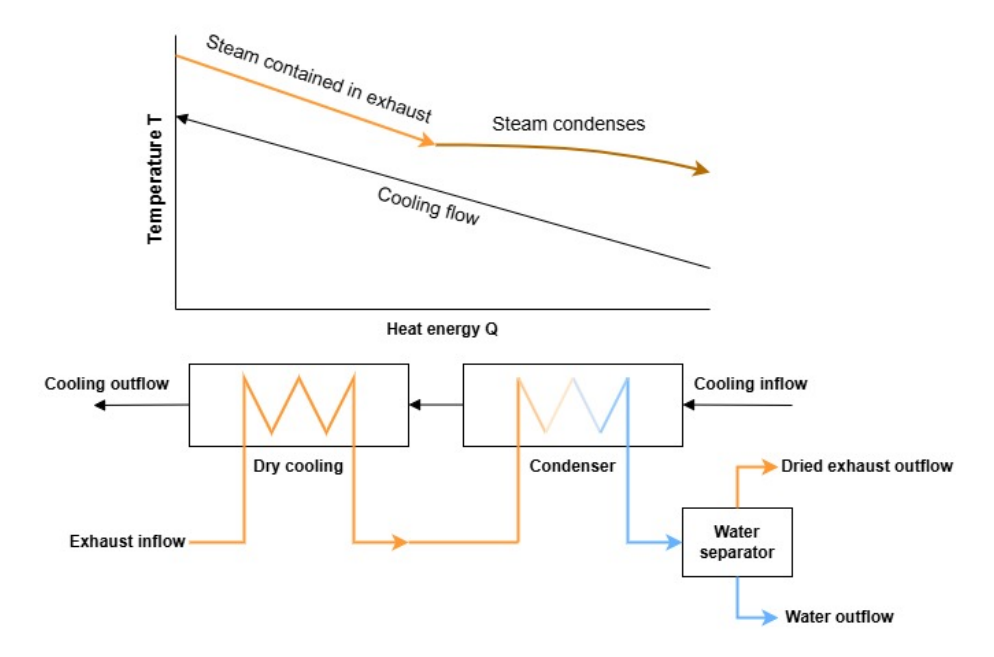


Figure 2.12: Overview of a condenser with average temperatures for both fluid streams plotted along the component

Thermal modelling of the condenser can be done in two sectors, with the dry cooling phase modelled as a single-phase vapour-to-vapour heat exchanger and the condenser part as heat exchanger with one single-phase side and one two-phase liquid-vapour side. The choice of cooling flow poses a challenge as a large amount of energy must be transferred, requiring flows with a large heat capacity or thermal conductivity, or a large temperature difference between the two flows. Currently the bypass air, or a

fraction of it, is chosen but the temperature difference between the evaporator exhaust air flow and bypass air might be small, especially at cruise. In the case of hydrogen the fuel line could provide added cooling, or additional ram air may be required. Given the high volume of the bypass flow and the fact that condensing flow is usually located on the tube-side [12], cooling flow could be allocated to the shell-side of the heat exchanger. However, the configuration depends on the total capacities of each stream as well as the configuration of the other heat exchangers and the final choice is elaborated further during detailed analysis of all three heat exchangers in Subsection 4.6.7.

In order for the steam cycle to be closed, the condenser must be able to condense and separate as much water from the core exhaust as is injected into the combustor. The *water recovery ratio* WRR is introduced in [16] to measure the fraction of water recovered from the exhaust, $\dot{m}_{wat,rec}$, to the steam flow injected into the combustor, $\dot{m}_{st,inj}$.

$$WRR = \frac{\dot{m}_{wat,rec}}{\dot{m}_{st,inj}} \tag{2.28}$$

In steady operation at the design point, the cycle should ideally be closed, making the water recovery ratio WRR=1. This might not be possible at every operating point due to varying available ΔT between the cooling air flow and core exhaust flow, necessitating some initial water storage on board. If WRR<1, external water supply is required, necessitating a larger tank and water reserves for a flight mission. If WRR>1, more water is recovered than injected, which is possible considering that the combustion of kerosene and hydrogen both produce water, the latter certainly more than will be required for steam injection. However, considering the large amount of energy required to condense water out of the core exhaust flow, this situation is unlikely at most operating points.

Evaporator

In its basic form, an evaporator is a heat exchanger that facilitates evaporation, providing the thermal energy needed for the phase transition of the working fluid from liquid to vapour. The evaporator in the steam injection cycle is also referred to as a *Heat Recovery Steam Generator* (HRSG), as it uses the heat energy of the core exhaust to heat the entering water and produce steam of sufficient quality for downstream components.

The component more specifically consists of three sections: the economiser where the inflowing water reaches its saturation point, the evaporator where water undergoes a phase change and exits as steam, and the superheater where the steam is further heated to the required temperature. Although the specific design of the evaporator flow configuration is not known, currently it is considered a counterflow heat exchanger, which individual passes of the shell-and-tube configuration may be modelled as. An overview of the three sections as well as the average flow temperature evolution for both the cooling exhaust stream and water/steam stream is given in Figure 2.13.

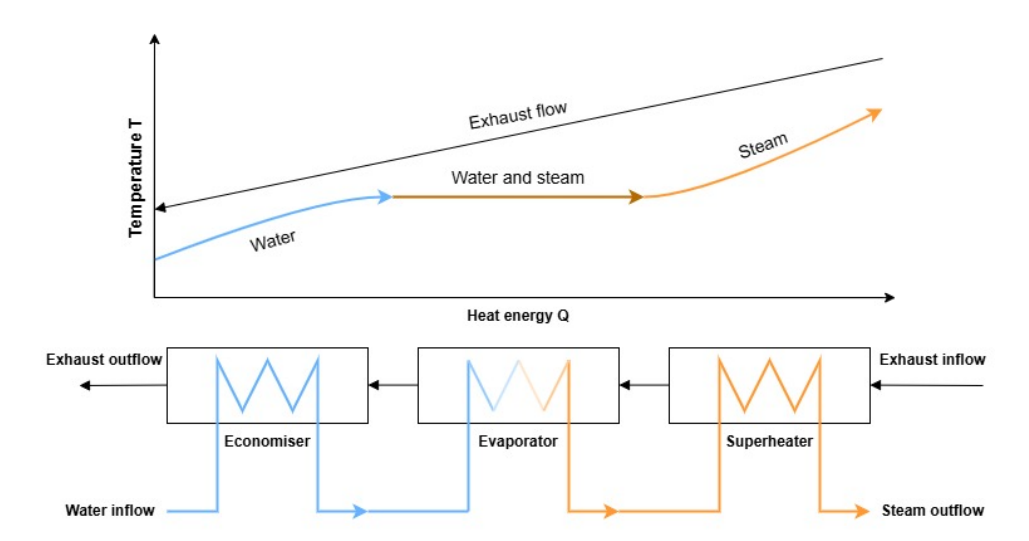


Figure 2.13: Overview of the HRSG with average temperatures for both fluid streams plotted along the component's length

There is a slight drop in temperature during evaporation due to pressure dropping, which lowers the boiling temperature of water. The superheater section is necessary as the steam must be of high enough temperature to ensure no liquid water droplets are present in the flow entering the downstream steam turbine, nor that any may form during the expansion of steam through the turbine, preventing damage to the turbine.

The three sections in Figure 2.13 can be modelled in sequence to account for the changing overall heat transfer coefficient and temperature differences. The sections can be modelled as an indirect-contact heat exchanger. A multi-pass shell-and-tube configuration could be considered, with water/steam on the tube-side and the exhaust flow on the shell-side, allowing the evaporator to be placed directly in the exhaust of the core. The choice of tube- and shell-side flows is motivated by the lower heat transfer coefficient of the exhaust flow, as well as its higher volumetric flow compared to the water flow.

2.3.3. Steam cycle components

The steam injection cycle is a combined cycle combining a Brayton, or gas turbine, cycle with a Rankine, or steam turbine, cycle. The addition of a secondary steam cycle to the primary gas turbine requires a number of new components to be added to the system, including but not limited to water storage and treatment, a water pump, a steam turbine and additional water/steam piping and feed system components. The first three mentioned components are briefly introduced.

Water tank

The water tank is necessary if the Rankine cycle is not fully closed, or in other words the water recovery ratio is less than 1. In this case, additional water must be available to meet the required flow rate for steam injection. Considering the fluid properties of water and that the tank will most likely not need to be under high pressures nor require significant insulation, its specific design is not deemed critical to the current work. However, a weight and volume penalty is expected for the overall system and the tank will need to be designed for the operating point with the lowest water recovery ratio achieved.

Water treatment

In considering water recovery, the quality of condensed water can be a concern. The water should be treated for impurities prior to entering the evaporator in order to protect the evaporator and downstream steam turbine from degradation, as well as insure the injection of undesirable compounds into the combustor which may increase emissions or otherwise negatively impact combustion. If the condensed water contains too many combustion products, chemical treatment might need to be considered, which would lead to additional complexity and cost. For hydrocarbon fuels, the potential of impurities in the water is higher than for hydrogen. Although there are is no known data for the purity of water recovered from aircraft turbofan exhaust, the analysis of the natural gas turbine at the "Carrozzeria Bertone" plant [45] showed that condensed water could easily be put back into the cycle without little treatment [46].

Water pump

A water pump will be necessary to move water from the tank to the evaporator and increase its pressure before entering the evaporator. The pumping power for water is low and the design of water pumps is understood well: as such, the pump will not be a critical component, nor should it impose a significant weight or volume penalty. For powering the pump, an electric drive can be considered, with power drawn, for example, from the steam cycle's own turbine. A point of concern for the pump design may be cavitation, as the entering water will be at fairly low pressures - to counter this, the water could be cooled prior to entering the pump.

Steam turbine

A steam turbine is included in the cycle to take advantage of the pressurised steam flow exiting the evaporator, allowing for the generation of shaft power and thus improving the overall cycle efficiency. The critical concern for the steam turbine is condensation: high enough pressures must be maintained throughout the turbine to prevent steam from condensing and damaging the component.

2.4. Hydrogen-fuelled engines

Noting the uncertainty of affordable future supply and the environmental impacts of currently used hydrocarbon fuels, there is great momentum to explore alternative energy sources in the aviation industry. The viability of an alternative energy source depends on its impact on design mission capability, as illustrated in the mass of fuel and containment system relative to range plotted for various energy sources in Figure 2.14. For the foreseeable future, the only alternative energy source able to compete with kerosene for missions of all ranges is shown to be liquid hydrogen. While battery-powered flight and hydrogen fuel cells (not pictured) may be a solution for regional and short-range missions, liquid hydrogen shows the most promise for the larger section of mid-range to long-range flights. Alternative fuels such as liquid natural gas, methanol and ethanol have also been investigated, but none would provide a more competitive advantage in performance and emissions [7]. Note also that in Figure 2.14 no allowance has been made for energy use to fulfill reserve requirements, which has a proportionally greater effect on the available mission range for battery-powered and gaseous hydrogen-fuelled aircraft.

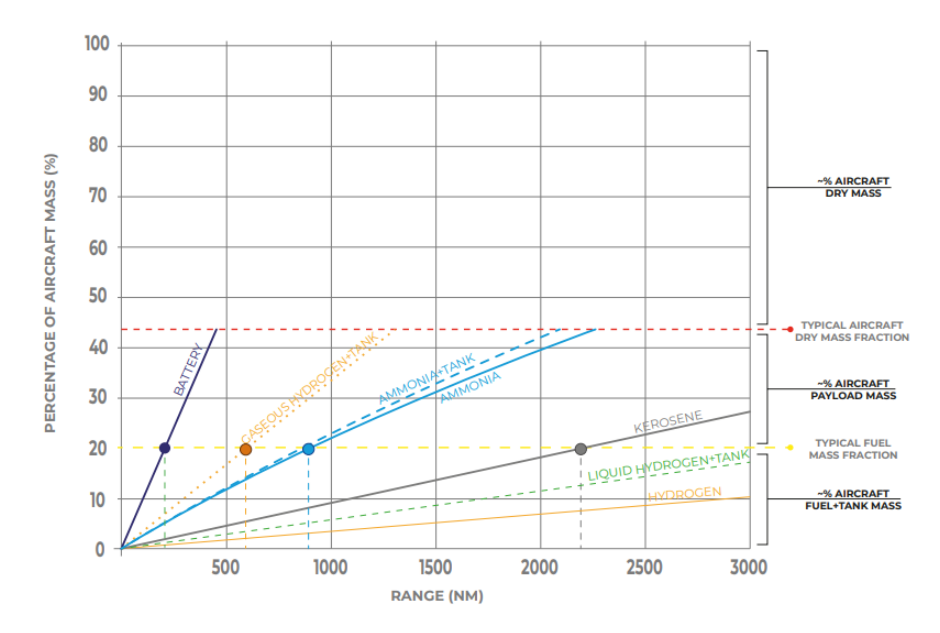


Figure 2.14: The fuel (and tank) mass fraction for various energy sources as a function of aircraft range (2030 technological assumption) [9]

The same potential is illustrated by the Breguet equation given in Equation 2.29 which relates the range of an aicraft to the engine's total efficiency η_{tot} , the lift-to-drag ratio L/D of the aircraft and the propellant mass, expressed in the ratio of initial to final total aircraft mass m_i/m_f . The range is shown to be proportional to *lower heating value* LHV of the used fuel, which would in principle promise a significantly higher possible range for an aircraft of otherwise identical characteristics powered by hydrogen rather than kerosene.

Range
$$= \frac{\eta_{tot}LHV}{g} \frac{L}{D} \ln \left(\frac{m_i}{m_f} \right)$$
 (2.29)

The potential improvements in mission capability, however, come at the expense of a lower volumetric energy density, higher complexity of fuel system and engine design.

2.4.1. Application in aircraft

The history of hydrogen as an energy source stretches back centuries. The first airborne vehicle fuelled by hydrogen was a balloon launched by Jacques Charles and Robert Brothers in 1783 [47], followed by the designing of the *Zeppelin* [48] in the late 19th century. The first hydrogen-fuelled engine was the *Heinkel Jet Engine*, flown in 1939 under a Heinkel He 118 dive bomber [49].

By the second half of the 20th century, NACA's Lewis Field laboratories were actively researching the use of hydrogen for high-altitude aircraft applications. This resulted in the first hydrogen-powered aircraft *Project Bee* [50], a modified Martin B-57 bomber redesigned to run on hydrogen. Whilst only one engine was configured to run on hydrogen, the aircraft flew successfully in 1957, switching between jet fuel and hydrogen 38 times in flight. The project showed the feasibility of modifying turbojet engines for hydrogen fuel and gave insight into the safe handling of hydrogen. Another significant contribution to the development of hydrogen aircraft technology is the *CL-400 Suntan* [50], a project of the Lockheed Skunk Works department. The prototype design was a high-altitude reconnaissance aircraft powered by two liquid hydrogen-fuelled engines mounted on the aircraft's wingtips. While the programme was scrapped due to budgetary pressure and difficulties achieving sufficient range, it included a successful conversion of an existing turbojet engine to run on hydrogen and importantly established the industrial infrastructure for high-volume hydrogen production that would later be utilised by the *Apollo* and *Space Shuttle* programmes [50].

Another important innovation was the soviet *Tupolev Tu-155*, a modified Tu-154 aircraft with one of its three engines capable of running on hydrogen combustion [51]. First taking flight in 1988, the aircraft made around 100 flights, although some of those were run on natural gas rather than hydrogen. The project was scrapped in the fall of the soviet union, but the aircraft demonstrated the feasibility of operating a turbofan engine on hydrogen and the integration of a cryogenic tank on aircraft [51].

At the turn of the millenium, the Airbus-led *Cryoplane* study assessed numerous configurations, systems, engines, safety and environmental compatibility of hydrogen-fuelled civil aircraft, including transition scenarios [52]. In recent years, emissions reduction and the energy transition are topics of high interest in aviation. In 2020, Airbus announced *Airbus ZeroE*, a collection of three hydrogen-fuelled aircraft concepts for varying mission ranges [5]. These include a conventional tube-and-wing configuration turboprop and turbofan aircraft, and a *blended-wing body* aircraft, all powered by the direct combustion of hydrogen stored in cryogenic tanks. The programme aims to put the first climate-neutral, zero-emission aircraft into service as early as 2035 [5]. While previously focusing on *sustainable aviation fuels* (SAFs), Boeing has completed research into hydrogen fuel cells and cryogenic tanks, as well as visualising hydrogen direct combustion as a feasible aircraft power source for the years 2040 and beyond [53].

Finally, there are further initiatives, including the European Clean Aviation Joint Undertaking [6] established in 2021, enabling among other topics research into hydrogen aircraft technology with the goal of cutting fuel consumption and related CO_2 emissions in future aircraft. Specifically, the use of liquid hydrogen in aircraft as a disruptive technology is seen as a promising option for meeting the European Green Deal objective of climate neutrality by 2050 [1].

2.4.2. Evaluating the use of hydrogen

In evaluating the advantages and disadvantages of using hydrogen as fuel, the baseline comparison is chosen as kerosene, the umbrella term for today's hydrocarbon aviation fuels. Both kerosene and hydrogen are used in a similar manner to power a turbofan engine, being burned in a combustor in order to add heat energy to the incoming air flow. However, their differing chemical composition introduces an array of differences in their properties and emissions as well as their storage, feed systems and safety concerns. In addition to this, the production of hydrogen has a contribution to its overall climate impact and holds implications for the infrastructure required to realise the use of hydrogen as an aviation fuel.

Production

Kerosene is produced from the fractional distillation of crude oil obtained from natural reservoirs. To current knowledge hydrogen does not, save for rare cases at extreme depths [54], exist in its pure state in nature. Molecular hydrogen must be produced, which is generally achieved by decomposition of a hydrogen-containing compound or *feedstock*.

Associated color	"Grey"	"Blue"	"Turquoise"	"Green"
Primary feedstock	Natural gas	Natural gas	Natural gas	Water
Production technology	Steam methane reforming (SMR)	SMR with carbon capture & storage (CCS)	Methane pyrolysis (MP)	Polymer electrolyte membrane water electrolysis (PEMEL)
Technology readiness level (TRL)	Commercial (TRL 9)	Industrial scale (TRL 8-9)	Research & Development (TRL 3-4)	Commercial (TRL 9)
Process-related CO ₂ emissions	High-CO ₂	Low-CO ₂	CO ₂ -free	Carbon-free

Figure 2.15: A selection of hydrogen production processes and their greenhouse gas emissions[55]

The production process as well as the energy carrier can vary, having an impact on the total environmental impact of the produced hydrogen. In Figure 2.15, some production technologies which are identified likely to be suitable for large-scale production of hydrogen in the near to medium-term future are highlighted [55]. Today, 75% of the world's hydrogen is produced using the *steam-methane-reforming* (SMR) process [56], an endothermic process which separates natural gas into hydrogen and the greenhouse gas carbon dioxide, with hydrogen produced in this manner called *grey* hydrogen. In the case that most of the greenhouse gas emissions are captured by trapping and storing the CO₂ produced, the hydrogen can be called *blue* [55].

[55] An alternative process is the electrolysis of water, another hydrogen carrier [57]. While the process itself produces no greenhouse gas emissions, an external energy source is required. In the case of a renewable energy source such as solar or wind power being used, the hydrogen is referred to as *green*. As of 2020, less than 0.1% of global hydrogen production is green [58]. The topic of hydrogen production is important to consider the wider environmental impact of fuel choice, as limiting emissions purely at the engine level does not translate to the same reduction in total emissions.

Chemical properties

Kerosene is a liquid at standard atmospheric conditions, and is stored at low pressure, simplifying storage system and pump design. Despite its high mass-specific energy density as expressed by the LHV, hydrogen is a gas at standard atmospheric conditions and would require unreasonably large tanks to supply an equal amount of energy to kerosene. Hence, it must be stored either at low temperature (cryogenic) or high pressure in order to compete with the volumetric energy density of kerosene. In Table 2.1, the storage conditions, density, LHV and volume-specific energy are given for kerosene, gaseous hydrogen and liquid hydrogen.

	Liquid hydrogen	Gaseous hydrogen	Kerosene
Storage temperature [K]	20 K	298 K	298 K
Storage pressure [MPa]	0.15	70	0.1
Density [kg/m ³]	71	39	804
Lower heating value (LHV) (MJ/kg)	120	120	43.2
Volume-specific energy (GJ/m ³)	8.25	4.68	34.7

Table 2.1: Comparison of storage properties and energy densities of liquid hydrogen, gaseous hydrogen and kerosene [9]

Storing hydrogen in its gaseous form requires a tank built to withstand the high pressures, which will have a large impact on the mass of the aircraft. Liquid hydrogen tanks, in turn, are complex due to the level of insulation and/or heat management required to maintain cryogenic conditions. However, the near doubling of the volume-specific energy when compared to gaseous hydrogen, as well as the reduction in tank mass, leads to liquid hydrogen storage being preferred for aircraft applications. As such, the following discussions assume that liquid hydrogen is to be employed in the engine.

Molecular states of hydrogen

Hydrogen has further specific considerations relating to its storage. Molecular hydrogen can exist in two different states depending on the nuclear spins of each atom, and these states have some differing characteristics. As illustrated in Figure 2.16, *ortho*-hydrogen or $o-H_2$ has two hydrogen atoms with the same spin, and *para*-hydrogen or $p-H_2$ two with opposing spins.

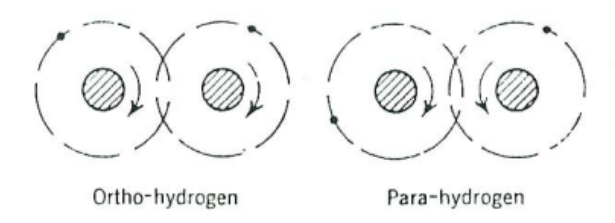


Figure 2.16: The spin direction of the two hydrogen atoms for ortho-hydrogen and for para-hydrogen

Regular or *normal* hydrogen in equilibrium at ambient temperature consists of 75% ortho- and 25% para-hydrogen and is designated as $n-H_2$. However, at cryogenic conditions of 20.4K, liquid hydrogen is 99.8% para-hydrogen with only a minor 0.2% ortho-hydrogen fraction [59]. As such, liquid hydrogen can be considered as $p-H_2$. The process of ortho-to-para-hydrogen is slow unless catalysed, and exothermic. This means unconverted hydrogen will have storage losses due to boil-off resulting from the heat released during the conversion. For long-term storage of liquid hydrogen, conversion is required and is catalysed by Nickel powder or ferric oxide as examples [59].

In Figure 2.17, the differing thermal capacities of normal hydrogen and liquid hydrogen are presented. As can be seen, liquid hydrogen has a higher heat capacity at temperatures between around 100K to 400K, which is beneficial as it increases its heat sink capability.

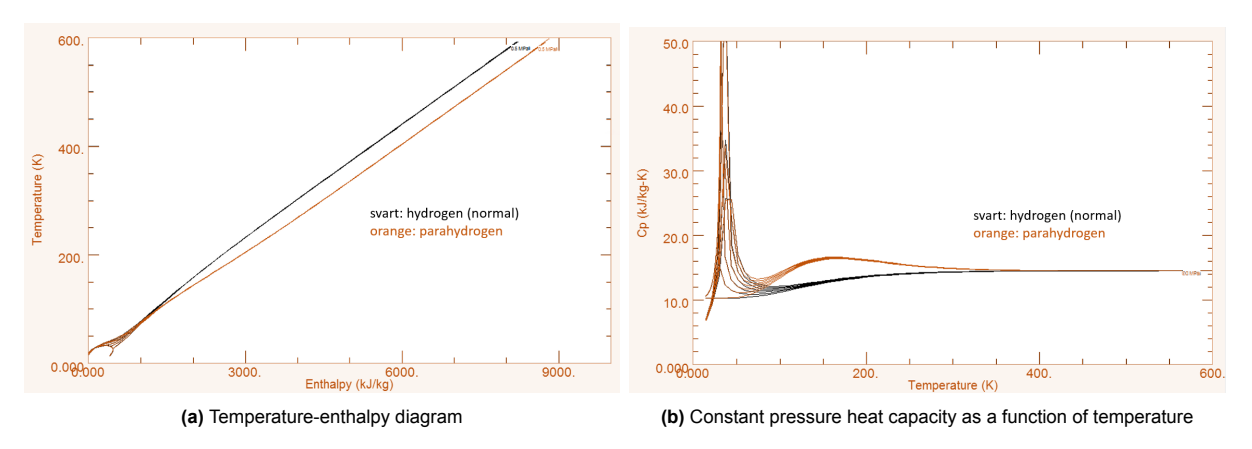


Figure 2.17: Comparison of the thermodynamic properties of normal $(n-H_2)$ and liquid hydrogen $(p-H_2)$ [60]

The uncatalysed conversion process is slow [59] and heating hydrogen to the combustion temperature inside the engine happens much faster, so liquid hydrogen may stay largely in para-state for short time scales at elevated temperatures. However, it can not be said with certainty what the molecular state of hydrogen is inside the combustor and heat exchangers. When modelling the hydrogen gas turbine, the molecular state of hydrogen must be considered in selecting appropriate chemical properties and is specifically important for estimating heat transfer.

Thermodynamic properties

The combustion characteristics for kerosene and hydrogen vary, which is of high relevance for the hydrogen-fuelled aircraft engine's combustor. The differences in the adiabatic flame temperature as a function of equivalence ratio Φ and specific heat at constant pressure of the exhaust mixture for the two fuels are shown in Figure 2.18.

The heat capacity of the combustor exhaust is plotted for the same inlet temperature of 800K[10]. Considering a standard range of combustor outlet temperatures between 1400-1800K, the heat capacity for hydrogen combustion products is 3.7% to 7.1% higher due to the higher content of water. The advantage is a higher potential for the turbines to extract work at the same combustor outlet temperature, which is generally a critically limiting temperature in an engine. Furthermore, the high heat capacity and low storage temperature of liquid hydrogen means it is a great heat sink, which is advantageous. Various components in an engine require cooling, such as turbomachinery, the engine oil, and specifically for the steam injection and water recovery cycle, the condenser. However, the higher heat capacity of hydrogen also influences heat transfer at the turbine blades, thus possibly introducing a different cooling air demand [16].

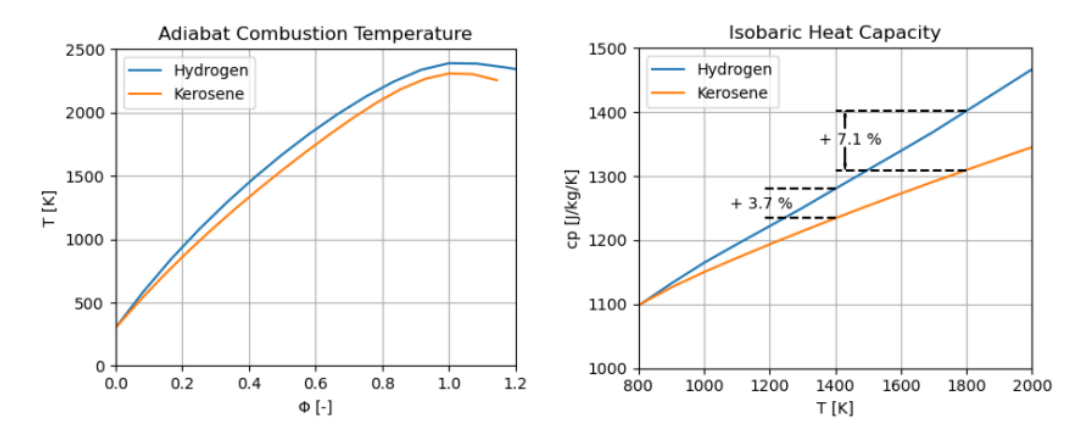


Figure 2.18: Comparison of the adiabatic flame temperature and isobaric heat capacity (of the exhaust mixture) for kerosene and hydrogen[10]

The adiabatic flame temperature for hydrogen is higher, surpassing that of kerosene by around 3.5% at its maximum near stoichiometric conditions (Φ =1). A higher flame temperature implies higher NO_X emissions due to the strong dependence of the primary NO_X formation pathway on temperature [21]. While modern turbofan combustors run lean to minimise regions of stoichiometric combustion [16], hydrogen's higher LHV also means that stoichiometric combustion is reached at lower fuel-to-air ratios. However, hydrogen has a significantly higher flammability range [8], allowing the combustor to operate at leaner equivalence ratios than with kerosene.

This effect is further illustrated in Figure 2.19. The lean blowout limit is significantly lower for hydrogen, allowing for lean low- NO_X combustion. Furthermore, for the same combustor inlet temperature the maximum combustor temperature at full load is lower than that for kerosene due to the higher energy density of hydrogen. The wider flammability range, however, means that hydrogen is highly reactive and prone to flashback, which has implications for the design of hydrogen fuel injectors.

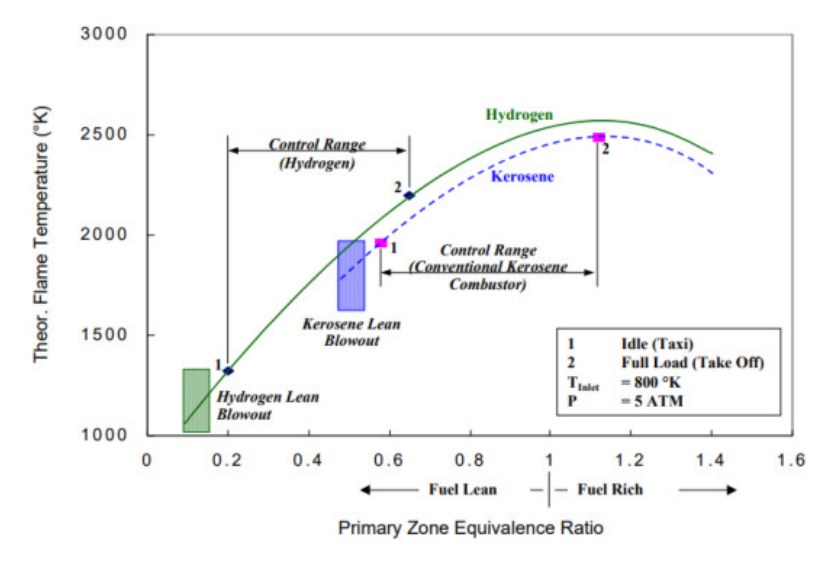


Figure 2.19: Flammability range and adiabatic flame temperature for kerosene and hydrogen [8]

The phase temperature-entropy diagram for hydrogen is given in Figure 2.20. At atmospheric pressure, the evaporation temperature is around 20 K, so storage of liquid hydrogen implies high demands on insulation and/or active cooling of the tanks. While kerosene is injected as a liquid into the combustor, doing so for liquid hydrogen would lead to a performance penalty due to its low temperature: hence, hydrogen is evaporated before combustion [61]. Furthermore, keeping hydrogen a liquid in the fuel control system could lead to the freezing of control valves [62], as well as lead to embrittlement. Considering the critical pressure is 1.315 MPa, which is lower than the pressures inside the engine, evaporation, or rather the heating, of hydrogen will happen in the supercritical state.

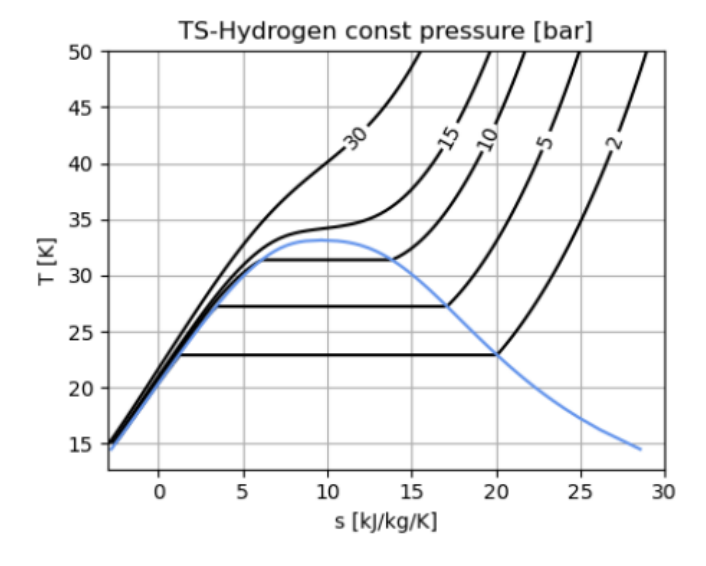


Figure 2.20: Temperature-entropy phase diagram for hydrogen with isobars plotted in black [10]

2.4.3. Combustion emissions

Unlike hydrogen, kerosene is a *hydrocarbon*, consisting of hydrogen and carbon atoms and this leads to a different composition in the engine exhaust depending on the fuel choice. The simplified combustion reactions assuming complete consumption are given in Equation 2.30 and Equation 2.31 for kerosene and hydrogen, respectively. In brackets, the additional products for non-ideal combustion are given. While kerosene is in reality a mixture of hydrocarbons, it is represented by the average formula of $C_{12}H_{23}$ [21].

$$C_{12}H_{23} + O_2 \rightarrow 12CO_2 + 11.5H_2O$$
 (+ CO, NO_X, soot, SO_2 , UHC) (2.30)

$$H_2 + O_2 \to H_2O$$
 (+ NO_X) (2.31)

It becomes obvious that exhaust from hydrogen combustion is cleaner, lacking undesirable carbon compounds, and significantly more humid. Considering the simplified equation, the combustion of a single kg of kerosene produces around 3.16 kg of CO_2 and 1.24 kg water. For a 0.36 kg mass of hydrogen, which provides the same energy content as a kg of kerosene, the mass of water is 3.21 kg, nearly triple that for kerosene.

The exhaust composition depends on altitude and thrust setting, and the combined environmental effect of an engine is complex. As a simplified overview, a comparison of the *Global Warming Potential* (GWP), a measure of the environmental impact of various gaseous emissions, was developed for the Cryoplane project and is shown in Figure 2.21. Hydrogen engines are shown to have a smaller overall impact on global warming, owing largely to the elimination of carbon dioxide emissions which is a greenhouse gas. NO_X emissions are reduced and can be further minimised by the use of premixing in the combustor. The impact of water vapour, however, is shown as a higher fraction of the total.

However, this analysis does not consider the higher energy usage of hydrogen aircraft which results from the configuration changes necessary to accommodate hydrogen storage systems, increasing aircraft drag and mass. As such, there is an increase in total emissions, and as a percentage this must be smaller than the percentage reduction in emissions potential in order to end up with a total overall benefit for choosing hydrogen.

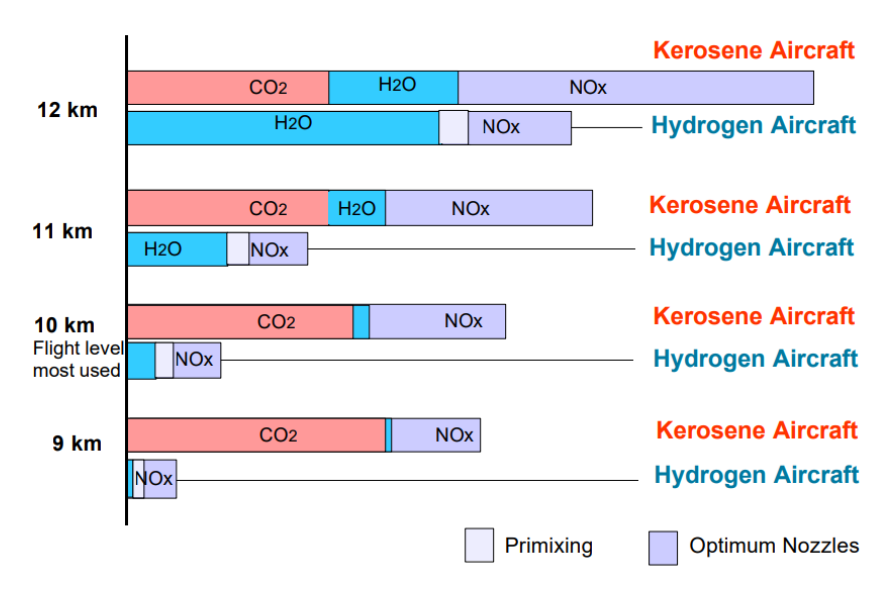


Figure 2.21: The Global Warming Potential of emissions from kerosene and hydrogen aircraft at varying altitudes [63]

An important conclusion is to realise that the impact of any one exhaust product can not be quantified by simply their amount, but depends also on the environment in which it is emitted. Furthermore, various metrics can be devised to describe the effects emissions have on the environment, from warming/cooling potential to toxicity and impacts on ecosystems. The science of modelling aircraft emissions and their impact is complex and a large deal of uncertainty exists, especially with the formation and impact of condensed water vapour, or contrails.

This is especially true for hydrogen engines as none are in service today, giving no quantitative data on contrail formation, persistence and impact. For determining the impact of contrails, three factors are important:

- Formation: This is a function of the exhaust and ambient temperatures as well as the composition of exhaust. A more humid exhaust will have more water to condense, a cooler exhaust will require less energy to condense, and more particles in the exhaust will provide more nucleating particles for ice crystal formation. Contrail formation is generally limited to ambient temperatures below 233K[64], hence their prevalence at higher altitudes.
- Persistence: How fast the contrail dissipates determines the impact of it and its persistence is a factor of ambient humidity [65]. As they exit the engine, exhaust gases mix with the surrounding air if this is fairly dry, any contrails formed of the engine exhaust humidity are short-lived. Persistent contrails are formed if the ambient air is supersaturated with respect to ice. The engine exhaust locally induces ice formation by providing nucleating particles of condensed water. This triggers the formation of wide spreading ice cirrus layers, as the ice particles grown until all vapour excess of ice saturation is deposited on them. The contrail dissipates either when its relative humidity drops below ice saturation, by mixing with dry air, subsedience or radiative heating, or alternatively if the particles sediment into drier air [65].
- Atmospheric heating and cooling: Contrails have two competing effects they reflect incoming radiation from above, while also trapping radiation from the Earth's surface. The total difference in energy exchange determines whether a cooling or heating effect is observed and is a complex function of the environment, the time of day and engine efficiency [65].

While hydrogen engines produce a higher absolute mass of water vapour in their exhaust, the exhaust composition has fewer nucleating particles in the form of soot and unburnt hydrocarbons. The formation of contrails, also at a wider range of altitudes, is certainly more likely given the humidity and higher temperature of the hydrogen exhaust. However, the smaller amount of particles in the exhaust is likely to lead to the formation of fewer, but larger droplets and ice particles [65]. Such a contrail has a smaller optical thickness despite the higher humidity and the particles would sediment earlier than for a larger initial particle density [65]. Hence, it may be that hydrogen contrails persist shorter and have a smaller climate impact than kerosene contrails. The research on this topic is ongoing and as discussed before, uncertainty in the total climate impact is large.

2.4.4. Hydrogen combustor

Hydrogen combustion is characterised by a high laminar flame speed, wide range of flammability and low flame emissivity. Gaseous hydrogen could theoretically work in a conventional kerosene combustor [62], but the large diffusive scales and fast kinetics of hydrogen combustion would lead to high-temperature stoichiometric layers, significantly increasing NO_X production [10]. Hence, the design of hydrogen combustors focuses on achieving sufficient mixing, generally featuring a large array of small-diameter injectors, increasing complexity of the component.

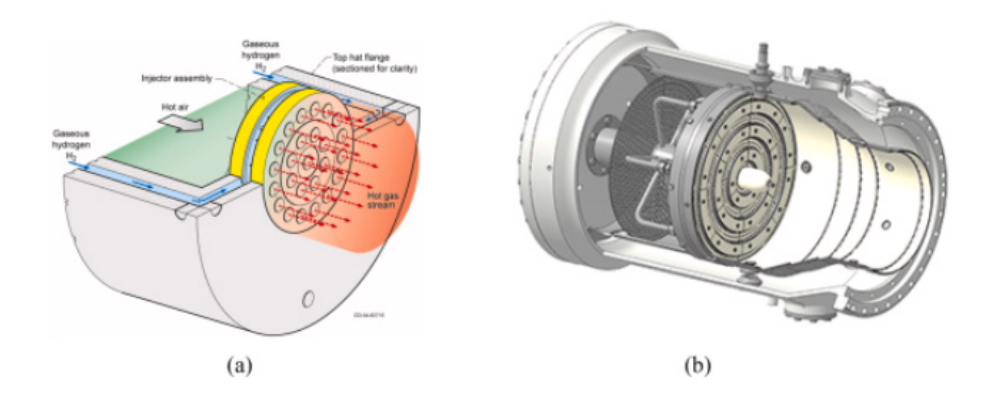


Figure 2.22: Hydrogen combustor design examples: (a) NASA direct lean injector [66] (b) a Kawasaki micromix combustion system [67]

In Figure 2.22, two technologies are shown. Premixed combustion allows for a further reduction in NO_X emissions, but the susceptibility of hydrogen to flashback must be avoided and is accomplished in [66] by the use of fuel inlets smaller than the fuel quenching diameter. Micromixing as a concept has been researched in many studies, exploiting the idea of minimizing the scale of the combustion zone by introducing thousands of uniformly distributed diffusing flames, offering improved turbulent mixing and reducing local residence time. The benefit is a high reduction of NO_X emission, and micromix combustor research is ongoing.

2.4.5. Hydrogen evaporator

As discussed, to ensure sufficient mixing, reduce local hot spots and avoid the performance penalty of injecting cold fuel into the combustor, a hydrogen evaporator is to be integrated into the cycle to heat the hydrogen from its cryogenic conditions prior to combustion. The evaporator will be a heat exchanger with hydrogen on one side and a higher temperature fluid on the other. Since there are various choices of flows in the engine higher than hydrogen's 20K storage temperature, the evaporator can also provide a cycle efficiency benefit if the heating flow is chosen wisely. Previous work has investigated various choices for this.

Brewer [61] summarises the results of several technological studies performed by NASA and Lockheed to investigate a liquid-hydrogen-powered long-range commercial jet in the late 1970s [61]. For the placement of the hydrogen fuel evaporator, five options were considered in an engine design study and their preliminary performance compared against a baseline theoretical high-bypass kerosene turbofan engine. The change in SFC and engine weight, and the added heat exchanger weight were determined and combined in a performance metric, the change in direct operating cost (DOC). Out of these five, three were also investigated in a 2022 article by Görtz and Silberhorn [10], whose results are used for further comparison. The SFC and TSEC, included due to the differing density and LHV of hydrogen, were compared to a theoretical kerosene-fuelled geared turbofan engine. While weight estimates were not made, the heat exchanger parameter kA was determined and used as a qualitative measure for size.

The five configurations are outlined below and their estimated performance compared. Simplified versions of the full cycle schematic presented in Figure 2.5 are employed to illustrate the placement of the hydrogen evaporator. Finally, some additional configurations which were not covered are introduced to demonstrate the wide design space for cycle architecture.

Compressor precooling

The first option is the *compressor precooling* (PC) configuration presented in Figure 2.23 which utilises the air between the fan and LPC to cool hydrogen, thereby also *precooling* the *compressor* inlet air.

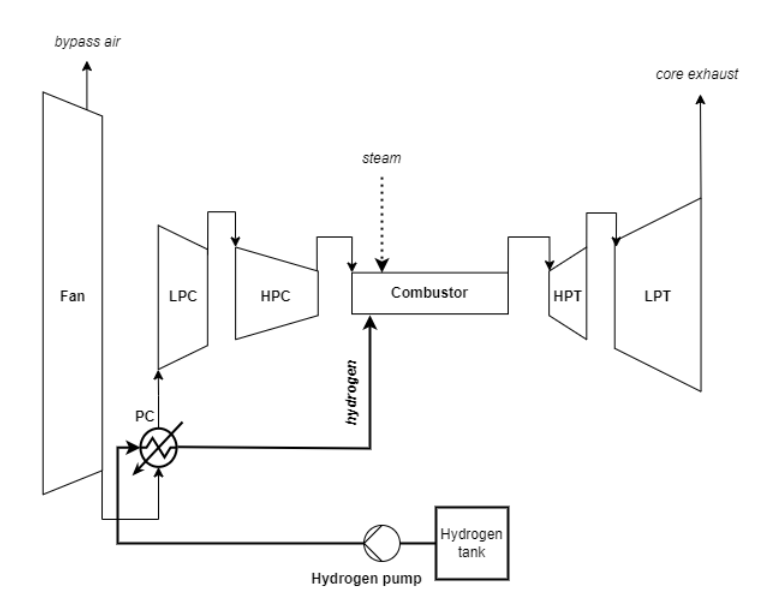


Figure 2.23: Compressor precooling configuration

An advantage of this configuration is the reduction in compressor work due to a cooler inlet temperature, reducing the size and weight of the gas generator. However, air-side pressure loss in the compressor will offset these advantages. Brewer [61] reported a 1.86% reduction in SFC and a moderate reduction in engine weight. Accounting for the added heat exchanger weight, the overall DOC improvement was calculated to be a reduction of 1.33% [61]. However, detailed heat exchanger design analysis revealed a severe air-side freezing problem, as well as a serious problem with susceptibility of the heat exchanger to damage due to foreign object ingestion [61], which could contribute to why this concept has not been considered in modern studies.

Compressor intercooling

Similar to compressor precooling, the hydrogen could instead be heated by the flow between the low-pressure and high-pressure compressor, referred to as compressor *intercooling* (IC) [10] and is presented in Figure 2.24. The advantage is similarly to compressor precooling a reduced compressor work and a reduction in gas generator size, with the drawback being a pressure drop in the core flow.

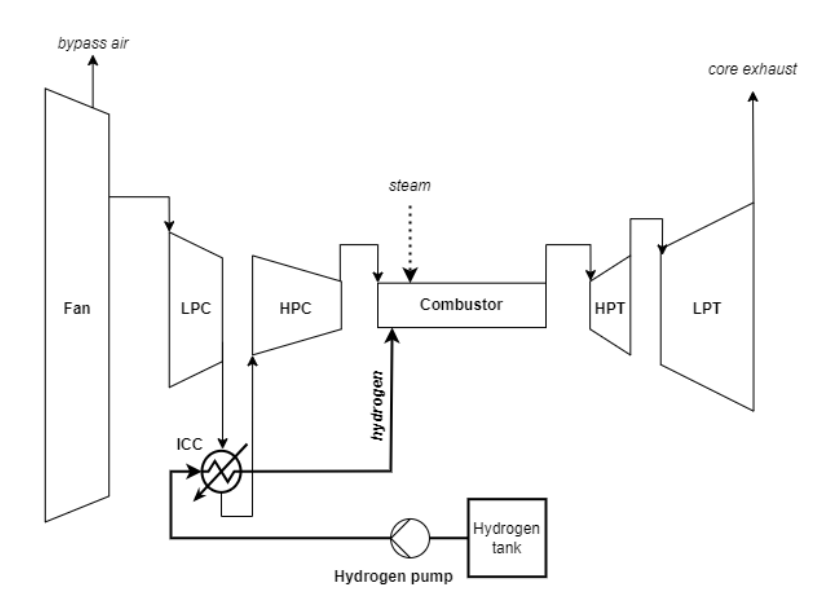


Figure 2.24: Compressor intercooling configuration

Brewer determines a reduction in SFC of 0.93%, half of the compressor precooling configuration, with a 33% smaller reduction in engine weight and a 33% higher heat exchanger weight, leading to only a 0.57% overall reduction in DOC [61]. The TSEC reduction was found to be 4.6% by Görtz and Silberhorn[10], which is the highest out of the explored options and the only one out of the three that does not increase the energy consumption of the engine. The main reason for this is that intercooling reduces the outlet temperature of the compressor, allowing for a higher realisable OPR [10]. Compared to the EC and CCA concepts, the OPR for IC was around 19% higher. While weight estimates are not made, the IC heat exchanger parameter kA is used as a found to be more than twice as large as the EC and CCA concepts [10]. The reason for the differing results in the two studies is likely the significantly higher OPR of 63.5 (53.3 for the EC and CCA configurations) in Görtz and Silberhorn's study [10], compared to 25.3 for Brewer [61]. The cycle benefit of compressor intercooling increases with total pressure ratio [21] and considering the general trend of increasing OPR for turbofan engines [17], intercooling technology provides a greater performance benefit in modern engines.

Cooled cooling air

The *cooled cooling air* (CCA) configuration, shown in Figure 2.25, places the evaporator such that hydrogen is heated by and used to cool the turbine cooling air which is drawn from the latter stages of the high-pressure compressor. Brewer states as an advantage the belief that cooling the turbines with colder flow would reduce the required flow rate to be extracted from the compressor and the concept was identified as a promising concept for future challenges, as it would allow for higher TIT and thus OPR [61].

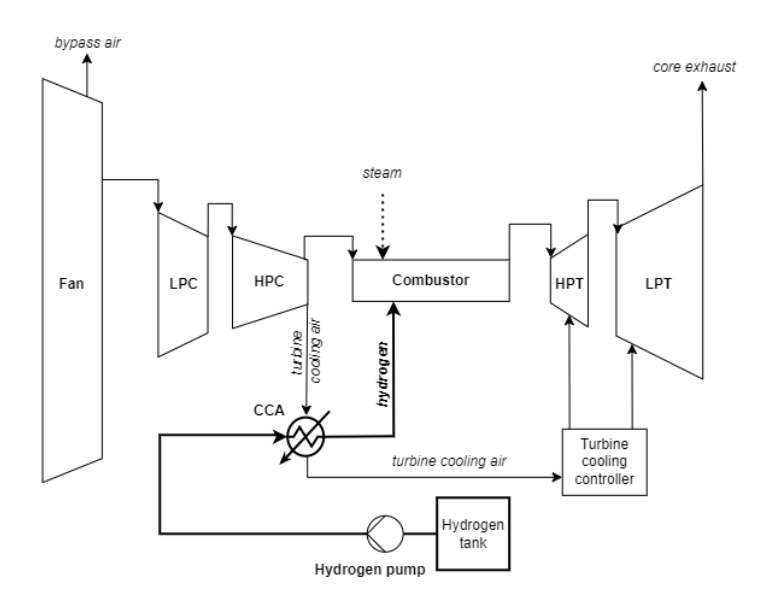


Figure 2.25: Cooled cooling air configuration

Brewer found a 0.53% reduction in SFC, a smaller engine weight reduction than the PC and IC configurations and a considerably smaller weight increase due to the heat exchanger, leading to an overall DOC reduction of 0.41%. However, it was noted that the baseline engine cooling requirement was low and as such the cycle benefit was small [61]. Görtz and Silberhorn found a 1.7% reduction in TSEC, the poorest of the investigated concepts, while also reporting the smallest heat exchanger size for this configuration [10].

Exhaust cooling

The next concept, shown in Figure 2.26, is regenerative heating of the hydrogen by the hot exhaust flow, named the *exhaust cooling* (EC) configuration [10]. While there is a decrease in engine effectiveness due to heat being removed from the exhaust, the work output increase of the core engine due to the heating of fuel makes up for this penalty.

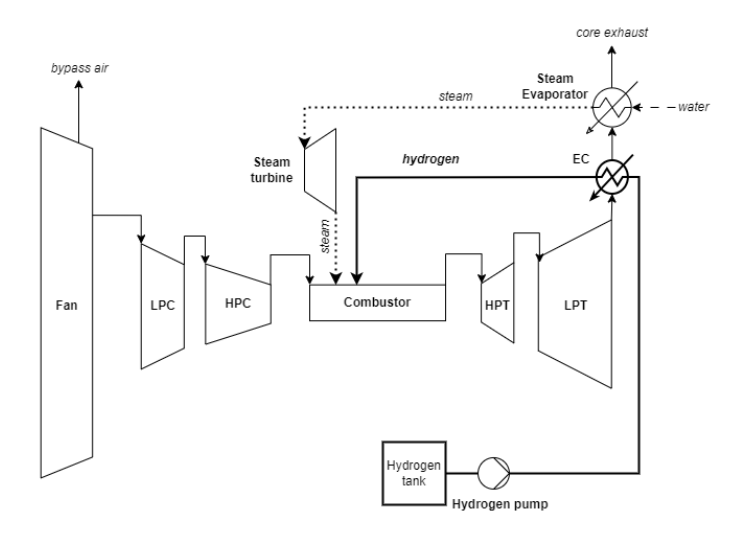


Figure 2.26: Exhaust (regenerative) cooling configuration

Brewer finds a 4.31% reduction in SFC, but in comparison to the previous three configurations with an increase in engine weight [61]. With the highest heat exchanger weight increase, the total DOC reduction is 2.9%, the highest among the concepts along with the expander cycle [61]. Görtz and Silberhorn find a 2.9% decrease in TSEC and a heat exchanger size slightly higher than the CCA configuration, ranking the EC concept in the middle of the three investigated [10].

Hydrogen expander cycle

A concept outlined by Brewer was to add a hydrogen turbine to the EC configuration in order to provide the accessory power required by the aircraft, illustrated in Figure 2.27. This would eliminate the accessory power load on the core engine and remove the gearbox weight penalty, but the latter would likely be offset by the addition of a turbine [61].

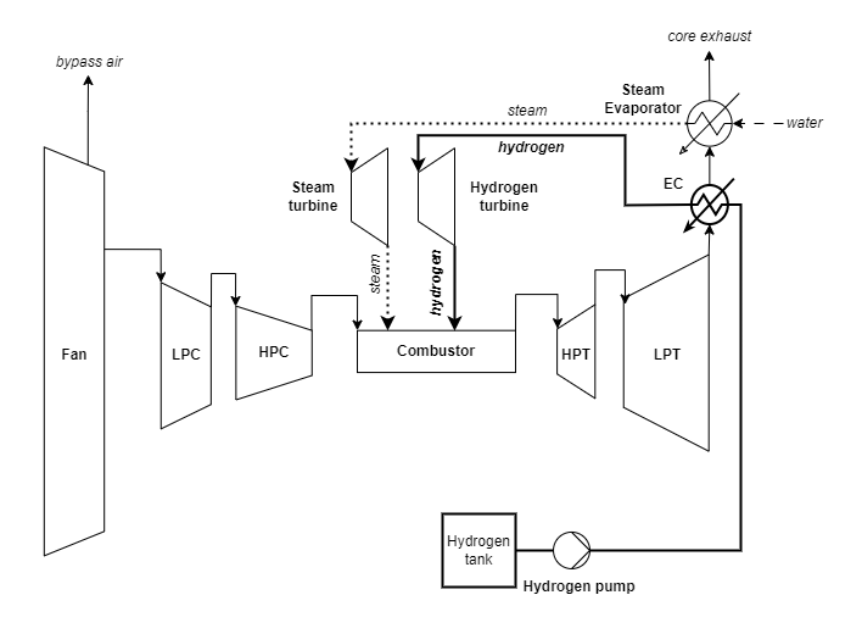


Figure 2.27: Hydrogen expander cycle configuration

As the concept is based on the EC configuration, the same SFC reduction and heat exchanger weight penalty were reported. With the weight penalties offsetting each other, the net result is the same reduction in DOC. The concept was not recommended for further study for the reason that the same benefits were achieved by EC, a configuration with lower complexity [61].

Alternative configurations

The above list and figures are not the comprehensive summary of possible configurations. Multiple alternative heat sources exist, and concepts may be combined. Some other options are outlined below.

- Oil cooling: The engine oil must be cooled and hydrogen is a good choice for this given its efficacy as a heat sink, but this will not be sufficient to heat the hydrogen to combustor injection temperature. An oil-to-hydrogen heat exchanger is recommended to be used in conjunction with additional heat exchangers in [61].
- Cabin air cooling: The bleed air taken from the compressor for the cabin needs to be cooled, and can be used to also heat the hydrogen. Similarly, this is recommended to be used in conjunction with additional heat exchangers in [61]. Currently in modern engines, the cabin air is generally cooled by the engine bypass air.
- Ram air: Ram air is readily available, but its use to heat hydrogen does not provide a cycle benefit. A benefit is that leakage of hydrogen to the ram air flow does not pose a significant danger to the engine, as it may do for the flows considered in the other heat exchanger placements.
- Bypass air: Bypass air is also readily available and leakage of hydrogen to the flow does not pose a significant issue. The bypass air will be warmer than ram air, allowing for higher total heat energy transferred.
- Combustor cooling: Given the high temperatures of the combustor, direct cooling of the combustor walls can be seen as an option. The main problem is hydrogen embrittlement: the diffusion of hydrogen into the metal structure leads to a loss of ductility and load bearing capability, resulting in fracture. Furthermore, there is no cycle benefit.

Given the cryogenic storage conditions of liquid hydrogen, the first heat exchanger hydrogen passes through has a high risk of icing and as such the second flow should not be too humid or cold. If engine exhaust or air, both humid, are to be used in the hydrogen evaporator, the hydrogen may need to be pre-heated or alternatively a hydrogen re-circulation loop implemented to bring hydrogen to a higher temperature prior to entering the heat exchanger.

2.4.6. Hydrogen tank and feed system

Hydrogen has an extremely low volumetric density. Even at cryogenic conditions, the volume-specific energy of liquid hydrogen is four times higher than kerosene, highlighting the importance of hydrogen tank design. The extremely low storage temperature combined with hydrogen's small molecular size further impose strong requirements. A metric to quantify the storage efficiency of a tank is the *gravimetric efficiency* η_{tank} , defined as:

$$\eta_{tank} = \frac{W_{H_2}}{W_{H_2} + W_{tank}} \tag{2.32}$$

The gravimetric efficiency represents the weight penalty incurred by a given hydrogen storage solution, and this has impacts on overall aircraft design. For low gravimetric efficiencies, the performance of hydrogen aircraft worsens with respect to kerosene aircraft the longer the range, whereas for high gravimetric efficiencies the opposite trend is observed [68]. Hence, aircraft configuration and tank design are interconnected and affect the potential for benefit from using hydrogen over kerosene.

In Figure 2.28, some existing and proposed hydrogen tanks are plotted. Liquid hydrogen has a higher gravimetric efficiency and storage density at the cost of increased complexity in storage solutions. Notably, the performance of some tanks such as the Space Shuttle's is inflated by the fact that fuel was used in a much shorter time span, and the tank was larger and single use, requiring less insulation and reducing concern for boil-off. The assumed Clean Sky 2 and ICCT tanks show a more realistic range of tank characteristics for aircraft.

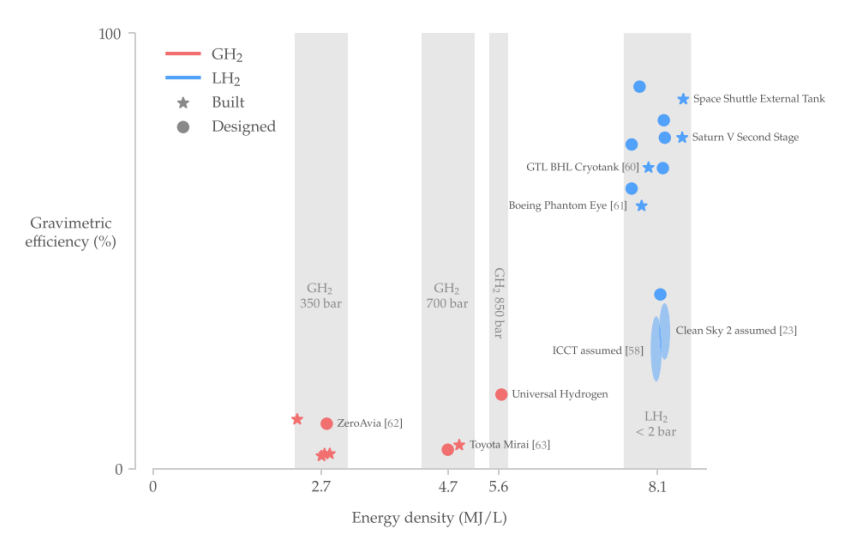


Figure 2.28: Gravimetric efficiencies of proposed and existing hydrogen tanks [69]

As discussed before, cryogenic liquid storage of hydrogen is identified as the most feasible solution for aicraft applications. This increases complexity and brings new challenges in the form of insulation, shape choice and pressure control.

Cryogenic tanks benefit from a low surface area-to-volume ratio as this reduces the boil-off rate. However, this does not favour aircraft configuration, increasing drag and reducing the lift-to-drag ratio. In Figure 2.29, these effects are highlighted. The surface area-to-volume ratio decreases with increasing aircraft volume, which reduces heat leak. For the same overall volume, tanks closer in shape to a sphere have a lower surface area-to-volume ratio. Spherical tanks thus have less boil-off, but lead to a higher fuselage diameter and a drag penalty, which is why cylindrical tanks are preferred in aircraft.

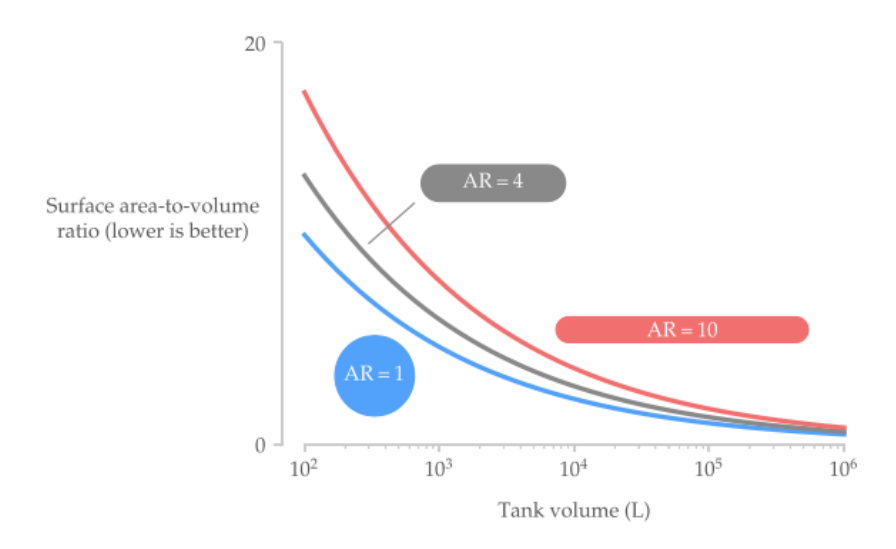


Figure 2.29: Surface area-to-volume ratio and tank volume [69]. AR is the length-to-diameter ratio

Liquid hydrogen is stored at pressures on the order of a few atmospheres [69] to avoid the risk of air leaking into the tanks and freezing. This means they must be designed to carry these loads efficiently, but the relatively low pressure means some design alteration is possible to conform tanks to the airframe, improving aerodynamic integration while incurring a weight penalty.

In order to minimise boil-off of hydrogen, the tank must be insulated. Most commonly considered passive types are foam insulation and vacuum-based insulation or a combination of these [69]. Active refrigeration has been considered but is more complex, with the added weight greatly surpassing the weight of fuel saved [61]. Foam insulation is prone to cracking or delaminating [69], being sensitive to cyclical variations in temperature, which makes it less optimal for aircraft use. However, the higher achievable gravimetric efficiency means it is still suggested by Brewer[61]. Vacuum insulation has much lower heat leak and higher reliability [69], while the tank weight increases due to requiring two walls to support the vacuum. Furthermore, a venting system should be designed to account for the risk of the vacuum failing, causing a dramatic increase in boil-off rates.

Hydrogen boil-off can not be completely negated, but is often limited to a rate of 0.1% hydrogen weight per hour of flight [69]. For a short-to-mid-range hydrogen civil aircraft, a total mission boil-off of around 2% of fuel has been found [70].

The choice of tank material is driven by strength-to-weight ratio, strength maintenance at cryogenic conditions and low cost. Aluminium alloys and composites are most commonly proposed for cryogenic liquid hydrogen tanks [69]. For composites, material challenges are cooling-induced stresses, cracking and potentially hydrogen permeability. For metals, embrittlement is a concern but aluminium has a low susceptibility as well as high strength and low cost, making it an attractive option overall.

2.4.7. Impacts on aircraft design

The chemical properties of hydrogen also have an impact on the aircraft level, which is summarised shortly below. Some benefits of choosing hydrogen over kerosene are:

- Lower fuel mass: The higher mass-specific energy content of hydrogen means that for the same energy consumption, fuel mass will be reduced, reducing the takeoff weight of the aircraft. However, this must be considered together with the mass of tanks and auxiliary hydrogen components, as well as the increased energy consumption of hydrogen aircraft due to the low volumetric energy of hydrogen.
- **Smaller wing:** If a lower takeoff mass is achieved, the wing size can be reduced, further reducing drag and takeoff weight. However, this must be considered together with the drag increase imposed by configuration changes due to the low volumetric energy of hydrogen.
- Possibly reduced maintenance cost: There is speculation that hydrogen turbomachinery might have a longer service life and require less maintenance than kerosene components due to the cleaner combustion of hydrogen [69].

Some of the negative aircraft design impacts of hydrogen as a fuel are:

- Higher tank volume: The low volume-specific energy of hydrogen imposes a volume penalty.
 Furthermore, for cryogenic tanks, shapes with low surface area-to-volume ratios are favoured.
 Hydrogen tanks are most commonly placed in the fuselage rather than the wings [69], meaning an increase in aircraft volume and/or reduction in passenger/cargo capacity.
- Lower L/D: The penalty of increased tank volume leads to higher drag and a lower lift-to-drag ratio.
- **No wing load alleviation:** As the wing no longer houses fuel tanks and fuel, it does not benefit from load alleviation, probably resulting in a heavier design [69].
- Configuration complexity: The shape and placement of the hydrogen tank(s) needs to be considered with regards to aircraft stability, drag, weight and safety. Conventional tube-and-wing-configurations would need to be extended in length or diameter or alternative configurations considered, both of which add development cost.
- Cost increase: The acquisition cost of hydrogen aicraft will be higher due to the hydrogen storage tank and system integration. Maintenance cost may also be higher due to the complexity of hydrogen operations.
- Complex ground operations: The fuel supply and maintenance of a hydrogen aircraft will impose new safety and operational concerns.

The net effect of these effects is disputed, as research into hydrogen aircraft configurations has shown varying changes in energy consumption, drag and takeoff weight. As an example, Verstraete [71] predicts a takeoff weight reduction of 25% and a 15% lower energy consumption for a long-range hydrogen-fuelled aircraft compared to kerosene, while Project Cryoplane found a takeoff weight reduction of only 14.8% and an energy consumption increase of 9% [52]. The aircraft range must also be considered, with the added complexity and penalty of hydrogen storage having a greater impact in short-range aircraft [69].

2.4.8. Safety

Hydrogen poses both advantages and disadvantages from a safety point of view. While hydrogen flames burn hotter, hydrogen rapidly vaporises and dissipates in air, reducing fire hazard from spills. Unlike kerosene, hydrogen does not pool and as such does not result in long-lasting fires on the ground.

Material and handling-related safety concerns include the ability of hydrogen to permeate and embrittle metals. Sensors, material monitoring techniques and maintenance procedures must be developed or adapted for the use of cryogenic hydrogen. The small molecular size of hydrogen means it is prone to leaks and its large flammability range means these leaks pose a fire risk both to the engine and aircraft as well as passengers and ground personnel. Ignition sources near hydrogen must be reduced as much as possible to prevent fires.

Another aspect of safety is perceived safety, which is important in the case of civil aircraft. The memory of the Hindenburg disaster [48] means that many associate hydrogen with a significant fire hazard and reluctance to fly on a hydrogen aircraft may be higher. The location of the tank, as well as operational procedures, must be developed in a way that passenger comfort and perceived security are high.

2.4.9. Infrastructure

In order for hydrogen-fuelled aircraft to enter operational service, the supporting infrastructure must be developed. Hydrogen aircraft are limited to travel between airports that are able to supply hydrogen and provide operational support for hydrogen systems. There are various options for airports, from full production and storage of hydrogen on-site to simply fuelling liquid hydrogen which is delivered from off-site. In any case, a suitable network of available liquid hydrogen supply must be developed, requiring initial development investment as well as possibly increasing operational costs of the airport.

2.5. The hydrogen-fuelled steam injection cycle

Aviation trends indicate a drive towards lower emissions, lower fuel consumption and higher cycle efficiency. The modern turbofan engine will continue to improve in these aspects, but disruptive technologies can provide accelerated improvement, albeit at increased complexity and cost.

The case for the steam injection cycle, is presented in Section 2.2, highlighting that steam injection and water recovery in a turbofan engine can be expected to lead to a large reduction in NO_X emissions as well as decreased overall fuel consumption. While steam injection is a proven technology in land-based applications, its use on aircraft engines is limited to research such as the MTU WET Cycle [15],[16] and Pratt & Whitney HySIITE [11] projects. Achieving sufficient water recovery from the exhaust is not trivial and aircraft applications pose demanding compactness and weight requirements on the system, leading to a high degree of development complexity and uncertainty.

The use of liquid hydrogen as an alternative to kerosene is presented in Section 2.4. Hydrogen promises a superior mass-specific energy, theoretically complete reduction of CO_2 emissions and desirable combustion characteristics allowing for a wider combustor operation range. This is at the expense of a lower density, possibly higher NO_X emissions, added engine complexity, as well as additional safety and infrastructure concerns. Hydrogen-powered aircraft engines have been flight-tested and there are ongoing efforts by large players such as Airbus to bring a hydrogen aircraft to the civil market [5], but this prospect is not for the near future.

With two technologies promising increased performance, efficiency and emission reduction, their combination can provide a greater benefit than either by itself. The use of steam injection and water recovery with a hydrogen-fuelled gas turbines shows a promising synergy which is summarised below and has been investigated in the Pratt & Whitney HySIITE [11] project as well as the Hydrogen-WET study carried out by MTU [16].

Advantages of the Hydrogen-fuelled steam injection cycle

- The exhaust of a hydrogen-burning gas turbine is significantly more humid, making condensation of water out of the exhaust gases easier. This would lead to a higher likelihood of condensing enough water to reach self-sufficiency in the steam injection loop.
- Liquid hydrogen is a good heat sink due to its high heat capacity and low temperature. This can be utilised to support condensation of water out of the exhaust.
- The lower density of hydrogen increases the energy consumption of hydrogen aircraft compared to kerosene. Steam injection reduces the fuel consumption, helping offset this difference.
- Hydrogen can have high NO_X emissions due to its high adiabatic flame temperature. Steam injection reduces NO_X emissions, offsetting this effect.

The challenges of integrating steam injection into a hydrogen-fuelled engine stem mostly from challenges specific to hydrogen as a fuel but some specific concerns exist with regards to steam injection. the importance of condenser design is evident, as is the high complexity of this cycle.

Challenges of the Hydrogen-fuelled steam injection cycle

- The higher adiabatic flame temperature of hydrogen leads to a higher exhaust temperature, which can make condensing sufficient water difficult.
- Combining two complex technologies leads to a high level of risk and increased complexity for the overall engine and aircraft.
- Hydrogen combustors are at a lower technological readiness level than conventional kerosene combustors. The combustor, as well as hydrogen storage and supply systems, must be developed, increasing development time and cost.
- Hydrogen heat exchangers have a high risk of icing and embrittlement, so further heat exchangers and/or a hydrogen recirculation loop must be implemented, increasing complexity.

Both of the presented technologies are highly complex and novel for application in aircraft. Investigating both at once provides an added level of uncertainty in the interaction of the two technologies, as well as likely increasing complexity significantly. However, the potential benefits of combining the two, especially easier condensation of water out of the exhaust for a hydrogen engine, show the cycle as an attractive option to improve engine fuel consumption and reduce emissions.

2.6. Numerical Propulsion System Simulation (NPSS)

The modelling section of the thesis will be completed using *Numerical Propulsion System Simulation*, abbreviated as NPSS. NPSS is a component-based object-oriented engine cycle simulator developed by NASA's Glenn Research Center in conjunction with the U.S. aeropropulsion industry and the Department of Defense which is designed to perform cycle design, steady-state and transient off-design performance prediction and test data matching, among many other cycle simulation tasks [13].

The choice of software is motivated by ease of access, as well as the technological capabilities and industry importance of NPSS. The software is in use at GKN Aerospace Sweden, where the thesis work will be carried out, and as such there is ready access to the program and expertise in its usage. Furthermore, previously developed full models and element models can be used to support the modelling work. NPSS allows for realistic modelling of engines with an advanced system architecture that supports implementing models at various levels of dimensional fidelity. This allows for the use of existing known element models and focusing development resources to the components critical for the steam injection cycle which have not previously been modelled. Finally, NPSS is in use at many large aerospace companies, certifying its value in the industry.

2.6.1. Input files

An engine model in NPSS is defined completely in one or multiple input files, requiring no alteration of the source code. The input syntax is a full-featured programming language which is modeled after *C++*. Input files are text files, created and modified using a text editor, and contain commands to achieve the following:

- · Identify the thermodynamic gas-properties package to use.
- Define model components and their linkages, the required calculations and desired outputs.
- · Initiate the solution of specified cases.

2.6.2. Previous model development

It is important to highlight the previous work of A. Feim [14] on the simulation of a kerosene-powered steam injecting and water recovering turbofan engine. The work was completed at GKN Aerospace prior to the start of this project and comprised the development of a cycle model in NPSS, including the development of custom elements for the evaporator and condenser. Although the model was configured for a kerosene-fuelled and larger engine than the one considered in this work, the model was able to be used as a baseline, with modifications and improvements made as required. The custom evaporator and condenser elements were also used successfully for the general cycle simulation. The resulting reduction in modelling work allowed for further refinement of the model and notably more time for the investigation of cycle parameters, studying water sufficiency, and even simulating off-design conditions. This would not have been achievable during the project duration were it not for the work of A. Feim.

Problem definition

In order to guide the project, an objective for the thesis work is presented together with defining the research questions to be answered. Furthermore, the scope is discussed to bound the research and set realistic expectations. Finally, the baseline engine to be modelled is introduced and its desired performance stated.

3.1. Research objective

The research objective is outlined as follows:

The research objective is to determine the on-design and off-design performance of a hydrogen-fuelled engine with steam injection and water recovery for a short-to-medium range aircraft.

3.2. Research questions

With the research objective defined, two research questions are developed and presented below.

- 1. How can we model a hydrogen-fuelled engine with steam injection and water recovery?
 - (a) What is an efficient architecture for the engine?
 - (b) How can the engine be accurately modelled in a cycle evaluation tool?
- 2. What is the on-design and off-design performance of the engine?
 - (a) At which operating points can the engine be self-sufficient on water?
 - (b) What is the change in SFC of the engine compared to a hydrogen-fuelled engine without steam injection?

3.3. Thesis project scope

The development of a model and simulating both on- and off-design points for a novel engine cycle is a complex task with a high possible level of detail. The objective is to model the steam injection and water recovery cycle at large in order to evaluate its performance. In order to produce sufficient results for discussion in the time allocated to this work, the problem is bounded to a realisable scope by simplifying some aspects and neglecting others. These are outlined below.

- Detailed geometric design of the engine components will not be completed. This includes the overall volume of the engine, the standard turbofan components as well as the added heat exchangers, water pump and steam turbine. Thus, the final performance must be considered together with an understanding that the weight and volume penalty from added components is neglected.
- The influence of the use of hydrogen on the overall design of the aircraft is not considered. This
 includes the design and placement of the hydrogen tank and the detailed hydrogen supply system.
 This allows for the evaluation of the cycle's performance while recognising that the success of a
 hydrogen-fuelled aircraft requires considerable redesign of the fuel storage and supply systems.

- Emissions are not evaluated. While the steam injection cycle and the use of hydrogen are both of interest due to their reduction of engine emissions, the estimation of these is a complex task requiring further study. Quantitative estimation of the effects in Chapter 2 is deemed sufficient to motivate the investigation of this engine.
- Verification and validation of this engine are difficult due to the lack of present engines employing both steam injection and hydrogen as a fuel. As such, verification is limited to the verification of component models in NPSS, and some preliminary verification of the model is done by comparing values such as WAR with other studies modelling the steam injection cycle.

3.4. Engine operating point performance

In order to simulate a gas turbine cycle, the engine to be studied needs to be introduced. Referring to the research objective in Section 3.1, a short-to-medium range aircraft is chosen for investigation. There are no hydrogen-fuelled civil aircraft engines available on the market or in common use, and furthermore none employ hydrogen fuel as well as steam injection.

To make an estimate of the thrust and design conditions, sizing of the aircraft is based on the H2JET Project aircraft [72] designated HJ160VAC, a hydrogen powered aircraft with a capacity of 160 passengers. However, in this study, a slightly larger aircraft will be considered, with the typical seating capacity chosen as 176 seats per cabin, equal to the average typical seating capacity of an A320 [73]. The aircraft is also sized for a larger 2000-3000 nm range. In an internal study, the ratio of maximum take-off weight (MTOW) between the baseline of this project and the H2JET aircraft was found to be 1.4, from which a scaling factor of 40% was applied to the thrust of the H2JET aircraft.

Three operating points are defined: take-off or T/O, top of climb or TOC, and cruise, with the latter referring to the aircraft's performance at its weight at the midpoint of cruise for a typical mission. In Table 3.1, the altitude, flight speed and temperature deviation from the standard atmosphere ΔT_{ISA} are given for all points. The slightly higher velocities for the chosen baseline engine compared to the H2JET aircraft are due to the relative sizes of the aircraft.

Aircraft	Mission point	Altitude [ft]	Mach [-]	ΔT_{ISA} [K]	Net thrust [kN]
HJ160VAC	Take-off	0	0.25	15	98.71
HJ176VAC					138.194
HJ160VAC	Top of climb	35000	0.75	10	27.27
HJ176VAC			0.78		38.178
HJ160VAC	(Mid-)Cruise	35000	0.75	0	20.49
HJ176VAC			0.78		28.686

Table 3.1: Operating point conditions and thrust for the reference HJ160VAC aircraft and chosen HJ176VAC aircraft

4

Methods

After defining an objective and research question, the concrete methods to answer these must be defined. In this section, the general approach to modelling in NPSS is described in Section 4.1, followed by presenting the model setup specific to this thesis work in Section 4.2, covering the general cycle as well as individual components. In Section 4.3, the setup of the solver is explained, and in Section 4.4 the approach to simulating a baseline reference engine described. A number of engine parameters are chosen for detailed study and explained in Section 4.5. Finally, the development of a detailed heat exchanger model is outlined in Section 4.6, together with how it integrates into the overall model in Section 4.7. A short overview of verification and validation is given in Section 4.8.

4.1. Modelling in NPSS

Simulating an aircraft engine in NPSS requires setting up a model of that engine, configuring the solver and running a simulation. A brief general overview of this process is given in this section.

4.1.1. Model definition

A model in NPSS consists of various component *elements* which may feature *sockets* connected to *subelements*, *functions*, or *tables*, and *ports* connected by *links* to ports of other elements. A thermodynamic package must be chosen for completing calculations relating to the flow in the model.

Thermodynamic packages

Specifying the thermodynamic package is one of the first steps in an NPSS model and must be done before any elements are added. A standard NPSS release features the following packages:

- CEA: NASA chemical equilibrium code.
- Janaf: National Institute of Standards and Technology gas properties prepared by Honeywell.
- GasTbl: Pratt & Whitney package based on Therm, with added humidity calculations and some chemical equilibrium capabilities.
- AllFuel: General Electric package containing gas and fuel properties.
- FPT: Used to define NPSS tables and/or functions that describe the thermodynamic properties of the fluid.

Furthermore, REFPROP is not included in NPSS, but there is built in functionality to get properties from REFPROP if the user has the REFPROP code in the working directory.

Multiple thermodynamics packages can be used in a single model, but care must be taken as the enthalpy and entropy bases for packages can vary. In this work, the $\rm Janaf$ and $\rm FPT$ thermodynamic packages will be used. Standard engine models developed at GKN are set up with the $\rm Janaf$ package, which is sufficient for most stations. However, in order to model liquid water and steam, the $\rm FPT$ package is used for relevant flow stations.

Elements

An NPSS model is constructed from linked elements. These are a class of NPSS objects which are used to model components in an engine cycle, such as compressors, combustors, turbines and nozzles. Their definition is accomplished in the following order:

- 1. Keyword Element (optional)
- 2. The specific element type
- 3. The object name
- 4. (Optional) block of statements executed when the object is instantiated

Subelements are children of other elements or subelements and are used to perform certain major calculations on behalf of the parent: an example of a subelement could be compressor maps. Their definition follows a similar approach:

- 1. Keyword Subelement (optional)
- 2. The specific subelement type
- 3. The object name
- 4. (Optional) block of statements executed when the object is instantiated

Subelements are plugged into elements by a *socket*, which can also accept functions or tables, but accept only one object. Elements and subelements may have multiple sockets, and not all need to be filled.

Ports and linkages

The interactions between elements in a model are accomplished by links through *ports*. A port signals a collection point for fluid properties, fuel properties and shaft properties to be shared with another element. For data ports, a single value is shared and for file ports, a file or more are shared. The five kinds of ports in NPSS are:

- fluid
- fuel
- shaft
- data
- file

Generally, every port on an element is connected to a port on another element, providing a mutual boundary condition. Most elements create the ports they require, but for some it is allowed or necessary to create ports. These are defined in a similar way as elements.

Once ports have been created, they can be connected using a linking command. This command also causes a station to be created, for which a given name is assigned. Ports must be of the same type to be connected. For fluid, fuel and shaft ports, every port must be linked to one and only one other port. For data ports, a single transferred value is defined, and no error is generated if data ports are not linked. Data output ports may be linked to more than one data input port. Data input ports, however, are only allowed to be linked to a single data output port. File ports are used to transfer files from one element to another and follow the same rules, with output ports allowed to be linked to more than one input, unlike input ports.

Assemblies

A collection of connected elements can be grouped as an *assembly*, which is then treated by the rest of the model as a single element. Assemblies may have their own dedicated solvers, and can contain further assemblies. The entire model is a *top-level assembly*, with any other assemblies being contained within it.

4.1.2. The solver

The solver's function is to drive a defined model to a *converged* state by iteratively solving the set of interdependent equations that comprise the system. A high degree of flexibility and user control is provided by NPSS, but may not be necessary for all cases. The solver controls provide the ability to direct the solution by defining independent variables, dependent variables, and solver constraints.

4.1.3. Problem setup

The problem setup defines the solution goals and constraints and consists of gathering the required inputs for a valid solution, defining outputs and the solution cases to be run. With the solver and problem setup complete, a simulation can be run, in which the solver attempts to converge to a solution satisfying the input targets and constraints.

4.1.4. Output files

After a converged solution is reached, there are a variety of ways to view the output data. Data can be sent directly to the screen or to a designated output file and is identified for output in the problem setup. Outputted data can also easily be imported into external tools for data processing and visualisation.

4.2. Model setup

The modelling objective is both to improve the existing model for steam-injected gas turbine cycles as well as adapt it for use with hydrogen as a fuel. This is done by starting with a model previously developed at GKN for a steam injection and water recovery cycle fuelled by kerosene [14]. Certain element models can be altered and adapted for the hydrogen system, and at the full engine level existing linkages can be utilised. Building upon previous work decreases the development time of many simpler components, providing more time for the development of more complex models, as well as improving the accuracy of existing ones.

A simplified modelling flow diagram is presented in Figure 4.1.

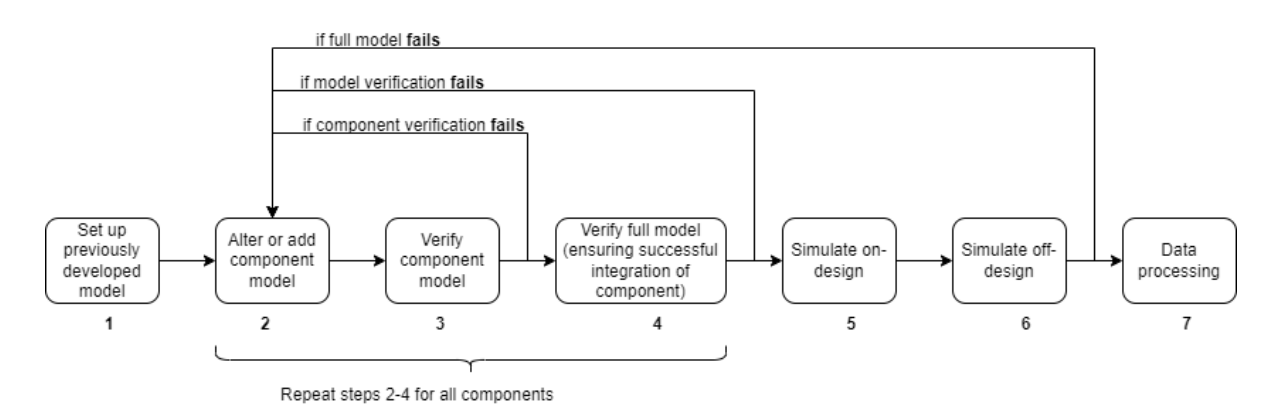


Figure 4.1: Modelling approach flow diagram

The model is to be altered component by component, allowing for parallel verification of both the component and the full model. Compared to developing component models individually and then integrating them, this provides more frequent checks for the compatibility of components when linked, as well as allowing preliminary simulation of (sections of) the full engine model. The development is presumed to happen at the on-design condition, but after running the model at off-design, components may need to be altered once more to ensure a converged solution for off-design points.

Once the model is developed and functional, the engine model can be run at various operating points to produce the desired output data. This data is output and processed externally to NPSS, with the final objective being tables, graphs and any other presentation of the results. A sensitivity analysis will also be completed to determine the effect of input parameters on the output of the model. Furthermore, verification will happen alongside the development work and some partial validation will be completed after obtaining results, both of which are discussed below.

4.2.1. Cycle model overview

An overview of the steam injection and water recovery cycle is given in Figure 4.2. While a general cycle diagram was presented in Section 2.2, the detailed setup of the model, its components and configuration are now presented. The critical changes from a standard turbofan model are discussed below.

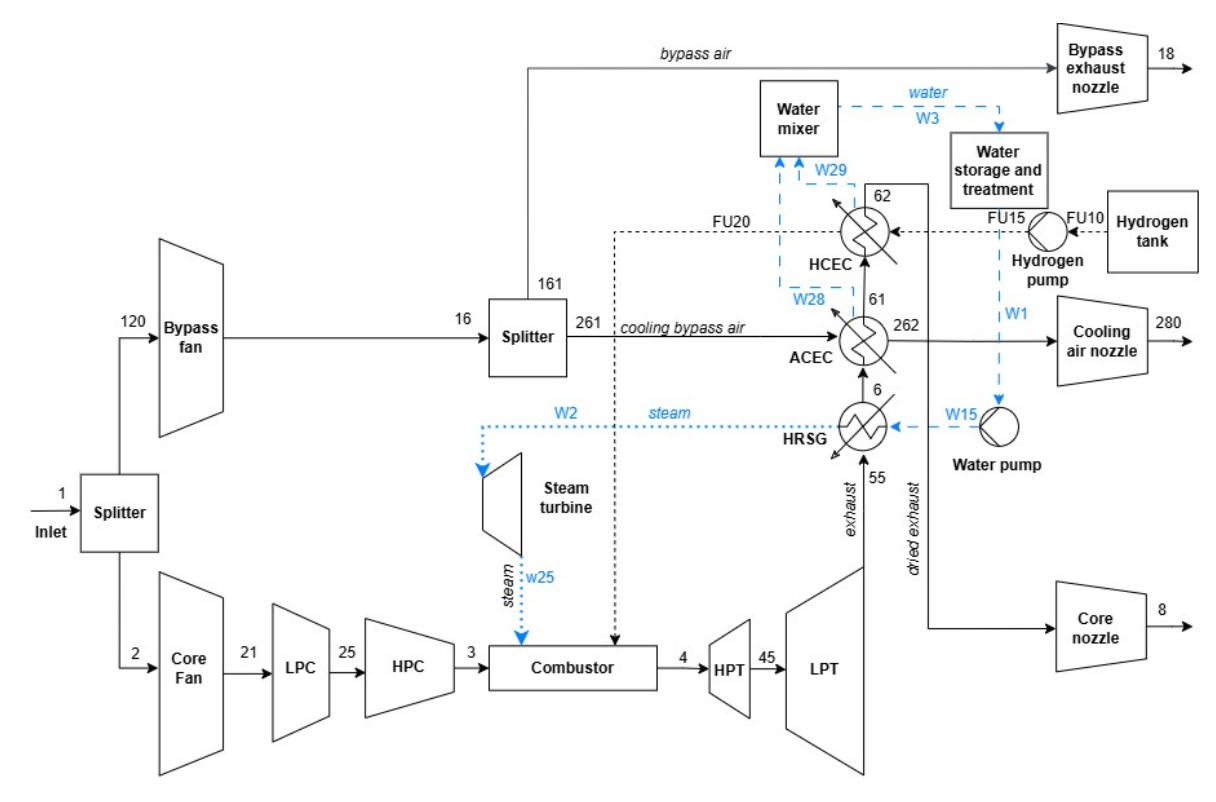


Figure 4.2: Overview of the cycle model with station numbering

Flow inlet and outlets

A splitter is included in the model to split the inlet total mass flow between the core and bypass flow streams. The core of the engine is largely unaltered from a standard turbofan model, except for a series of heat exchangers added to the core exhaust path between the LPT and primary core nozzle. For the bypass stream, a secondary splitter is introduced in order to separate a section of bypass mass flow for cooling in the air-cooled exhaust condener. This cooling flow is expanded through a tertiary cooling air nozzle while the undisturbed bypass flow is expanded through the secondary bypass nozzle. The nozzles are not mixed as this was determined in preliminary studies and previous work [14] to result in frequent instabilities and convergence errors in the model. Mixing is common in military applications as it reduces noise and the thermal signature of an engine, while for civil applications noise improvement but more importantly a gain in specific thrust are reasons to consider mixing. However, thorough mixing is not easy to achieve without sacrificing compactness or pressure loss. Furthermore, it is unclear whether a performance benefit might be gained from mixing the flows, as this has not been investigated in detail for the steam injection and water recovery cycle.

Heat exchangers

In order to recover water from the exhaust and produce steam for injection into the combustor, an evaporator and condenser are required. The *heat recovery steam generator* HRSG between stations 55 and 6 is the first heat exchanger in the path of the core exhaust, where energy is extracted from the core flow in order to evaporate an incoming stream of water for steam injection. After the HRSG, the exhaust flow passes through two exhaust condensers: the *air-cooled exhaust condenser* ACEC and the *hydrogen-cooled exhaust condenser* HCEC. In the ACEC between stations 6 and 51, a flow of cool bypass air split from the total bypass flow by a splitter at station 16 exchanges heat with the exhaust,

resulting in cooling and condensation of the water contained in the humid exhaust. In the HCEC, further cooling is achieved by the even cooler hydrogen flow, providing added condensation.

Water recovery and steam injection

The separation of condensed water is not modelled in detail, but the condensed flows from the ACEC and HCEC are mixed in a mixer before station W3, after which the total condensed water flow is treated and stored, before being pumped back to the HRSG. As the water passes the HRSG between W15 and W2, it is evaporated and expanded through a steam turbine before injection into the combustor, providing some additional shaft power.

4.2.2. Modelling heat exchangers

Modelling the HRSG, ACEC and HCEC is a critical step in simulating the steam injection and water recovery cycle. Custom elements are developed in NPSS for this purpose, with their calculation logic explained in the following section.

Heat exchanger effectiveness

The effectiveness of the heat exchangers is defined in relation to the maximum possible rate of heat transfer.

$$\varepsilon = \frac{\dot{Q}}{\min(|\dot{Q}_{1,max}|,|\dot{Q}_{2,max}|)} \tag{4.1}$$

In Equation 4.1, \dot{Q} refers to the total rate of heat transfer over the heat exchanger, while $\dot{Q}_{1,max}$ and $\dot{Q}_{2,max}$ refer to the maximum possible heat transfer rates in streams 1 and 2, respectively. For stream 1, this is reached if the fluid outlet reaches the inlet temperature of stream 2, and conversely for stream 2 if its outlet reaches the inlet temperature of stream 1. The rate of heat transfer is determined by setting the outlet enthalpy according to the outlet pressure and opposite stream's inlet temperature, as shown in Equation 4.2 and Equation 4.3.

$$\dot{Q}_{1,max} = \dot{m}_1(h_{1,out,max} - h_{1,in}) \quad h_{1,out,max} = h(T_{2,in}, P_{1,out})$$
 (4.2)

$$\dot{Q}_{2,max} = \dot{m}_2(h_{2,out,max} - h_{2,in}) \quad h_{2,out,max} = h(T_{1,in}, P_{2,out})$$
 (4.3)

4.2.3. Heat exchanger elements

The cycle model includes three heat exchangers: an evaporator or HRSG and two condensers, the ACEC and the HCEC. In order to model these, Evaporator and Condenser elements are developed in NPSS by [14] and further expanded upon in this work. Both elements are configured to support four calculation methods: specified rate of heat transfer, specified outlet temperature, specified effectiveness or specified coefficient of heat transfer. This allows for various methods to estimate the performance of, or size, the heat exchangers at different points during design studies, verification and off-design.

Specified rate of heat transfer

If a rate of heat transfer Q_{in} is specified, the outlet conditions are set by determining the outlet enthalpy from the inlet enthalpy and \dot{Q}_{in} . The pressure at the outlet is set by the specified percentage pressure drop.

$$\dot{Q} = \dot{Q}_{in} \tag{4.4}$$

$$h_{1,out} = h_{1,in} - \dot{Q}/\dot{m}_1 \tag{4.5}$$

$$h_{2,out} = h_{2,in} + \dot{Q}/\dot{m}_2$$
 (4.6)

$$P_{1.out} = (1 - \Delta p_1) P_{1.in} \tag{4.7}$$

$$P_{2,out} = (1 - \Delta p_2) P_{2,in} \tag{4.8}$$

Knowing either the outlet temperature or enthalpy means that the other is also known. NPSS allows the user to set a flow station's enthalpy and pressure, from which the program internally calculates temperature, or a temperature and pressure can be set, from which the enthalpy is determined.

The specified heat transfer rate Q_{in} may not be physically possible in the heat exchanger, leading to an effectiveness greater than one. In order to prevent this, a conditional is inserted into the code to set the heat transfer instead to the maximum possible (corresponding to $\varepsilon=1$) and print out an error message to alert the user that the requested rate of heat transfer is not possible.

if
$$\dot{Q}_{in} > \min(|\dot{Q}_{1,max}|, |\dot{Q}_{2,max}|), \ \dot{Q} = \min(|\dot{Q}_{1,max}|, |\dot{Q}_{2,max}|)$$
 (4.9)

The effectiveness is estimated by Equation 2.8 and the NTU and heat transfer area are found as:

$$C_{rat} = \frac{C_{min}}{C_{max}} = \frac{\min((\dot{m}c_p)_1, (\dot{m}c_p)_2)}{\max((\dot{m}c_p)_1, (\dot{m}c_p)_2)}$$
(4.10)

$$NTU = rac{\ln rac{arepsilon-1}{Rarepsilon-1}}{C_{rat}-1}$$
 (4.11)

$$A_h U = NTU \cdot C_{min} \tag{4.12}$$

The product of the total heat transfer area and heat transfer coefficient $A_h U$ is also determined. The overall heat transfer coefficient needs to be estimated to determine the heat exchanger area, but this is difficult due to the varying heat transfer coefficients of fluids along the heat exchanger, especially in the condensing and evaporating streams. Total heat transfer area is thus not determined in the cycle model and will instead be investigated further in Section 4.6.

Specified outlet temperature

If the outlet temperature $T_{2,out}$ of the evaporating or condensing stream is specified, its outlet conditions are set and the corresponding rate of heat transfer calculated as:

$$h_{2,out} = h(T_{out,2}, (1 - \Delta p_2)P_{in,2})$$
 (4.13)

$$\dot{Q} = \dot{m}_2 (h_{2,out} - h_{2,in}) \tag{4.14}$$

(4.15)

If this heat transfer is higher than the possible maximum across the heat exchanger, the conditional statement specified in Equation 4.9 is similarly applied.

The outlet conditions are set the same as for the first case as expressed in Equation 4.5-Equation 4.8, and the heat exchanger performance is similarly determined by Equation 4.10-Equation 4.12.

Specified effectiveness

If an effectiveness is specified, the heat transfer rate is calculated as:

$$\dot{Q} = \varepsilon \cdot \min(|\dot{Q}_{1,max}|, |\dot{Q}_{2,max}|) \tag{4.16}$$

Once again, the outlet conditions are set by Equations Equation 4.5-Equation 4.8, and the NTU and $A_h U$ found by Equations Equation 4.10-Equation 4.12.

Specified heat transfer coefficient and area

If the product A_hU is supplied as input, the solving procedure is iterative. A guess is made for the outlet enthalpy of the condensing or evaporating stream, and the total heat transfer rate found as:

$$h_{2,out,guess} = h(T_{2,out,guess}, (1 - \Delta p_2)P_{2,in})$$
 (4.17)

$$\dot{Q} = \dot{m}_2 (h_{2 \text{ out avess}} - h_{2 \text{ in}}) \tag{4.18}$$

An effectiveness based on the heat transfer rate ε_Q is calculated by Equation 2.8. Following this, effectiveness is also calculated based on NTU as:

$$C_{rat} = \frac{C_{min}}{C_{max}} = \frac{min((\dot{m}c_p)_1, (\dot{m}c_p)_2)}{\max((\dot{m}c_p)_1, (\dot{m}c_p)_2)}$$
(4.19)

$$NTU = A_h U / C_{min} (4.20)$$

$$\varepsilon_{NTU} = \frac{1 - e^{(C_{rat} - 1)NTU}}{1 - C_{rat}e^{(R-1)NTU}} \tag{4.21}$$

The outlet guess $h_{2,out,guess}$ is iterated inside the element until convergence at $\varepsilon_Q = \varepsilon_{NTU}$.

4.2.4. Estimating condensation

In the Condenser element, condensation phenomena are modelled in order to predict the amount of water condensed out of the exhaust stream. The methodology for this is explained in detail in [14]. The flow in the condenser is split into a *dry gas* flow \dot{m}^{dg} and a *water vapour* flow $\dot{m}^{w,vap}$.

$$\dot{m} = \dot{m}^{dg} + \dot{m}^{w,vap} \tag{4.22}$$

For a given outlet temperature of the condensing stream, the outlet saturation humidity WGR_{out}^{sat} is checked against the inlet absolute humidity WGR_{in} in order to determine whether condensation occurs.

if
$$WGR_{in} \leq WGR_{out}^{sat}$$
, no condensation (4.23)

if
$$WGR_{in} > WGR_{out}^{sat}$$
, condensation occurs (4.24)

(4.25)

If the amount of water vapour in the mixture is greater than what it can hold as vapour under the given conditions, condensation occurs. The outlet humidity is set to saturation humidity, with the difference in water vapour flow between inlet and outlet determining the liquid water flow \dot{m}^w condensed.

$$\dot{m}_{out}^{w,vap} = \dot{m}^{dg} W G R_{out}^{sat} \tag{4.26}$$

$$\dot{m}^w = \dot{m}_{in}^{w,vap} - \dot{m}_{out}^{w,vap} \tag{4.27}$$

4.2.5. Water separation

In order to remove the condensed water from the exhaust flow, a water separation mechanism is required. A possible water separator for a hydrogen-fueled steam injection engine is outlined in [74], with the component including an input, a primary water outlet, and an exit with a plurality of exit guide vanes to straighten the core gas flow that proceeds through the exit. These guide vanes include a secondary water outlet to remove condensed water from the flow.

Within the scope of this thesis, detailed design of a water separator is not completed. However, it may be difficult to ensure full separation of all condensed water from the exhaust mixture. As such, a water separation efficiency $\eta_{separation}$ is introduced:

$$\eta_{separation} = \frac{\dot{m}_{inj}}{\dot{m}_{cond}} \tag{4.28}$$

The separation efficiency is set at a fixed value of 95%. For the design case, this means the condenser is sized in order to account for this, resulting in a positive 5% margin on the total required condensed flow.

$$\dot{m}_{wat,req} = 1.05 \dot{m}_{inj}$$
 (4.29)

4.2.6. Hydrogen components

In order to configure the engine model for use with hydrogen, some alterations are made in the NPSS model. The Burner element is redeveloped with small changes in order to properly set the fuel composition and allow for integration with the rest of the components. Hydrogen is assumed to be supplied to the hydrogen pump at 40 K and 0.15 MPa. The hydrogen pump is configured using the $\operatorname{Dynamic}$ Pump element, which is included in NPSS.

4.2.7. Water/steam loop components

In order to model the water/steam loop, some further components are neccessary. A custom Water Mixer element is developed to provide a rudimentary model for water separation. This sums the condensed flows exiting from both the ACEC and HCEC, with the outflow temperature set as the massaverage of the two streams. A separation efficiency of 95% is added to the outflow of the mixer to account for non-ideal separation of condensed water in the exhaust condensers. Water storage is not modelled in detailm while the water pump is similarly to the hydrogen pump modelled with a $\operatorname{Dynamic}$ Pump element, the power of which is set as an off-take of the low-pressure shaft. The steam turbine is modelled as a standard turbine and placed also on the low-pressure shaft, providing extra power. However, if the quality at the end of the turbine is not above one or if the pressure before the turbine falls lower than the required overpressure at combustor entry, the turbine power is set to zero by the model in order to prevent power being drawn from instead of added to the low-pressure shaft.

4.2.8. Compressor scaling effects

As will further be discussed in Subsection 5.2.6, the steam injection and water recovery cycle favours a high overall pressure ratio and also features a comparatively smaller core flow to a conventional engine. The resulting reduction in size of core components can lead to size-dependent performance penalties which need to be considered when varying the overall pressure ratio of the engine in parameter studies. Furthermore, the blade height is important to be considered in evaluating the overall performance benefits of steam injection and water recovery technology.

A critical component is the high-pressure component, whose outlet is the smallest compressor stage in the engine. As such, the blade height is calculated at this critical location to determine the possible penalty imposed on component efficiency. The root-to-tip ratio r_r/r_t for the HPC is chosen as 0.925 [75] and the blade height assuming infinitely thin blades calculated in the model code as:

$$A_{annulus} = f(\dot{m}, T, P, M) \tag{4.30}$$

$$r_t = \sqrt{\frac{A_{annulus}}{\pi (1 - (r_r/r_t)^2)}} \tag{4.31}$$

$$h_{blade} = r_t (1 - r_r/r_t)$$
 (4.32)

In [75], a correlation is given for the efficiency correction depending on blade height. This correction is coded into the cycle model in order to account for changing final-stage blade height in the HPC. The resulting variation in blade height and polytropic efficiency are shown in Figure 4.3. As can be seen, for the range of OPR investigated the blade height does not drop below a value of 13 mm, after which a polytropic efficiency penalty is applied in [75]. However, it is noted that this choice of 13 mm as a reference blade height with 0% correction for the polytropic efficiency might not be appropriate for this engine. Still, it is notes that a sharp drop-off in efficiency is noticed only after a blade height of around 10 mm, which is not reached for the range of OPR investigated.

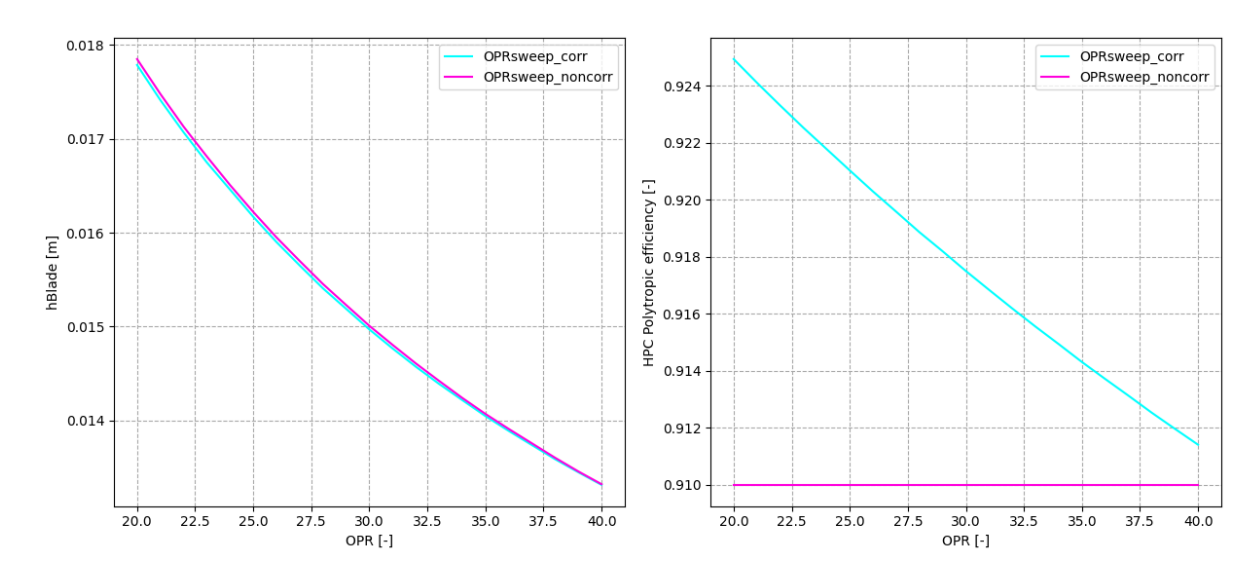


Figure 4.3: Blade height and HPC polytropic efficiency with scaling correction applied for varying OPR

4.3. Solver setup

With a model defined, the NPSS solver needs to be set up to allow for simulation of the cycle. The solver setup consists of choosing a number of independent and dependent parameters, allowing for an iterative search of a combination of design parameters to match a desired output performance. These are introduced for both design and off-design simulation, with the latter following a different engine performance calculation logic.

4.3.1. Fixed parameters

A number of parameters are fixed in order to constrain the design problem and provide a desired performance target.

Parameter	Value
Total inlet corrected mass flow rate \dot{m}_{corr} [kg/s]	917
Inner (core) fan isentropic efficiency $\eta_{fan,in}$	0.88
Outer (bypass) fan isentropic efficiency $\eta_{fan,out}$	0.92
IPC (booster) isentropic efficiency η_{IPC}	0.89
High-pressure compressor HPC isentropic efficiency η_{HPC}	0.87
High-pressure Turbine HPT isentropic efficiency η_{HPT}	0.93
Low-pressure Turbine LPT isentropic efficiency η_{LPT}	0.94
Steam Turbine isentropic efficiency η_{steam}	0.87
Water pump efficiency $\eta_{pmp,w}$	8.0
Hydrogen pump efficiency η_{pmp,H_2}	0.5

Table 4.1: Fixed engine and component parameters

In addition to this, bleed and cooling flows are accounted for in the model and are not changed from the existing engine model based on a conventional turbofan engine.

4.3.2. Solver variables

In order to solve the system of equations introduced by the definition of a cycle model, dependent and independent parameters need to be introduced. Independent parameters will be those that the NPSS solver iteratively changes, seeking a value which matches target performance, expressed as a dependent variable of fixed required value. An overview of the independent and dependent variables in design and off-design is given in this subsection.

Design point solver variables

The independents and dependents are largely chosen as pairs, with the independent being varied in order to match the target dependent. The choice of these is largely based on previous experience and common practice in gas turbine engine design, in various tools but also specifically previous engine models developed in NPSS at GKN.

For cruise, the solver pairs are introduced below. It is noted that while these are described as pairs which for a real engine are expected to be linked, in NPSS all independents and dependents are treated in a single pool. Nonetheless, the pairs are introduced as such to highlight the logic behind the choice of varying and target variables.

Independent: Bypass ratio BPR

• **Dependent**: Net thrust F_n

The BPR of the engine is allowed to vary to match the thrust, because the inlet corrected mass flow is treated as a fixed parameter and the fuel flow is varied to target the burner outlet temperature.

• Independent: Fuel flow \dot{m}_{fuel}

• **Dependent**: Burner outlet temperature T_4

The fuel flow into the combustor is varied to keep a constant burner outlet temperature, which is a common design parameter for turbofan engines.

• Independent: Steam injection flow rate \dot{m}_{inj}

• Dependent: Water-to-air ratio WAR

The water-to-air ratio is a fixed parameter that is achieved by varying the flow of steam injected into the combustor. This means that the WAR is assumed possible even if the total flow of condensed water is less than the flow of injected steam, or WRR < 1. This is fixed in order to allow for easier comparison of the cycle performance depending on parameter variation.

Independent: ACEC effectivenessDependent: Condensation margin

As is discussed in Subsection 4.2.5, the exhaust condensers need to supply a total condensed water flow higher than the injected water flow in order to account for en efficiency in water separation from the exhaust flow. In order to size the exhaust condensers in the overall model for this condition, the ACEC effectiveness is varied to target the desired total flow rate. This is chosen as the HCEC contributes only a small fraction of the total condensed water, and if its effectiveness were to vary another condition would need to be fixed in order to set both the ACEC and HCEC effectiveness.

- · Independent: Fan pressure ratio FPR
- Dependent: Ideal exhaust jet velocity ratio ζ

The ideal exhaust jet velocity ratio is a parameter of interest in studying the cycle, so a way to vary it is required. This is achieved by varying the fan pressure ratio, as the BPR and inlet corrected flow fix the bypass and core flow rates.

- Independent: High-pressure compressor pressure ratio PR_{HPC}
- Dependent: Overall pressure ratio OPR

The overall pressure ratio is another parameter of interest, and is varied by changing the pressure ratio of the HPC.

• Independent: HPC adiabatic efficiency $\eta_{is,HPC}$ • Dependent: HPC polytropic efficiency $\eta_{p,HPC}$

This pair is included as NPSS does not allow for the specification of polytropic efficiency. Due to the changing size of the turbomachines in parameter studies, assuming constant isentropic efficiency is not accurate, with constant polytropic efficiency being a better choice. This is achieved by setting a target polytropic efficiency, which is reached by iteratively varying the adiabatic efficiency. The effects of scaling are most important in the HPC, and as such only the HPC polytropic efficiency is introduced in solver variables to limit the computational complexity of the system.

• Independent: Steam turbine PR

• Dependent: Steam overpressure at injection

The steam turbine PR is set by maximally expanding the steam exiting the HRSG, with the limit set by a required overpressure of 1 atm at the injector. This prevents the flow of combustion gases into the water/steam loop fluid lines.

• Independent: Hydrogen pump PR

• Dependent: Hydrogen overpressure at injection

Similarly, the hydrogen pump is sized to ensure that hydrogen is pumped to a pressure that is 30% higher than the combustor pressure to prevent flashback.

• Independent: Water pump PR

Dependent: Requested pressure after pump

The pressure in the water/steam loop is also investigated in parameter studies, with the desired value achieved by varying the water pump PR.

Off-design solver variables

NPSS supports off-design simulations by altering the calculation procedure of model elements depending on the design condition, toggled by the conditional variable $\operatorname{switchDes}$. When running off-design cases, the design case must first be run in order to fix the geometry of the engine.

In design, switchDes "DESIGN" and geometry and scale factors are calculated to achieve a specified performance. In the current model, an example of this is a requested net thrust, inlet corrected mass flow and BPR, which will determine the geometric areas of the fan face, bypass nozzle and core nozzle.

In off-design mode, switchDes = "OFFDESIGN" and specified geometry and scale factors which are fixed from the design calculations are used to calculate resulting performance. A target is still set in off-design performance - in this model, net thrust is also targeted for the off-design points, but the parameters varied to reach that thrust are now different.

- Independent: Steam injection flow rate \dot{m}_{inj}
- Dependent: Water-to-air ratio WAR

The steam injection flow and WAR pair remains from design, as the WAR is kept constant over all operating points.

In off-design, describing the independent and dependent variables as discrete pairs becomes more difficult, and hence larger groups will be introduced.

• Independent: Fuel flow \dot{m}_{fuel}

• Independent: Inlet total mass flow \dot{m}_{inlet}

• **Dependent**: Net thrust F_n

In off-design, a target thrust is once again set, but is reached by instead varying the fuel flow and inlet mass flow.

• Independent: Fan BPR

Independent: Bypass cooling flow splitter BPR

• **Dependent**: Primary nozzle area A_8

Dependent: Secondary nozzle area A₁₈
 Dependent: Tertiary nozzle area A₂₈₀

The nozzle areas are fixed in design, and are achieved in off-design by a combination of varying the inlet mass flow introduced above and BPR at the two splitters: the fan split, and the bypass cooling flow split.

The performance of turbomachines in off-design is estimated in NPSS with the use of integrated performance maps. Knowing the corrected flow in a turbomachine and the torque balance on the relevant shaft, efficiency and PR are determined by moving along the R-line on the performance map.

Constraints

In addition to the specified independent and dependent variables, a constraint is set on the steam turbine pressure ratio. In order to prevent leading-edge erosion and the resulting efficiency drop in the steam turbine due to the formation of water droplets, the quality throughout the turbine must remain above 1. This is achieved by setting a constraint on the outlet quality χ_{out} of the turbine.

$$(\chi_{out})_{steam} >= 1 \tag{4.33}$$

4.3.3. Simulation limitations and challenges

A number of challenges were faced in setting up the cycle model and especially in running the simulations. Solver setup, model architecture as well as initial variable values had a strong influence on whether the solver converged to a valid solution in a reasonable time, or whether code was able to run without fatal errors. The amount of time required to mitigate these errors and produce converged results is significant enough to warrant their mention.

In setting up the model, a number of choices influenced the outcome of the solver sequence. For the bypass flow splitter which controls the cooling flow rate passing through the ACEC, the use of a $\operatorname{Splitter}$ element increased the total computational time of running a simulation significantly. This is likely due to the cooling flow rate being defined as a multiple of the core flow. As the core flow changes over each iteration due to changes in the engine cycle, the splitter BPR needs to be calculated accordingly. Furthermore, the flow downstream of the splitter affects the upstream flow as the model is also targeting a fixed nozzle exit velocity ratio between the bypass and core nozzles. With the incoming flow to the splitter also being a function of the fan BPR, which is similarly varying, the splitter's BPR depends on multiple different variables and cycle stations while simultaneously affecting those values. To mitigate this, the splitter was instead modelled as a Bleed off-take from a bypass flow duct with a pressure drop equal to the splitter pressure drop applied. In the Design mode, this proves a reduction in computational time while having a negligible, if any, impact on the cooling and undisturbed bypass flow rates. However, the behaviour of a Bleed port in off-design is significantly different to that of a splitter. After a W_{cool}/W_{core} ratio was fixed in design and a $\operatorname{Splitter}$ element with the corresponding fixed BPR reinstated, which was used for off-design simulations.

The NPSS solver employs the Newton-Rhapson method, which is a powerful and simple root-solving algorithm with a few key weakness. As the method requires evaluating the slopes of functions, the method can fail to converge in regions where the slope becomes infinite or is not well-behaved. The method is also highly dependent on initialisation and incorrect initial point choice may lead to convergence to an unphysical solution, oscillation or inability to converge. Manual variation of initial conditions guided by expected values helps mitigate this problem. Furthermore, moving between different design points is done in a gradual manner, simulating a few points along a line in the design space connecting the two points.

While independent and dependent variables are introduced as pairs in Subsection 4.3.2, the solver does not consider these pairs, instead considering all dependents and all independents in one set. If a dependent does not respond to a perturbation in an independent, the solver produces an error and the solution is halted. If that dependent is not physically linked to the independent, a response may not be expected and as such this situation is not erroneous. A work-around is reducing the maximum solver step in the independent expected to affect that dependent the most, such that convergence for that specific variable pair is slowed enough to allow for the other independent to converge.

4.4. Baseline engine simulation

In order to have a baseline for performance comparison, the cycle model is simulated for a hydrogen-fuelled engine without steam injection and water recovery. This is completed by setting the target water-to-air ratio WAR to 0 and ideal exhaust jet ratio ζ to 2/3 [76]. In other aspects, the engine model is unchanged and the engine is sized for the same net thrust and corrected mass flow rate at the design point.

4.5. Parameter studies

A number of key cycle parameters are defined and investigated when designing the engine. These are fixed before a simulation is run to size the engine, but are varied in parameter *sweeps*, observing the resulting impact on engine performance and sizing.

4.5.1. Ideal exhaust jet velocity ratio

The simulated Steam Injection Cycle features three separate nozzles for the core flow, the bypass flow and the cooled bypass flow which passes through the condenser. The ratio of the ideally expanded jet velocities of the core nozzle and bypass nozzle is defined as the ideal exhaust-jet velocity ratio, given in Equation 4.34.

$$\zeta = \frac{V_{I,18}}{V_{I,8}} \tag{4.34}$$

For a conventional Brayton cycle with a fixed bypass ratio and specific thrust, the value of ζ that minimizes the required power output from the engine core is estimated by Guha [77] as equal to the product of the fan and the LPT isentropic efficiencies:

$$\zeta_{opt} \approx \eta_{fan} \eta_{LPT}$$
(4.35)

However, this condition does not account for the impact of weight and drag on the mission fuel burn, so fulfilling the condition at one operating point does not guarantee it at another. The final cycle design will require a trade-off between mission fuel burn and the direct operating cost (DOC)[76]. The value of ζ which minimises DOC at the top-of-climb (ToC) point was found by General Electric to be around 2/3

For the Steam Injection and Water Recovery Cycle, the core exhaust stream passes through a series of heat exchangers before the nozzle. In the HRSG, energy is extracted from the flow in order to generate steam, and in the ACEC and HCEC the flow is further cooled in order to condense and separate water from the flow. Furthermore, there is a pressure drop over all heat exchangers. As such, the flow entering the core nozzle will have reduced enthalpy and the optimum ideal exhaust-jet velocity ratio will change, and is likely higher. The addition of heated steam into the burner, as well as any benefit gained from its expansion in the steam turbine, are seen to reduce the core size as discussed in Subsection 5.2.6, further having an impact on the optimum.

In order to investigate the effect of ζ , simulations were carried out for a fixed cooling flow rate of $W_{cool}/W_{core}=7.9$, fixed WAR=0.33 and fixed overall pressure ratio of OPR=40. In order to vary the ideal exhaust-jet velocity ratio, the fan pressure ratio was varied in order to target a desired value of ζ .

As the inclusion of the ACEC introduces a third (cooling bypass flow) nozzle, an additional related parameter is defined in the tertiary-to-core ideal exhaust jet velocity ratio $V_{I,280}/V_{I,8}$. Given a fixed 5% pressure drop and an extraction of energy for cooling in the ACEC, this ratio will differ from ζ . No research has investigated the influence of this on the cycle performance and it may be a parameter that could further be optimised. To vary this ratio, a study is performed where an additional booster stage is added to the cooling bypass flow stream, with further compression changing the tertiary nozzle velocity. The relationship between ζ and $V_{I,280}/V_{I,8}$ is given in Figure 4.4.

4.5. Parameter studies 54

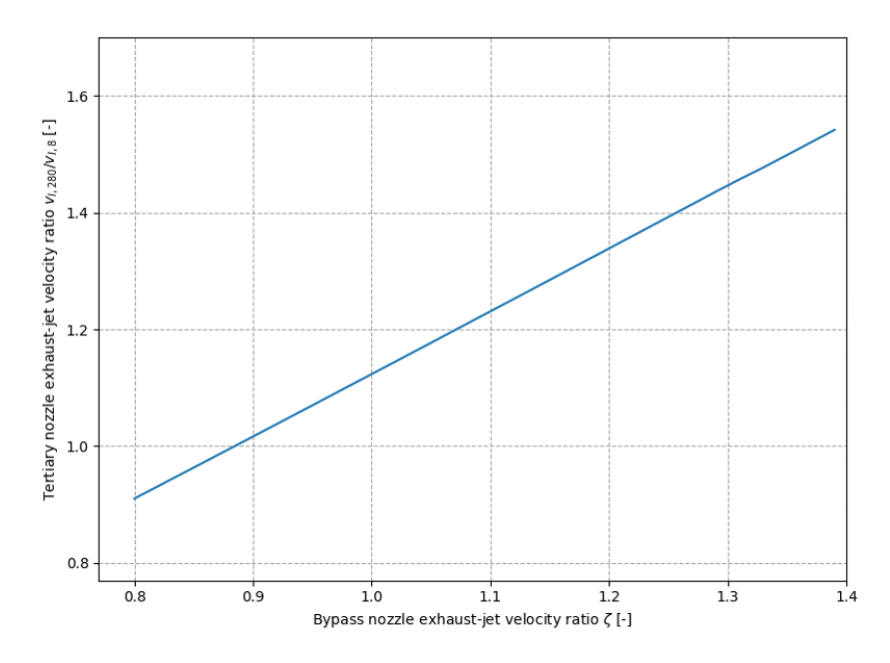


Figure 4.4: Tertiary-to-core nozzle ratio as a function of ζ

4.5.2. Overall pressure ratio OPR

The overall pressure ratio OPR is an engine parameter of interest in the study of Brayton cycles, with the cycle thermal efficiency improving for increasing OPR. Given the change in cycle from a simple Brayton cycle to a combined cycle in this engine, the optimal OPR may vary from conventional engines. The OPR is varied for a range of values from 20 to 40, corresponding to a common range of values for top of climb. As the fan pressure ratio is varied as an independent variable and the booster pressure ratio is set to achieve a constant pressure ratio over the booster and fan, the HPC pressure ratio is altered in order to vary OPR. It is important to note that the simulation model suffers from increased instability, longer computational times and convergence problems at high values of OPR, so investigating values above 40 was not feasible.

4.5.3. Steam pressure

The pressure in the water/steam loop after the water pump is chosen for investigation as it may impact the performance of the HRSG, and will determine in part how much power is able to be produced in the steam turbine. The pressure is varied by varying the pressure ratio of the water pump, with a range of 20 to 100 bar or 2 to 10 MPa investigated.

4.5.4. Water-to-air ratio WAR

The water-to-air ratio is varied from 0 to 50% at the burner inlet. In previous simulation of a kerosene steam injection cycle at GKN [14], the achieved WAR at design point was around 15%, while other projects have investigated values between 0-30% [15], and further 0-40% for a hydrogen steam injection cycle [16]. In present work, the model often became unstable, failing to converge or leading to fatal errors in flow calculation, at higher WAR.

4.5.5. Cooling flow rate

The cooling flow rate W_{cool}/W_{core} refers to the cooling flow of the air-cooled exhaust condenser ACEC and is defined in relation to the core mass flow rate before steam injection.

$$W_{cool}/W_{core} = \dot{m}_{261}/\dot{m}_{25} \tag{4.36}$$

The cooling flow rate has a significant influence on the amount of condensed water in the ACEC and is thus of interest for reaching water self-sufficiency. The cooling flow rate is varied by varying the bypass flow splitter BPR, but is defined in relation to the core flow as opposed to the bypass flow to

relate it to the core mass flow. This is to give an estimate of the relative stream mass flows in the ACEC, as well as because the core flow can vary between model iterations.

4.6. Detailed heat exchanger model

The summarised parameter studies were completed with a simplified modelling approach treating the heat exchangers in the cycle model as singular blocks with a fixed effectiveness. This allowed for simulation of the entire cycle, but the accuracy of heat exchanger performance was compromised for a number of reasons, summarised here.

- Assuming constant effectiveness: The effectiveness of a designed heat exchanger will change
 with a change in operating conditions, which is the case in running parameter studies and offdesign. Modelling
- Treating the heat exchangers as a single element: The heat transfer coefficient varies strongly in the condensing and evaporating streams, and to a lesser extent in the cooling and heating flows.
- **Ignoring the pinch point**: As a combination of modelling the heat exchangers as a single element with fixed efficiency, the pinch point is not properly considered and infeasible heat transfer rates may be prescribed.
- No sizing of heat exchangers: The parameter $A_h U$ was left as a fixed product in cycle simulations. Estimating the total heat transfer area is important as it provides an estimate for the size of the heat exchangers, which is required for off-design simulation as well as evaluating the entire cycle.

Correctly estimating the performance of the HRSG and two exhaust condensers is highly important for the steam injection and water recovery cycle, as the cycle improvement gained over a conventional Brayton cycle is a result of heat energy and water extraction from the exhaust stream. The assumptions made in the overall cycle model can lead to an overestimation of heat transfer, which is specifically critical for the condensers, in which the rate of condensed water may be overestimated. In order to ensure the engine is capable of condensing sufficient water at the design point, and to accurately estimate heat exchanger performance, a separate detailed model is developed. Here, the HRSG, ACEC and HCEC are extracted from the overall model and simulated in a separate environment, as can be seen in Figure 4.5.

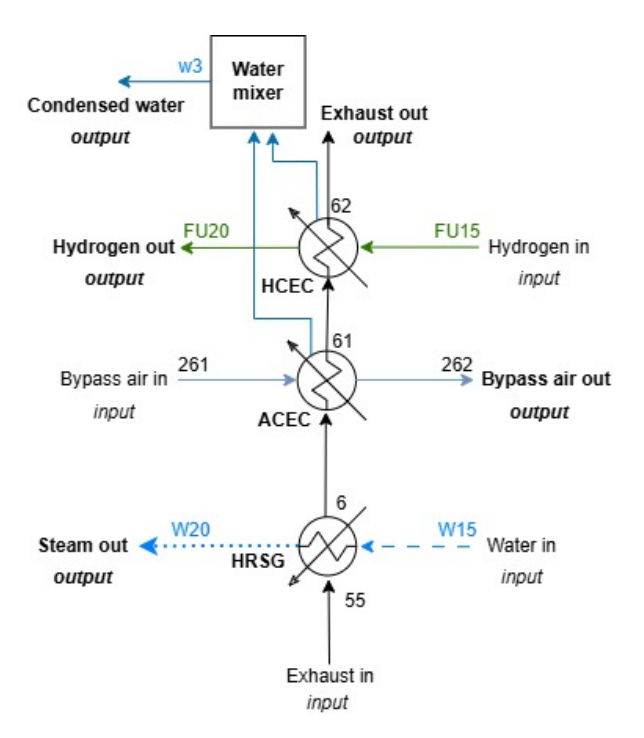


Figure 4.5: Detailed heat exchanger model schematic with station numbers and inputs/outputs

The heat exchangers in this detailed model will no longer be modelled with a fixed effectiveness, but with a varying set of boundary conditions and in multiple sections to capture phase variation and resulting changes in heat transfer. The HRSG will be modelled comprising of an economiser, evaporator and superheater, and the ACEC of a dry cooler and condenser. The model requires inlet conditions for incoming fluid streams as an input, with significant outputs being the total condensed water flow, total heat transfer area A_h for each heat exchanger and outlet conditions of the steam exiting the HRSG. The complete overview of inputs and outputs is given in Table 4.2.

	Input	Output
HRSG	Exhaust inlet T_t , P_t , \dot{m}	Exhaust outlet T_t , P_t , \dot{m}
	Water inlet T_t, P_t, \dot{m}	Steam outlet T_t , P_t , \dot{m}
	Superheater A_h or ε	Superheater A_h or ε
		Economiser A_h and $arepsilon$
		Evaporator A_h and $arepsilon$
ACEC	Exhaust inlet T_t , P_t , \dot{m}	Exhaust outlet T_t , P_t , \dot{m}
	Bypass cooling inlet T_t , P_t , \dot{m}	Bypass cooling outlet T_t , P_t , \dot{m}
		Dry cooler A_h and $arepsilon$
		Condenser A_h and $arepsilon$
		Condensed water flow $\dot{m}_{cond,ACEC}$
HCEC	Exhaust inlet T_t , P_t , \dot{m}	Exhaust outlet T_t , P_t , \dot{m}
	Hydrogen inlet T_t , P_t , \dot{m}	Hydrogen outlet T_t , P_t , \dot{m}
	HCEC A_h or $arepsilon$	HCEC A_h or $arepsilon$
		Condensed water flow $\dot{m}_{cond,HCEC}$

Table 4.2: Detailed model inputs and outputs

4.6.1. Pinch analysis

An important theoretical concept to consider is the pinch point, which refers to the point of minimum temperature difference between the two streams of a heat exchanger [78]. In process engineering, pinch analysis is a methodology for minimising the energy consumption of chemical processes by determining the pinch points, where the design is most constrained, and starting the heat exchanger design from there. In the context of this work, the pinch point is important as it helps determine the maximum possible heat transfer between the phase-changing and single-phase streams. This prevents the overestimation of heat exchanger that can occur when treating the heat exchangers as a single block with fixed effectiveness.

In Figure 4.6, two duty diagrams are shown plotting temperatures along the HRSG. In Figure 4.6a, the minimum distance between the cooling and heating streams is zero, and the heat exchanger is said to be *perfectly pinched*. This situation signifies the maximum possible rate of heat transfer in the heat exchanger, effectively limiting flow temperature between the economiser and evaporator. In Figure 4.6b, a physically infeasible duty diagram is drawn up, where the temperature change over the evaporator and economiser is overestimated. This would result in a cooler exhaust outflow, enhancing condensation further downstream, and/or hotter steam outflow, providing higher steam outlet quality and steam turbine power. Both of these lead to an overestimation of HRSG performance and cycle improvement.

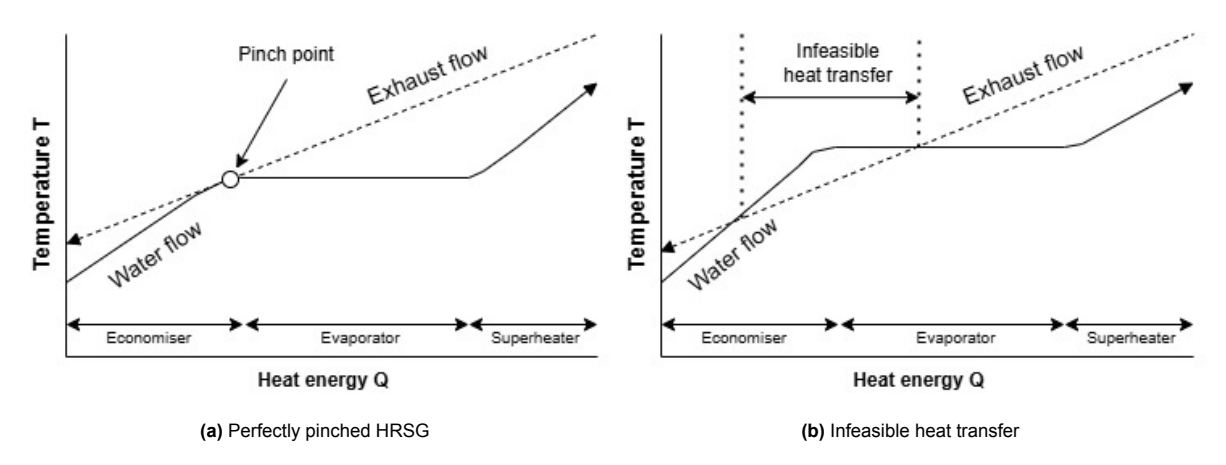


Figure 4.6: HRSG duty diagrams with pinch point

Similarly, duty diagrams are drawn up for the ACEC consisting of a dry cooler and condenser. In Figure 4.7a, the ACEC is perfectly pinched, whereas in Figure 4.7b, an infeasible situation is presented. The implication of ignoring the pinch point for the ACEC can lead to a significant overestimation of the outlet temperature, and thus the rate of condensed water, which is a critical parameter for overall cycle performance.

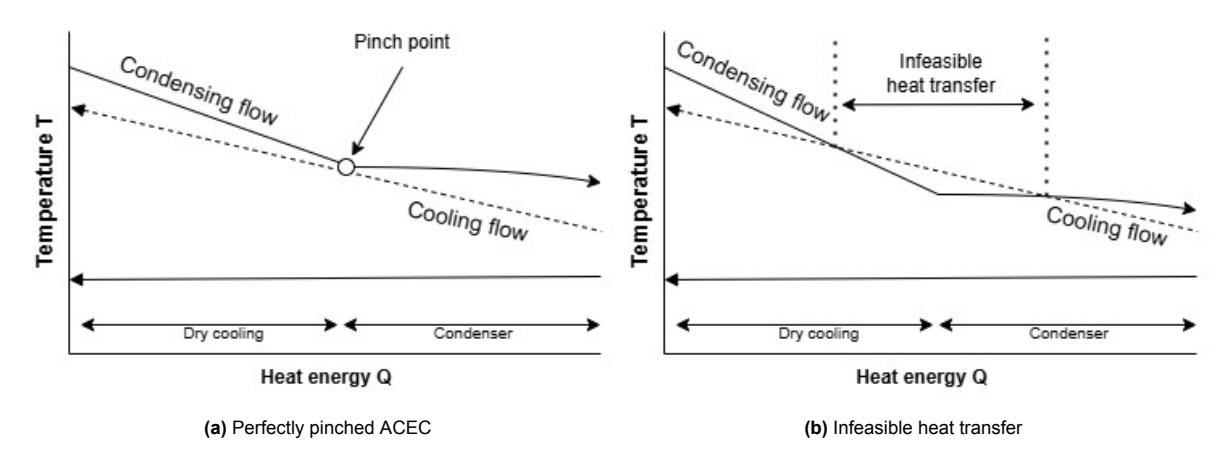


Figure 4.7: ACEC duty diagrams with pinch point

In the case of the overall model, the infeasible situation would not be detected as the HRSG and ACEC are treated as one block, with only the outlet and inlet temperatures of both fluids considered. If the outlet of either stream does not reach the inlet of the other, the prescribed heat transfer is considered possible. Prescribing an infeasible rate of heat transfer will overestimate the performance of the heat exchanger. This is the primary reason for developing a detailed heat exchanger model, treating each component in sections to capture the detailed temperature profile and more accurately model performance.

4.6.2. Heat exchanger type choice

In order to estimate the heat transfer and thus the total heat transfer area A_h , the type of heat exchanger must be defined. Two of the most common types of heat exchanger for similar applications are tube-and-shell and plate heat exchangers [12]. Their differences, advantages and disadvantages are summarised in Table 4.3.

	Shell-and-tube	Plate
Construction	Tubes	Flat plates
Efficiency	Typically lower	Typically higher (up to five times)
Heat transfer area	Lower	Significantly higher (compact)
Maintenance	Harder to inspect and maintain	Easier to inspect and maintain
Cost	Higher	Lower initial cost, but long-term
		costs possible
Operation	High pressures, high temperatures	Can withstand less pressure
Durability	Higher	Lower

Table 4.3: Comparison of shell-and-tube and plate heat exchangers

Due in part to the high pressure and temperature differences experienced in the heat exchangers as discussed in Equation 2.3.2, shell-and-tube configurations were chosen for the HRSG, ACEC and HCEC. Furthermore, shell-and-tube heat exchangers offer high durability and are commonly used in refrigeration[12], where condensers are a key component similar to the steam injection and water recovery cycle. While other types of heat exchanger such as plate heat exchangers may offer improvements in terms of efficiency and compactness, these considerations are treated qualitatively, as detailed geometric design is deemed outside the scope of this work. Choosing and fixing a configuration allowed for a narrowing of the already large design space for heat exchangers, and more time allocated toward developing this detailed sizing model.

4.6.3. Heat exchanger geometry

While detailed geometry design is not completed in this work, it is necessary to fix some geometric parameters in order to estimate the rate of heat transfer in the heat exchangers. For simplicity, these are chosen the same for all three heat exchangers. An overview of the estimated parameters is given below.

Parameter	Value
Tube outer diameter [mm]	5
Tube thickness [mm]	0.25
Pitch ratio S_T/S_L	1.15
$\overline{}_{V_{exhaust}}$ [m/s]	50
V_{bypass} [m/s]	50
V_{water} [m/s]	1.5

Table 4.4: Heat exchanger geometric parameters

The choice of tube diameter, wall thickness and the transverse-to-longitudinal pitch ratio S_T/S_L are chosen based on common practice and recommendations from private communication with industry experts.

The estimated flow velocities in the heat exchangers are based on suggested tube- and shell-side velocities [79]. For the exhaust and bypass flows, a velocity of 50 m/s is chosen as an estimate based on recommended vapour velocities. In reality, the exhaust flow passes through a number of heat exchangers and is thus expected to slow due to the pressure drop it experiences, but in order to limit complexity and avoid detailed geometric design, a constant value is used. For liquid water, a lower velocity of 1.5 m/s is chosen in the economiser, with velocity in the steam phase calculated in the code according to conservation of mass in the evaporator and the change in density of water to steam. Finally, hydrogen is allocated a velocity of 20 m/s.

4.6.4. General assumptions

Some general assumptions made in the detailed model are summarised below.

- The HRSG, ACEC and HCEC are modelled as counter-flow heat exchangers.
- The heat exchangers are modelled as tube-and-shell type.
- Boiling effects are neglected in the estimation of heat transfer in the evaporator.
- Constant and equal pressure drops are assumed over each of the HRSG, ACEC and HCEC.
- Heat transfer coefficients are calculated based on mean flow conditions calculated from the inlet and outlet values.

4.6.5. Heat Recovery Steam Generator

As discussed in Equation 2.3.2, the HRSG can be broken into three distinct sections: an economiser, an evaporator and a superheater. In order to accurately predict the temperature profile inside the HRSG, the three sections are modelled as individual evaporator elements in NPSS. With appropriate design constraints and estimation of heat transfer coefficients, each section can be sized individually and outlet conditions for the steam and exhaust flows can be predicted. These are presented in Figure 4.8.

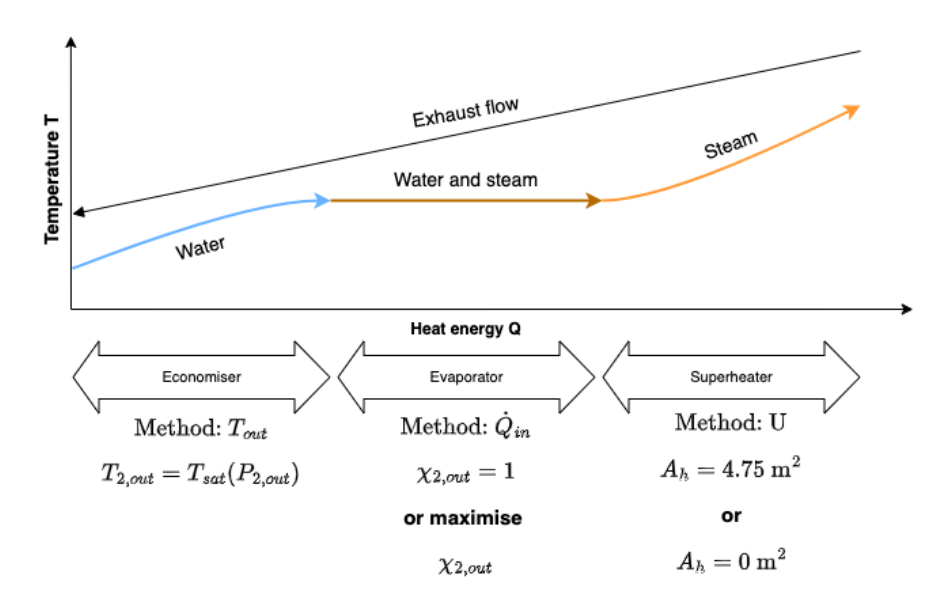


Figure 4.8: Detailed HRSG model calculations

The **economiser** brings the inflow of water to its saturation temperature at the HRSG internal pressure. The boundary condition is thus a fixed outlet water temperature, with the calculation procedure run for an input T_{out} .

In the **evaporator**, water changes phase from liquid to vapour. Knowing the incoming water flow properties, the boundary condition is an outlet steam quality of 1 corresponding to saturated steam. The calculation procedure is run for an input \dot{Q}_{in} , iterated until the outlet condition is matched. Alternatively, if the rate of heat transfer to raise saturated steam is not possible, the maximum possible outlet quality is sought.

Finally, the **superheater** further heats the produced steam. With the overall heat transfer coefficient U calculated from flow properties, the superheater has a number of possible designs, with a trade-off between heat transfer area and effectiveness.

A simple study is run in order to fix a superheater area for the design point. At the design condition, superheater area is varied and the HRSG sized. For higher superheater area, a higher steam outlet quality is reached, increasing steam turbine power, but the total heat transfer area of the HRSG grows accordingly. The steam turbine power increases linearly with superheater area, while the increase in total HRSG area accelerates with superheater area. To limit the weight penalty incurred by the superheater while ensuring some expansion is possible in the steam turbine, a value of 4.75 m² is chosen for the superheater.

4.6.6. Exhaust Condensers

A temperature-heat energy diagram for the two exhaust condensers is presented in Figure 4.9. The ACEC is broken into two sections: a dry condenser where the exhaust is brought to the water saturation temperature, and a condenser where steam begins to condense. The HCEC can be seen as an extension of this condenser segment.

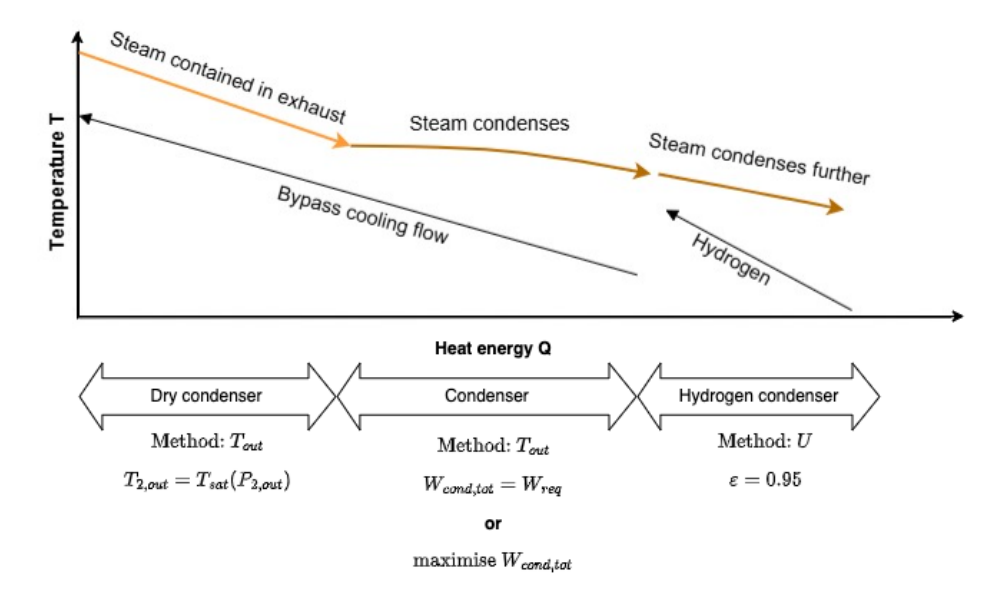


Figure 4.9: Detailed ACEC and HCEC model calculations

The **dry condenser** has the outlet boundary condition of saturation temperature for the exhaust floww at the outlet pressure, and the calculation is thus run for a fixed T_{out} . The **condenser** is also calculated for a fixed T_{out} , with the target being a total condensed water flow equal to the one required for the design point. If the requested heat transfer rate is impossible, the model instead sizes the condenser for a maximum condensed water flow, corresponding to an effectiveness of one. As an effectiveness of one will be difficult to achieve in reality and the condenser is limited on the bypass flow side, the bypass flow can be increased until the desired water flow is reached at a lower, achievable effectiveness. The total condensed flow also includes the HCEC condensed flow, but this is fairly constant and contributes a small amount of the total, so it is not iterated.

The **hydrogen condenser** is calculated for a fixed U. Here, a prescribed effectiveness of 0.95 is given as this is determined feasible to reach in detailed heat exchanger design. Knowing the total heat transfer coefficient, the area of the HCEC is calculated.

4.6.7. Flow configuration

In Section 2.3, a choice of heat exchanger type is made, and the flow configuration shortly discussed. Initial work assumed that the heat exchangers would be configured with the exhaust stream being allocated as the shell-side flow for all three. This is because the water in the HRSG and hydrogen in the HCEC are certainly allocated to the tube side. Construction of the ACEC, being between the two other heat exchangers, is simplified by keeping the exhaust on the shell side, essentially forming one large shell for the exhaust flow. However, in initial runs of the detailed model it was realised that the ACEC condenser, the largest heat exchanger, is limited in heat transfer on the bypass flow side. Thus, allocating the bypass cooling flow to the tube side leads to an infeasibly large ACEC total heat transfer area. Some alterations to the ACEC are thus considered to improve its heat transfer.

4.6.8. Heat transfer enhancements

A preliminary study to investigate the effect of some heat transfer enhancements was completed. In Table 4.5, a number of configurations are presented together with the resulting ACEC areas. *Out-out-out* refers to a flow configuration where the exhaust is on the shell side of all heat exchangers, while *out-in-out* refers to a configuration where the exhaust is allocated shell side for the HRSG and HCEC, while being tube side for the ACEC. In addition to the flow configuration, the impact of halving the tube diameter is explored, as is the enhancement of heat transfer on the limiting bypass flow side. The specific enhancement technique is not explored, but a 50% increase in heat transfer coefficient is applied in order to quantify the improvement in required total heat transfer area.

Case	Dry condenser	Condenser	Total ACEC
	A_{dry} [m 2]	A_{cond} [m^2]	A_h [m 2]
Exhaust out-out-out			
$D_{tube} = 5mm$	1257	5684	6940
No enhancement			
Exhaust out-out-out			
$D_{tube}=2.5 \mathrm{mm}$	853	5209	6062
No enhancement			
Exhaust out-out-out			
$D_{tube} = 5 \mathrm{mm}$	850	3435	4303
+50% bypass h enhancement			
Exhaust out-in-out			
$D_{tube} = 5 \mathrm{mm}$	810	1774	2584
No enhancement			
Exhaust out-in-out			
$D_{tube}=2.5 {\sf mm}$	753	1597	2350
No enhancement			
Exhaust out-in-out			
$D_{tube} = 5 \mathrm{mm}$	810	1182	1992
+50% bypass h enhancement			
Exhaust out-in-out			
$D_{tube}=5mm$	753	1065	1818
+50% bypass h enhancement			

Table 4.5: ACEC area for different heat exchanger configurations and ACEC parameters

For all explored configurations, the total heat transfer area is significant. A significant improvement is achieved by changing flow configuration to *out-in-out*, and as such this configuration is chosen for following calculations. Reducing tube diameter has a marginal improvement that does little to mitigate the large areas, with a slightly larger reduction achieved with an increased heat transfer coefficient. As detailed geometric heat exchanger design is not in the scope of the project and recognising the currently infeasible ACEC size, further calculations are completed in order to compare values between design and off-design points while a feasible ACEC design is recommended for future work. Choosing to instead use a plate heat exchanger, which provides a higher effectiveness and total heat transfer area, is expected to provide a hopefully feasible design.

4.6.9. Pressure drops

A heat exchanger will disturb the flow and as such a pressure drop is expected. Negating pressure drops can lead to an overestimation of performance and the resulting cycle benefit, so an estimation of pressure loss is included. With a lack of detailed geometric design of the heat exchangers, calculating exact pressure drops is difficult and deemed outside of the scope of research. Instead, a fixed 5% pressure loss over each of the HRSG, ACEC and HCEC in both flow streams is assumed.

Considering the size and flow phase variation along the heat exchangers, the pressure drop is unevenly split among the sections of the components. For the HRSG, the superheater is comparatively smaller than the economiser and evaporator, and is hence allocated a smaller pressure drop. The liquid water has a much lower pressure drop due to a significantly lower fluid velocity, so the pressure drop is split only among the evaporator and superheater for the steam, with the evaporator allocated a larger drop due to its larger area.

Stream	HRSG Δp [%]				
	Economiser	Evaporator	Superheater		
Exhaust	2%	2%	1%		
Water	0%	3%	2%		

Table 4.6: Pressure drop distribution over HRSG

For the ACEC, the condenser is a significantly larger component, and as such is allocated a larger share of the total pressure drop.

Stream	ACEC Δp [%]		HCEC Δp [%]
	Dry condenser	Condenser	Hydrogen condenser
Exhaust	1%	4%	5%
Water	1%	4%	-
Hydrogen	-		5%

Table 4.7: Pressure drop distribution over ACEC and HCEC

4.6.10. Off-design heat exchanger calculations

Once the heat exchangers have been designed and sized for the design point, their off-design performance can be simulated. The same detailed sizing model is used, however with some alterations in the calculation procedure. Most crucially, the total heat transfer area A_h is fixed from the design point.

HRSG off-design

The economiser is solved again for a water outlet temperature $T_{2,out}$ equal to the saturation temperature T_{sat} at the outlet pressure. The evaporator is also sized for an outlet quality of 1, or the maximum possible. In case 1 is achieved, the superheater is sized by Equation 4.37, and otherwise there is no superheater and the area is set to zero.

$$A_{super} = (A_h)_{HRSG} - A_{econ} - A_{evap} \tag{4.37}$$

ACEC off-design

The dry cooler is again sized to provide an outlet exhaust temmperature $T_{2,out}$ equal to the water saturation temperature T_{sat} at the outlet pressure, or the lowest possible temperature. If the saturation temperature is reached, the condenser section is sized by Equation 4.38.

$$A_{cond} = (A_h)_{ACEC} - A_{dry} \tag{4.38}$$

HCEC off-design

The area of the HCEC is fixed in design, and kept constant. The calculation is done for an input heat transfer coefficient U.

4.7. Integration of detailed model into overall model

Initially, the heat exchanger detailed sizing was aimed to be completed in the overall model along with the rest of the solver sequence. However, integration of the detailed model with a number of new dependent and independent variables increased computational complexity significantly, with convergence not reached even for a range of guiding input conditions and other mitigating features such as integrating some independent-dependent pairs as direct calculations in the code. The various heat exchanger sections, boundary conditions and counter-flowing streams increase the already high complexity.

A robust manual approach was chosen in order to have some feedback between the two models while limiting computation time. The overall cycle model is run, with the heat exchangers at a fixed effectiveness. From this model, the input conditions of the three heat exchangers can extracted and the heat exchanger assembly run in the detailed heat exchanger model. From this, an accurate estimate of the total condensed water flow rate, HRSG steam outlet conditions and calculated total effectivenesses of the heat exchangers are obtained. If the pinch point of the condenser is ignored in the overall model and the realistic condensed water flow rate is lower than required, the cooling flow rate can be increased in order to match the required value, giving a new splitter BPR. The effectiveness of the heat exchangers and splitter BPR, as well as HRSG outlet steam conditions are updated in the overall model. The overall model is run again, resulting in an updated steam turbine power and cycle performance values.

Complete integration of the detailed model may be possible with further time allocation towards this challenge, allowing for a higher accuracy of simulation within the timeline and scope of the project, producing some comparable results was prioritised and allowed for time spent on simulating off-design conditions. As the thesis studies the cycle at large, some reduction

4.8. Verification and validation

Verification is completed to ensure the developed models function correctly, producing the correct results for the implemented equations. Validation, which can only be done partially in this work, aims to compare the model's results to real-life experimental data.

Verification is be completed in a few ways. In the element modelling phase, the element models are verified by hand calculation of the set of equations. The same inputs are taken and the output of the programmed model is compared to the hand calculations or results from software. For the full engine model, results from the modelling work of other researchers such as the WET project [15],[16] are used to compare engine parameters and performance. While for many parameters data is sparse, the values of WAR are able to be compared. MTU and DLR studies show ranges of WAR around 0-0.5 [16] [15], with optimal values minimising SFC found anywhere from 0.15 to 0.25, with lower WAR values seen for a kerosene steam injection cycle than a hydrogen one. Pratt & Whitney's HySIITE claims a much higher WAR of 0.8 [11], but with a lack of publications it is unclear how this WAR is defined. The investigated WAR range of 0 to 0.5 is chosen as similar to the previous work mentioned, and the optimum found in this work is in this range, while being slightly higher than the values found by MTU and DLR.

Validation of results is complicated by the fact that no experimental data presently exists for an engine running a hydrogen-powered steam injection cycle. Even for individual components, such as the condenser, finding data may be difficult for the same operating conditions and fluid composition. Experimental data exists for ground-based gas turbines operating on Cheng cycles, but these are not hydrogen-powered and the Cheng cycle itself does usually not include water recovery, which means the cycle itself is different. At the full engine model level, validation is not feasible due to the lack of experimental data, and as such is not completed in this work.

Results and Discussions

The successful development of a general cycle model for a hydrogen steam injection and water recovery cycle is augmented by a detailed heat exchanger model for accurately determining the performance of the HRSG, ACEC and HCEC. This model is run with the specified solver setup and while varying a number of design parameters in order to reach a top of climb engine design. At this operating point, the geometry of the engine is fixed and off-design simulations at the mid-cruise and take off points completed. The results of the parameter studies are presented in Section 5.2, while design and off-design performance is compared in Section 5.3. The results of the detailed heat exchanger model simulations are given in Section 5.4. A baseline hydrogen engine simulation without steam injection and water recovery is also completed for top of climb, presented in Section 5.1. Finally, recommendations for future work are discussed in Section 5.5.

5.1. Baseline engine results

The performance of a baseline non-steam injection hydrogen-fuelled turbofan engine is given in Table 5.1.

Parameter	Value
F_n [kN]	38.178
Fuel flow \dot{m}_{fuel} [kg/s]	0.2
SFC [g/(kNs)]	5.215
Injected steam flow \dot{m}_{inj} [kg/s]	0
ldeal exhaust jet ratio ζ [-]	0.667
BPR	12.6
Inlet mass flow [kg/s]	342
Bypass mass flow [kg/s]	317
Core mass flow [kg/s]	25.2

Table 5.1: Overview of baseline hydrogen engine performance and size

It is important to note that this engine has not been optimised and as such the SFC could be improved from the stated one. However, due to a lack of reference performance data for a hydrogen steam injection and water recovery turbofan, the level of accuracy is accepted in order to provide some reference for quantifying the performance enhancement of these technologies.

5.2. Parameter studies

As discussed in Section 4.5, a number of parameters are investigated to determine an optimal engine. The main objective in these studies is two-fold: achieving water self-sufficiency, and minimising SFC. In addition, desirable properties are lower weight, complexity, and component losses. The parameters are presented one by one, the resulting changes in the cycle are discussed, and finally a choice for the design point is made.

5.2.1. Water self-sufficiency

The ability of the engine to condense the required water for steam injection is a primary point of interest. To limit the weight of an excess water tank and water on board which diminish the benefits of steam injection, the engine is designed to be water self-sufficient at least at its design point, and ideally through most of its typical mission duration. The cooling flow rate W_{cool}/W_{core} in the ACEC and cycle water-to-air ratio WAR are the key parameters affecting condensation. The cooling flow is critical due to the relatively larger size and cooling capacity of the ACEC compared to the HCEC and the fact that the flow is generally limited in capacity on the bypass side. The WAR has an impact on the amount of water available for condensation in the exhaust stream and thus is expected to impact condensation. The cooling flow rate and WAR are investigated largely together, as the fuel efficiency optimum and water condensation margin are a function of both parameters.

A range of 0-50% was chosen for simulation, while as can be seen in Figure 5.3 and Figure 5.1 above 35% there are signs of instability in the produced results.

The effect of WAR on the rate of condensation is first considered. In Figure 5.1, the condensed water flows of the ACEC and HCEC are plotted for a range of WAR together with the steam flow required for injection. Here, the cooling flow rate is fixed at 7.9 times the core flow. While the condensed and injected flow rates are dimensional, WAR is a non-dimensional parameter. The WAR is chosen to be studied because the core size changes with iterations in the model, leading to a varying core flow. The WAR is thus an indicator of the relative fraction of steam injection flow.

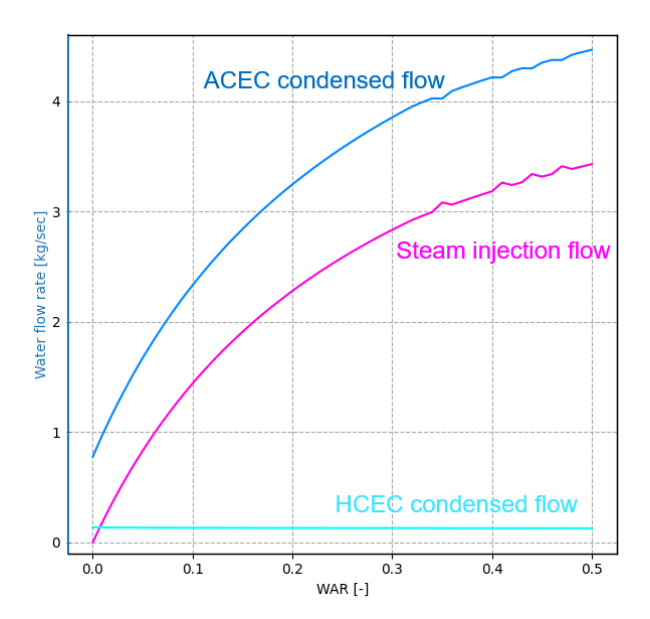


Figure 5.1: The condensed water flow rate and required flow rate for steam injection for WAR from 0 to 0.5, for a fixed cooling flow rate W_{cool}/W_{core} =7.9

A higher WAR leads to a higher amount of water in the core stream, which will aid condensation while simultaneously constraining it by requiring a higher condensed flow to be supplied if the engine is to be water self-sufficient. The benefit to condensation lies in both a higher fraction of water present in the flow to condense and a higher heat transfer coefficient due to the more humid air. Notably, the benefit from the increase of humidity in the core seems to outweigh the requirement for condensing more, as the two lines diverge slightly with increasing WAR. However, this analysis does not consider the size of the resulting ACEC, which can be expected to similarly increase with the total condensed flow rate.

It can be seen that even at a WAR of zero, there is still some water condensed. The reason for this is that hydrogen combustion produces water vapour, leading to a humid exhaust. The core engine flow is otherwise assumed to be dry in the NPSS model, so for kerosene a WAR of zero would be expected to have no condensation. This also highlights the synergy of water recovery and the use of hydrogen, as the increase in humidity is contributing to an already humid exhaust.

The HCEC condensed flow is minimal compared to the ACEC condensed flow, but also notably constant. This is because a constant effectiveness is assumed for the condenser and the HCEC is

limited in stream capacity on the hydrogen side. The stream capacity, which is defined as the product of the heat capacity and mass flow rate, is lower due to the significantly lower mass flow of hydrogen, despite its high heat capacity. This means that when increasing heat transfer in the exhaust stream the condenser is already operating at its limit and little gain can be found in the total heat transferred.

5.2.2. Cooling flow rate

The cooling flow rate W_{cool}/W_{core} is the key parameter affecting condensation. This is due to the relatively larger size and cooling capacity of the ACEC compared to the HCEC and the fact that the flow is generally limited in capacity on the bypass side, as the humid exhaust has a high heat capacity despite its lower mass flow. Figure 5.2 shows the rate of condensed water flow and the required steam injection flow for a range of cooling flow rates. Once more, a dimensional parameter is plotted against a non-dimensional one, which is done as the core flow rate is changing. The definition of a non-dimensional ratio allows for an easier understanding of the comparative flows in the condenser. Furthermore, while the condensed and injected flows could also be defined as ratios, he difference between them is of higher interest than their specific values, as this determines if water self-sufficiency is reached or how much water is required to be supplied from tanks if it is not.

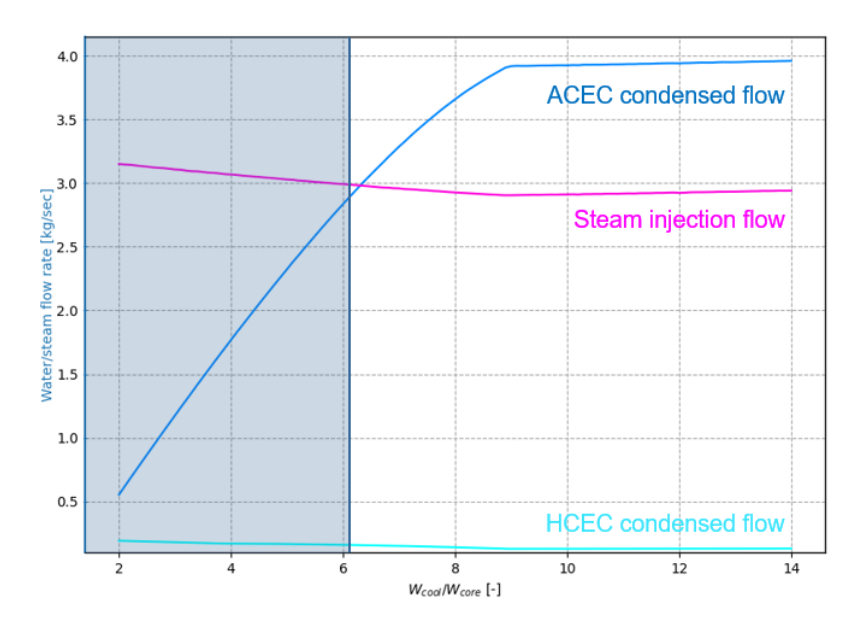


Figure 5.2: Variation in the injected steam flow rate and total condensed water with a change in bypass cooling flow rate

The feasible design space is highlighted right of a W_{cool}/W_{core} of 6, where condensation surpasses the required flow rate. The steam injection flow remains fairly constant, but small changes in the cycle due to a higher cooling flow rate lead to some variation in the core flow and thus steam injection flow. Increasing cooling flow rate expectedly increases the condensed water flow rate, but there is a point around W_{cool}/W_{core} =9 beyond which an increase in cooling flow gives no advantage in condensation. At this point, the ACEC becomes limited by the stream capacity of the exhaust flow, which together with the constant effectiveness assumption fixes the total heat transfer rate.

5.2.3. WAR and W_{cool}

The parameters of WAR and W_{cool}/W_{core} are more useful to consider together, as achieving a varying WAR will require a varying cooling flow rate. Furthermore, locating the SFC optimum requires considering both variables.

In Figure 5.3, a visualisation of the condensed and required water flows for a wide range of WAR and W_{cool}/W_{core} is given. It is noted that these results are produced in initial studies, and as such the magnitudes of flow rates may not match the values for the design point determined. However, this graph is included to explain the interdependence of W_{cool}/W_{core} and WAR and the phenomena resulting from the condenser calculation logic.

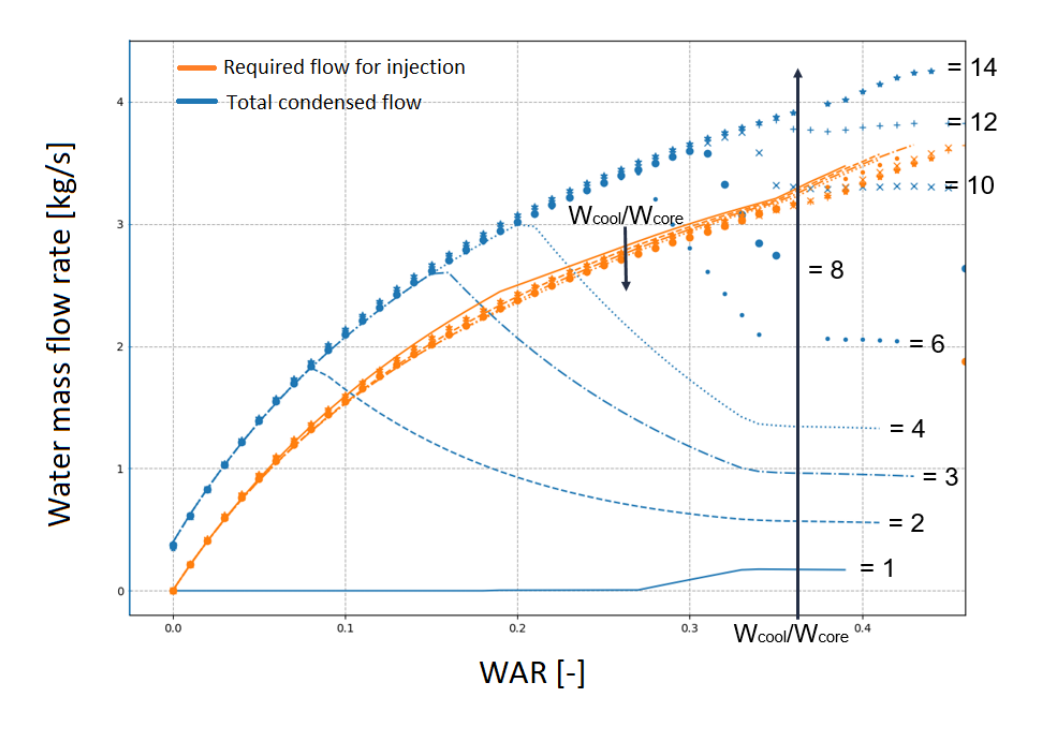


Figure 5.3: Condensed and required water flow rate for a range of WAR from 0 to 0.4 and W_{cool}/W_{core} from 1 to 14

The orange curves corresponding to the required steam injection flow are affected slightly by a change in W_{cool}/W_{core} , as the required flow rate depends solely on WAR and the core flow, which is only slightly affected by the cooling flow. However, a small decrease in the required flow for steam injection is noted.

The blue curves correspond to the total condensed flow. At a cooling flow ratio of 1, there is not enough heat transfer in the ACEC to condense any water out of the flow until a fairly high WAR. Increasing W_{cool}/W_{core} increases heat transfer, allowing water to be condensed. For a given W_{cool}/W_{core} , there is generally a maximum achievable WAR beyond which the ACEC has reached its maximum possible heat transfer and increasing WAR cools the flow, reducing condensation further until sufficient water is not condensed. It is noted that at high values of W_{cool}/W_{core} high rates of condensation are reached, but the size and weight of the ACEC will grow large, with more than half the bypass mass flow passing through the component and the high water condensation rate requiring a large total heat transfer area. In order to limit weight and volume penalties, excessive values of W_{cool}/W_{core} are to be avoided.

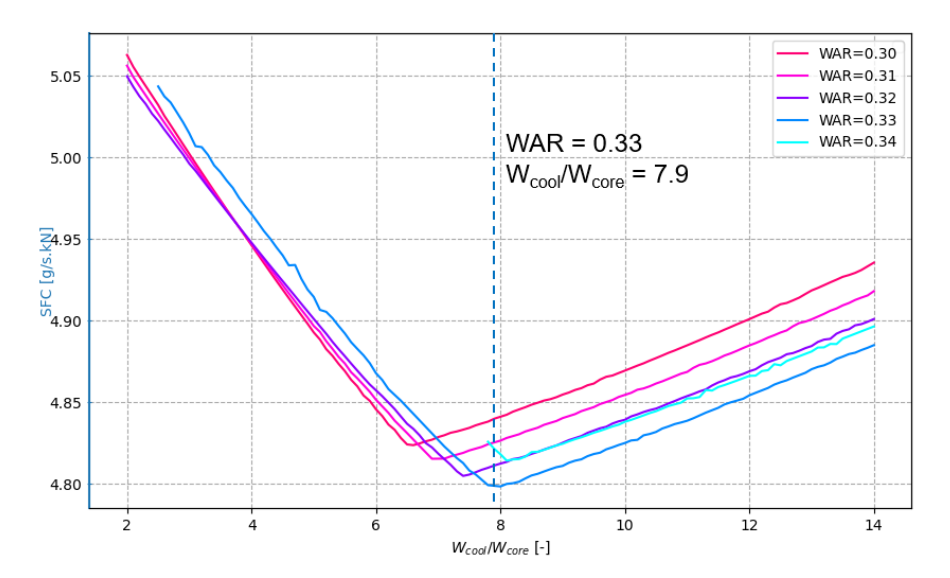


Figure 5.4: Fuel consumption as a function of the cooling flow rate and WAR

In Figure 5.4, the SFC variation with W_{cool}/W_{core} for a narrowed range of WAR is shown. Some instabilities in the model solving procedure are evidenced by the roughness of plotted lines as well as the discontinuity of the WAR=0.34 line before W_{cool}/W_{core} =8, but the SFC minimum is accurately captured. Following the logic of minimising SFC while limiting W_{cool}/W_{core} to limit weight penalties, the design point is chosen as WAR = 0.33 with a W_{cool}/W_{core} = 7.9, highlighted also in the figure.

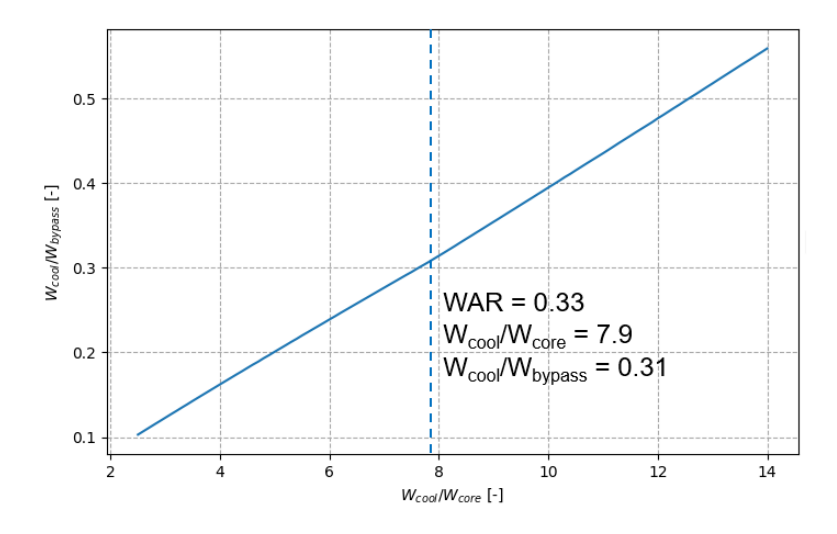


Figure 5.5: Cooling flow as a fraction of the total bypass flow

Figure 5.5 plots the cooling flow rate as a function of bypass total flow rate to illustrate the split of flows in the bypass stream. The observed relationship is a linear one as the BPR is constant. For the range of cooling flow rates investigated, the fraction of cooling flow varies from 10 to nearly 60% of the bypass and for the chosen design point, the cooling flow rate in the ACEC is 31% of the total bypass flow rate. Nearly a third of the total bypass flow is required in order to provide sufficient cooling in the ACEC, which will likely lead to a large condenser, increasing total engine weight. Furthermore, as most of the thrust, especially in the case of the steam injection cycle, is generated by the bypass stream, the impact of the ACEC on the total thrust can be significant. While currently a fixed 5% pressure drop is assumed for the bypass flow passing through the ACEC, a detailed analysis of pressure losses would provide a more accurate estimate of the impact, also at different operating points.

5.2.4. Cooling flow rate correction

As discussed in Section 4.7, after the overall model has been run and the engine sized for the design point, the detailed heat exchanger model is run in order to verify the performance of the HRSG, ACEC and HCEC. In fact, the overall model overestimates the total condensed flow as expected due to the assumption of constant effectiveness. As described by the iterative procedure, the cooling flow rate is increased by 40%, giving a higher final W_{cool}/W_{core} presented in Table 5.2.

ACEC Cooling flow [kg/s]	140
W_{cool}/W_{core} [-]	11.2
W_{cool}/W_{bypass} [-]	0.43

Table 5.2: Updated ACEC cooling flow rate

5.2.5. Jet exhaust velocity ratio

As discussed in Subsection 4.5.1, the fuel efficiency optimum for the ideal exhaust jet velocity ratio, around 2/3 at top of climb for a conventional turbofan engine [76], is expected to be higher due to energy being extracted from the core flow in the HRSG, ACEC and HCEC with mass extracted in the form of condensed water in the latter two as well. The calculated fuel consumption for a range of ζ between 80-150% is given in Figure 5.6. Above a value of around 146%, the model failed to converge, and thus higher values were not achievable. A possible reason is that as the fan inlet flow and thrust are constant, increasing ζ will reduce the core size, leading eventually to the core being unable to power the fan.

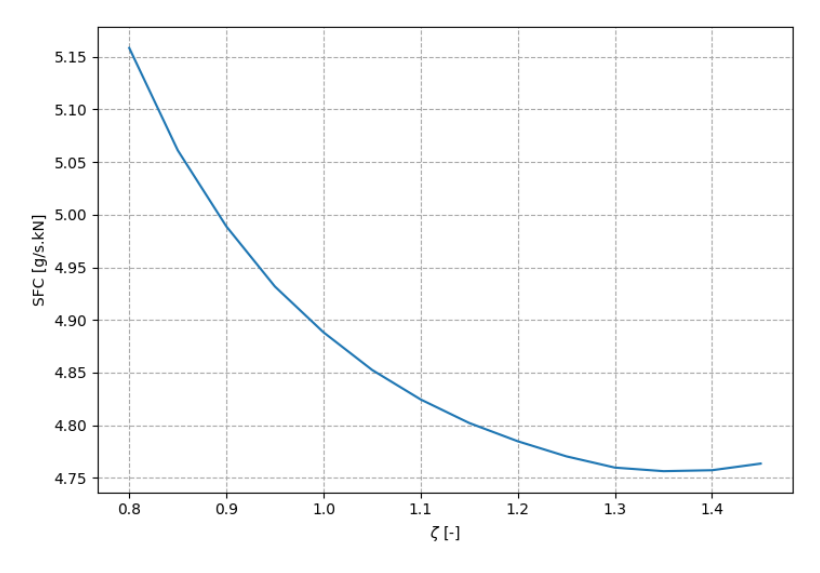


Figure 5.6: Fuel consumption as a function of the ideal exhaust jet ratio

The optimum ζ for fuel consumption at the design point is seen to be significantly higher than that of a conventional engine. The energy extraction from the core stream is enough that the bypass nozzle in fact has a higher exhaust velocity than the core. Another aspect to consider is that the engine core also reduces in size for the steam injection and water recovery engine due to the improved thermal efficiency and the injection of steam at the combustor, reducing the work and size of the high-pressure compressor. The reduction in core size can further reduce the core nozzle exhaust velocity, leading to a higher value of ζ .

The design point is chosen to be top of climb, but meeting the optimum ζ at this point does not guarantee an optimal value at other operating points. Cruise is the longest mission segment and as such there is a strong argument for minimising fuel consumption during cruise. The ideal exhaust jet ratio will not change as drastically from top of climb to cruise as it might from take-off to top of climb, but an increase in ζ is hypothesised as the engine throttle is reduced, reducing the core exhaust velocity relative to the bypass. This supports the choice of a slightly lower ζ at the top of climb design point, ensuring the cruise value is also close to or at optimum. Another aspect to note is that engines are in

practice likely designed with a lower ζ than the theoretical optimum $\zeta = \eta_{LPT} \times \eta_{fan}$ as when increasing ζ and thus power extraction from the core the added weight penalty and maintenance cost due to an added low-pressure stage outweigh the possible SFC decrease.

As discussed, the exhaust velocity ratio of the tertiary cooling bypass flow nozzle to the core nozzle is also varied by the addition of an additional booster in the bypass cooling flow stream. In Figure 5.7, the resulting fuel consumption is plotted. The ratio is varied in a range corresponding to the same resulting range in ζ as Figure 5.6, meaning that the two plots can be compared side-by-side.

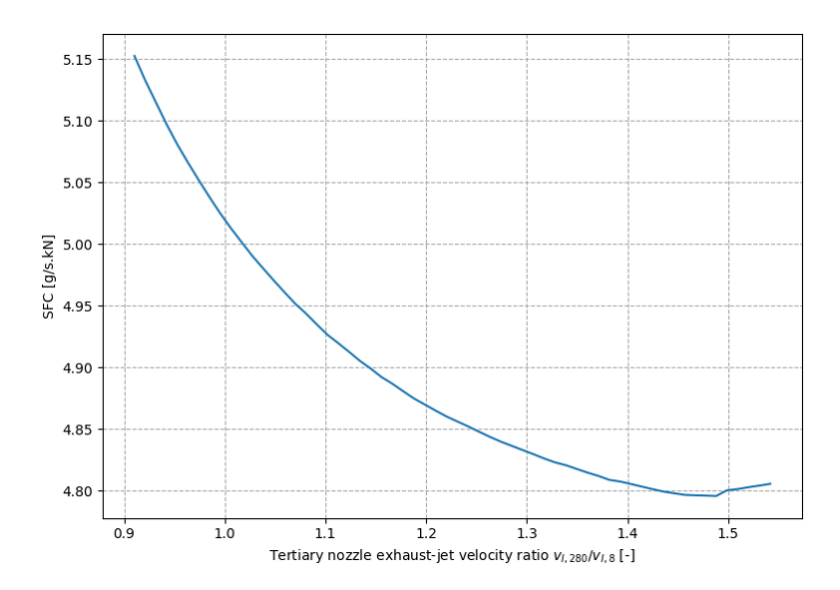


Figure 5.7: Fuel consumption as a function of the tertiary-to-core nozzle exhaust jet ratio

The trend is very similar between the two ratios, as the velocities are linearly dependent on each other. The optimum for the tertiary nozzle exhaust-jet velocity ratio lies slightly toward the right in comparison to the plot for ζ , but the added weight, cost of maintenance and complexity from additionally compressing the cooling bypass flow stream would outweigh the narrow performance benefit.

The change in ζ around the optimum value is small, which is beneficial as a wider range of operating points will be close to optimum. For the design point, a value of 130% is chosen for ζ , ensuring that in both top of climb and cruise the value is close to the optimum for fuel efficiency. This additionally ensures that should the calculation procedure lack accuracy, the value is still likely to be close to the optimum.

5.2.6. Overall pressure ratio

The change in SFC over WAR is plotted for a range of OPR in Figure 5.8.

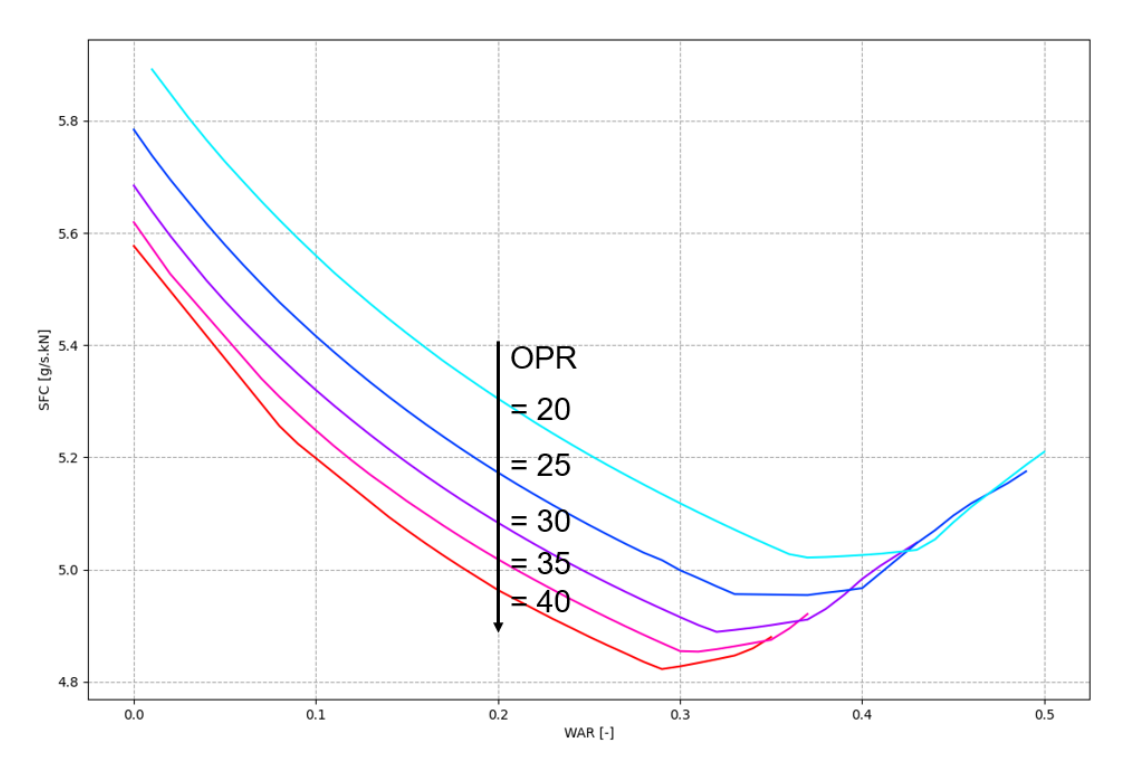


Figure 5.8: SFC variation with WAR for OPR ranging from 20 to 40

Increasing OPR leads to a reduction in SFC across most of the range of WAR, although SFC can be seen to be increasing with OPR for some higher values of WAR. These points are however away from the SFC optimum, and as such in general a higher OPR is favoured. There are diminishing benefits to an increasing OPR, however, with the same step increase in OPR leading to smaller improvements in SFC. In addition, the added weight and complexity of additional compressor stages is not included in this analysis, and would penalise the higher OPR. Instabilities in simulation prevented higher overall pressure ratios than 40 being simulated, so while a further optimum may exist, a value of 40 is chosen for the design point to ensure a solvable cycle model and recognising diminishing returns on SFC benefit as well as weight penalties.

Scaling effects are accounted for, with OPR up to 40 not having significant efficiency penalties due to the reduction of blade height in the final stages of the compressor. However, moving to higher OPR may well bring the blade height closer to the 10 mm limit expressed in Figure 4.3, leading to a rapid drop in compressor efficiency. Furthermore, the choice of 13 mm as a reference with no efficiency correction may need to be revised to ensure it is appropriate for the considered engine.

5.2.7. Steam pressure

In Figure 5.9, the fuel consumption for a range of steam pressures is shown. The SFC falls rapidly between 0 to 3 MPa steam pressure, but stays mostly constant after this. The reduction in SFC is additionally of lesser magnitude than for a variation in OPR, ζ , WAR or cooling flow rate. As such, the steam pressure is a less critical parameter in terms of fuel efficiency optimisation.

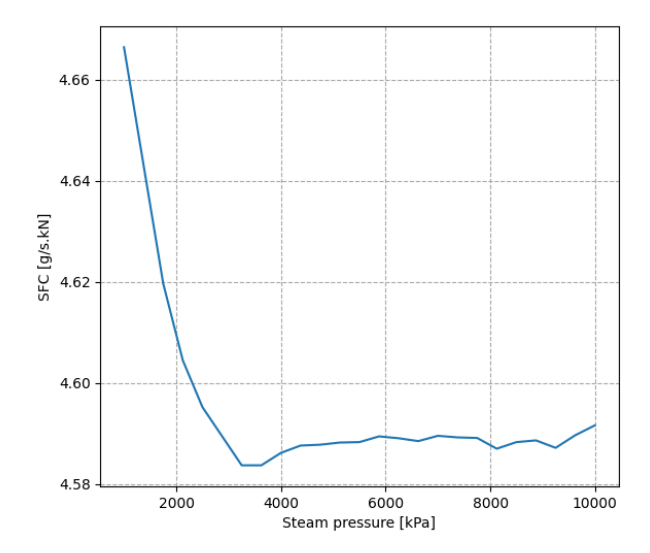


Figure 5.9: Fuel consumption variation with steam pressure

The sudden constant nature of the SFC curve after 4 MPa steam pressure predicts a limiting condition which restricts further improvements with further increasing steam pressure. This is seen also in Figure 5.10, where the steam turbine power is shown to rapidly increase with steam pressure before remaining constant after a steam pressure of 4 MPa. The power of the water pump is also plotted as a comparison. Water pumps are highly efficient and not expected to require a large amount of power, but it is still beneficial to ensure that the steam turbine produces at least enough power as the water pump requires, thus meaning the net shaft power from the water loop is positive.

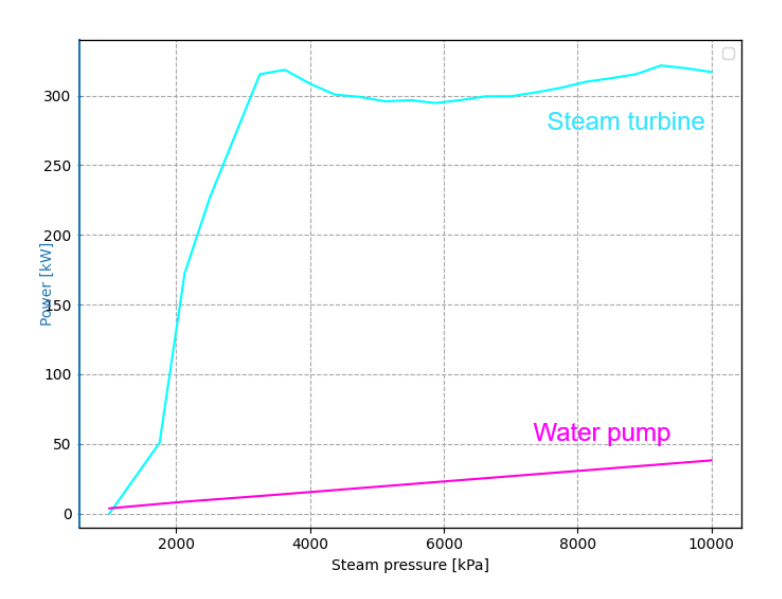


Figure 5.10: Steam turbine and water pump power as a function of steam pressure

In Figure 5.11, the pressures and steam quality at the inlet and outlet of the steam turbine are shown. As steam pressure increases, the quality before the turbine increases, while the quality after the turbine decreases. This can be explained by higher steam pressure before the turbine leading to further possible expansion in the steam turbine, reducing the outlet temperature of the turbine. For low steam pressures the steam turbine becomes infeasible, functioning instead as a compressor, which is due to the fact that the turbine outlet pressure is limited by a fixed overpressure of the steam for injection into the combustor, corresponding to a pressure of around 1.7 MPa.

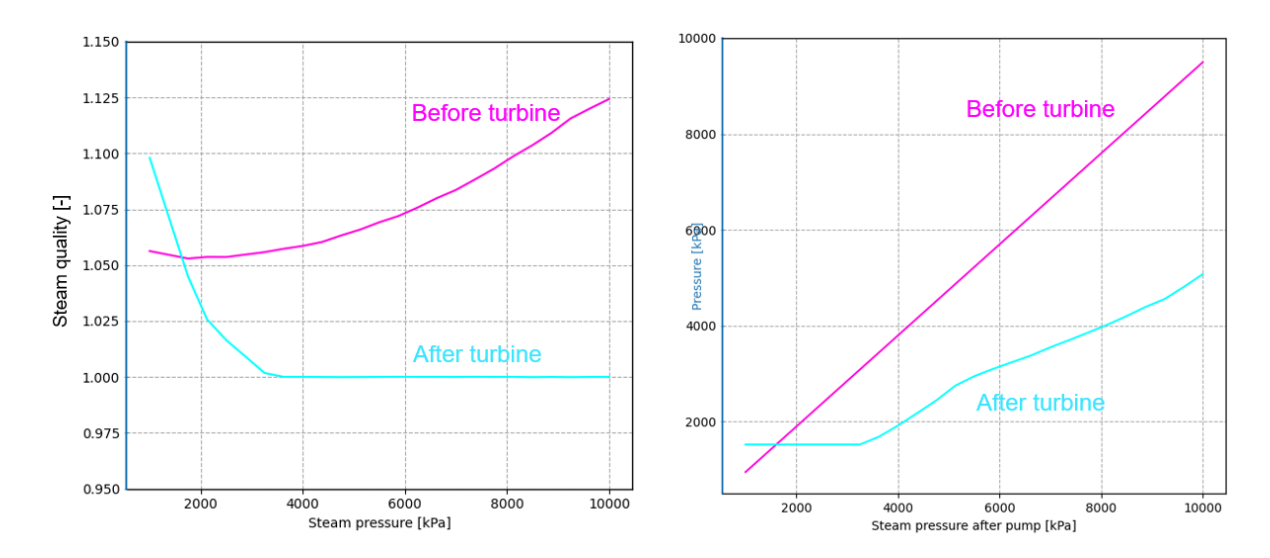


Figure 5.11: Flow quality and pressures in the steam turbine for varying steam pressure after the pump

The quality plot provides an explanation for the constant SFC and steam turbine power above 4 MPa steam pressure, as the turbine outlet quality limit is reached at this point. For lower steam pressures, the maximum possible expansion is reached in the steam turbine, with the outlet pressure equal to the steam injection overpressure limit. After 4 MPa, with further reduction in quality not being possible without compromising the turbine, the quality is fixed and the pressure after the turbine keeps increasing.

For the design point, a value of 4 MPa or 40 bar is chosen as the steam pressure after the pump, as beyond this there is no improvement in SFC, while higher steam pressures will lead to heavier steam loop components and feed lines.

5.3. Design and off-design performance

The engine is designed to be water self-sufficient at the top of climb point, and its geometric parameters and scaling factors fixed. The designed engine is then simulated for two off-design points: mid-cruise and take-off. The performance in all three points is presented and discussed in the following section.

5.3.1. Overall engine performance

An overview of the engine's design and off-design performance is given in Table 5.3. The operating conditions, target thrust and key cycle parameters are presented for top of climb, mid-cruise and take-off.

Top of climb (Design)	Mid-cruise	Take-off
35000	35000	0
0.78	0.78	0.25
10	0	15
38.178	28.686	138.194
0.177	0.122	0.393
4.645	4.269	2.974
2.94	2.48	6.95
3.09	3.43	2.26
2.92 (94.4%)	3.43 (97.9%)	1.92 (84.7%)
0.17 (5.5%)	0.070 (2.1%)	0.35 (15.3%)
+5%	+38%	-67.5%
134	0	4156
1.2%	0%	9.8%
	35000 0.78 10 38.178 0.177 4.645 2.94 3.09 2.92 (94.4%) 0.17 (5.5%) +5% 134	35000 35000 0.78 0.78 10 0 38.178 28.686 0.177 0.122 4.645 4.269 2.94 2.48 3.09 3.43 2.92 (94.4%) 3.43 (97.9%) 0.17 (5.5%) 0.070 (2.1%) +5% +38% 134 0

Table 5.3: Overview of design and off-design performance

The SFC reduction compared to the baseline engine without steam injection is around 11%, which is a significant improvement with the caveat that this neglects the impacts of the various added components to the cycle. Most notably, the weight penalty introduced by the heat exchangers is significant and likely to outweigh much of this benefit. Nonetheless, an increase this large is notable and with an optimisation of heat exchanger design a strong case can be made for the use of steam injection.

The injected steam flow rate is significantly higher at take off compared to the other two points due to a constant WAR being chosen for all operating points, as the core flow rate is significantly higher at sea level. This imposes a higher required condensation flow rate, while also meaning that a higher total mass of water is present in the flow for condensation. With temperatures throughout the engine core as well as in the bypass stream increasing, condensation is negatively affected as flow must be cooled by a larger temperature difference to be brought to the water saturation temperature and because the available temperature difference between the two streams drops.

The design point, as stated, is designed for a condensation margin of 5% to account for a 95% water separation efficiency. If the engine is water self-sufficient at top of climb, it is hypothesised that it will also be so for cruise for a number of reasons, and this trend is observed with a 39% condensation margin reached for the cruise point. With the engine throttle reduced from top of climb to cruise, core flow temperatures drop, leading to less required heat transfer in the condenser. As the bypass cooling flow temperature will remain similar with a similar mass flow rate, the ACEC is able to condense more water out of the flow. However, given that cruise is a large section of the mission profile, it may be that sizing the exhaust condensers for top of climb will lead to a very high weight penalty due to the size of the components, meaning the engine is overdesigned for much of its mission. In take-off, the temperatures inside the core are large and as such a large rate of heat transfer is required to condense water out of the flow. In addition, the bypass air is significantly hotter at lower altitude, further decreasing the total heat transfer possible in the exhaust condensers. As such, reaching water self-sufficiency is expected to be highly difficult at take-off, a fact that is confirmed by the negative -67.5% condensation margin. Thus, a water supply would be required for at least take-off and likely much of the climb phase if constant WAR is desired to be kept for the entirety of the mission. An improvement in heat transfer

could also be achieved by considering another type of heat exchanger, such as a plate heat exchanger. While less suitable for high pressure and temperature applications, plate heat exchangers offer significantly larger heat transfer area, effectiveness and compactness, all of which are desirable considering the demands set by the steam injection. The large size of the exhaust condensers and the resulting implications are discussed further in Section 5.4.

The steam turbine power increases significantly from top of climb to take-off due to the significantly higher steam flow as well as higher core temperatures, leading to a higher heat transfer across the HRSG and a greater possible expansion over the turbine. The turbine also provides a larger fraction of the total power of the engine, which shows that the advantage gained from steam injection is perhaps larger at take-off. However, the difficulty of condensing the required large water flow rate remains and in the current design, water would need to be carried on board for take-off and climb, likely negating the gained performance benefits.

In cruise, the reduction in core temperatures aids condensation but reduces the available temperature difference in the HRSG. The steam turbine power drops to zero as the HRSG is not able to transfer enough heat to raise steam, and as such expansion without damaging the turbine is not possible. This means either that the steam turbine cannot be included in the cycle, or a functionality for the steam flow to bypass the turbine needs to be implemented. The turbine cannot be used for an outlet quality less than 1, but this limit does not extend to steam injection, where the quality is not critical.

Point	Top of climb (Design)	Mid-cruise	Take-off
Engine inlet mass flow [kg/s]	342	327	28
Core mass flow [kg/s]	12.5	11.0	813
Bypass mass flow [kg/s]	329	316	785
ACEC cooling flow [kg/s]	140	135	334
Fan BPR [-]	26.40	28.78	27.96
Cooling flow splitter BPR	1.350	1.346	1.350

Table 5.4: Mass flows and BPR for design and off-design points

In Table 5.4, the engine mass flows and bypass ratios for the fan and cooling flow splitter are presented. Compared to the baseline engine and convenctional engines, the fan BPR for all points is fairly large. This is largely due to the reduction in core size observed in the steam injection cycle. The addition of steam in the combustor reduces the required work of the high-pressure compressor, leading to a smaller core flow. The fan BPR increases from the design point to cruise likely as the core flow drops as the engine throttle is reduced, while the bypass flow sees a smaller decrease. In take-off, the fan BPR is between the values of the top of climb and mid-cruise points.

The bypass cooling flow splitter has a low BPR, with around 31% of the bypass flow used for cooling in the ACEC at the design point. The splitter BPR stays constant for take-off, while a small reduction is seen from top of climb to cruise. While this difference may be introduced by the calculation procedure, it could also be a result of changing conditions or choking at the secondary and tertiary nozzles, as the nozzle areas are constant between design and off-design.

Net thrust F_n [kN]	Top of climb (Design)	Mid-cruise	Take-off
Primary (core) nozzle	0.89 (2.3%)	0.57 (2.0%)	3.84 (2.8%)
Secondary (bypass) nozzle	20.5 (53.8%)	15.5 (54.1%)	76.8 (55.6%)
Tertiary (bypass cooling) nozzle	16.7 (43.8%)	12.6 (43.9%)	57.5 (41.6%)
Total	38.2	28.7	138

Table 5.5: Total thrust and distribution over the primary, secondary and tertiary nozzles

Finally, the distribution of thrust between the three nozzles is given in Table 5.5. The distribution of thrust over the nozzles is fairly similar for all points. The core nozzle produces a marginal amount of the total thrust, making up between 2% and 2.8% of the total, compared to modern hgih-bypass

turbofan engines where 10-30% of the thrust might be produced by the core. This is in part due to the smaller core of this engine compared to a conventional engine, but more significantly due to the removal of energy from the core stream in the heat exchangers leading to a lower core exhaust velocity. Furthermore, while the cooling flow rate is less than a third of the total bypass flow, the thrust provided by the stream is over 40%. This is due to the heating of this cooling stream in the ACEC, which outweighs the pressure loss in the component. Furthermore, it can be hypothesised that the propulsive efficiency of this cycle will be higher than a conventional engine as a significantly larger fraction of thrust is produced by the bypass stream and the core size decreases, increasing the BPR and reducing the effective exhaust velocity.

The large contribution of the cooling flow to the thrust highlights the importance of estimating the pressure drop over the ACEC in the cooling stream. If the assumed pressure drop is low, the performance of the engine may be overestimated, or conversely for too high a pressure drop the total thrust may be underestimated. In either case, detailed analysis of the pressure drop is recommended for future studies in order to accurately determine the engine's performance.

5.4. Heat exchanger sizing

The detailed heat exchanger model is used to simulate the design case and both off-design cases. In Table 5.6, the calculated total heat transfer coefficients for all heat exchangers are given.

The overall heat transfer coefficient U stays fairly constant over the entire HRSG, which is expected as the flow is limited in heat transfer on the exhaust flow side, due to water and steam having a higher heat capacity than the gaseous exhaust mixture. The exhaust flow remains single-phase through the HRSG, but an increase in Reynolds number leads to a higher Nusselt number and thus heat transfer coefficient. As the exhaust cools over the HRSG, Re increases due to an increase in density that is not outweighed by the increase in dynamic viscosity with temperature. The overall heat transfer coefficient reduces also from top of climb to cruise. While the core flow is cooler the pressures in the core are also lower and the flow is less dense, leading to a lower Reynolds number and rate of heat transfer. The dynamic viscosity additionally increases with the decrease in temperature, further reducing Reynolds. During take-off, the core flow is much denser and hotter, leading to a higher Reynolds number and heat transfer coefficient.

Overall heat transfer coefficient [W/(m ² K)]	Top of climb (Design)	Mid-cruise	Take-off
Economiser U_{econ}	267	253	557
Evaporator U_{evap}	242	230	493
Superheater U_{super}	230	223	467
ACEC dry cooler $U_{ACEC,dry}$	58.0	54.2	41.7
ACEC condenser $U_{ACEC,cond}$	328	316	47.4
$oxed{HCEC\ U_{HCEC}}$	146	148	133

Table 5.6: Overall heat transfer coefficients for heat exchanger sections

The dry cooler is the component with the lowest heat transfer coefficient across all operating points, as both flows are single-phase vapour flows with moderate Reynolds number. The flows are also fairly balanced, having similar total stream capacity, and as such enhancing heat transfer on both the shell and tube sides should be considered if the total heat transfer area is to be minimised. The value of U drops from top of climb to cruise possibly due to a decrease in Re caused by lower core flow temperatures. In take-off, however, U drops further. In cruise and top of climb, the flow is limited in heat transfer coefficient on the exhaust side, while at take-off the bypass flow becomes limiting.

The condenser has a higher rate of heat transfer for the top of climb and cruise points, as condensation significantly improves the heat transfer coefficient. As the total In take-off however, the condenser U is significantly lower than for the other two points, being only 14% of the top of climb value. This is because the heat transfer is limited on the bypass side, where the heat transfer coefficient decreases. The exhaust will have a much higher coefficient of heat transfer due to condensation, so enhancing heat transfer on the bypass side could lead to great improvements in total heat transfer and help alleviate the lack of sufficient condendsation at take off. As the bypass flow is also the outer flow in this heat exchanger, an increase in heat transfer area could be achieved by adding fins to the outside of the heat exchanger tubes.

The HCEC heat transfer coefficient remains similar throughout the operating points as it is limited by the capacity of the hydrogen flow rather that the exhaust flow. As the hydrogen conditions stay fairly similar in the heat exchanger, the total heat transfer coefficient does not change much.

Point	Top of climb (Design)	Mid-cruise	Take-off
Economiser A_{econ} [m ²]	58.0	60.6	43.6
Evaporator A_{evap} [m ²]	224	226	208
Superheater A_{super} [m ²]	4.75	0	35.8
Total HRSG $(A_h)_{HRSG}$ [m ²]	287		
Dry condenser A_{dry} [m ²]	991	650	776
Condenser A_{cond} [m ²]	1965	2306	2180
Total ACEC $(A_h)_{ACEC}$ [-]	2956		
HCEC $(A_h)_{HCEC}$ [m ²]	52.7		

Table 5.7: Overview of total heat transfer area A_h distribution in design and off-design

In Table 5.7, the relative sizes of the sections of the heat exchangers are shown. The total HRSG, ACEC and HCEC heat transfer areas are constant as the design is fixed. The HRSG sizing does not change much from top of climb to cruise, with the caveat of the superheater missing in cruise due to the lower achieved steam quality. In take-off, the superheater is a lot larger and in accordance with this the outlet quality of the steam is higher.

The dry cooler is smaller than the condenser for all operating points, with the condenser once again highlighted as a critical component which currently leads to an infeasible engine. Even the dry condenser area is above what is considered reasonable and investigations into heat transfer enhancement as well as a change to a plate heat exchanger are encouraged.

The HCEC area is fixed according to a reasonable effectiveness of 0.95, and stays constant over the operating points.

Point	Top of climb (Design)	Mid-cruise	Take-off
Economiser effectiveness [%]	59.8%	64.5%	47.7%
Evaporator effectiveness [%]	92.9%	95.3%	88.2%
Superheater effectiveness [%]	7.74%	[-]	55.6%
Total HRSG effectiveness [%]	82.1%	79.7%	84.7%
Dry condenser effectiveness [%]	93.3%	84.2%	44.2%
Condenser effectiveness [%]	92.0%	91.6%	38.1%
Total ACEC effectiveness [%]	93.5%	75.7%	92.6%
HCEC effectiveness [%]	95%	98.9%	72.5%

Table 5.8: Overview of heat exchanger effectiveness

In Table 5.8, the effectiveness of the heat exchangers is presented for design and off-design conditions. The HRSG and ACEC both reduce in effectiveness in cruise, achieving a lower heat transfer rate of the maximum possible. At take-off, the performance of the HRSG improves mostly due to the superheater, as the evaporator and economiser individual effectivenesses decrease from their design values. The dry condenser and condenser effectiveness both see a strong decrease in individual effectiveness, but in fact the overall effectiveness found from inlet and outlet conditions decreases little.

Stream	Point	Top of climb (Design)	Mid-cruise	Take-off
Exhaust	HRSG (superheater) inlet T [K]	795	712	871
	Evaporator inlet T [K]	787	712	803
	Economiser inlet T [K]	542	537	550
	HRSG (economiser) outlet T [K]	414	381	475
	ACEC dry cooler outlet T [K]	349	346	383
	ACEC condenser outlet T [K]	314	290	354
	HCEC outlet T [K]	311	285	352
Water	HRSG (economiser) inlet T [K] (χ [-])	327 (-0.50)	293 (-0.61)	359 (-0.39)
	evaporator inlet T [K] (χ [-])	522 (0)	528 (0)	515 (0)
	superheater inlet T [K] (χ [-])	521 (1)	527 (0.71)	514 (1)
Steam	HRSG (superheater) outlet T [K] (χ [-])	533 (1.03)	527 (0.71)	670 (1.27)
Bypass	ACEC (condenser) inlet T [K]	289	268	338
	ACEC (condenser) outlet T [K]	344	340	368
	ACEC (dry cooler) outlet T [K]	353	344	409
Hydrogen	HCEC inlet T [K]	132	132	132
	HCEC outlet T [K]	305	288	295

Table 5.9: Overview of temperature and quality across heat exchangers in design and off-design

Finally, the temperatures across the heat exchangers are given in Table 5.9. For the water/steam flows, the quality is also presented. As can be seen, saturated steam conditions are not reached at the top of climb point, which prevents the use of a steam turbine with the current design. Conversely at take-off, a high outlet quality is achieved, allowing for further expansion in the turbine and a high resulting steam turbine power.

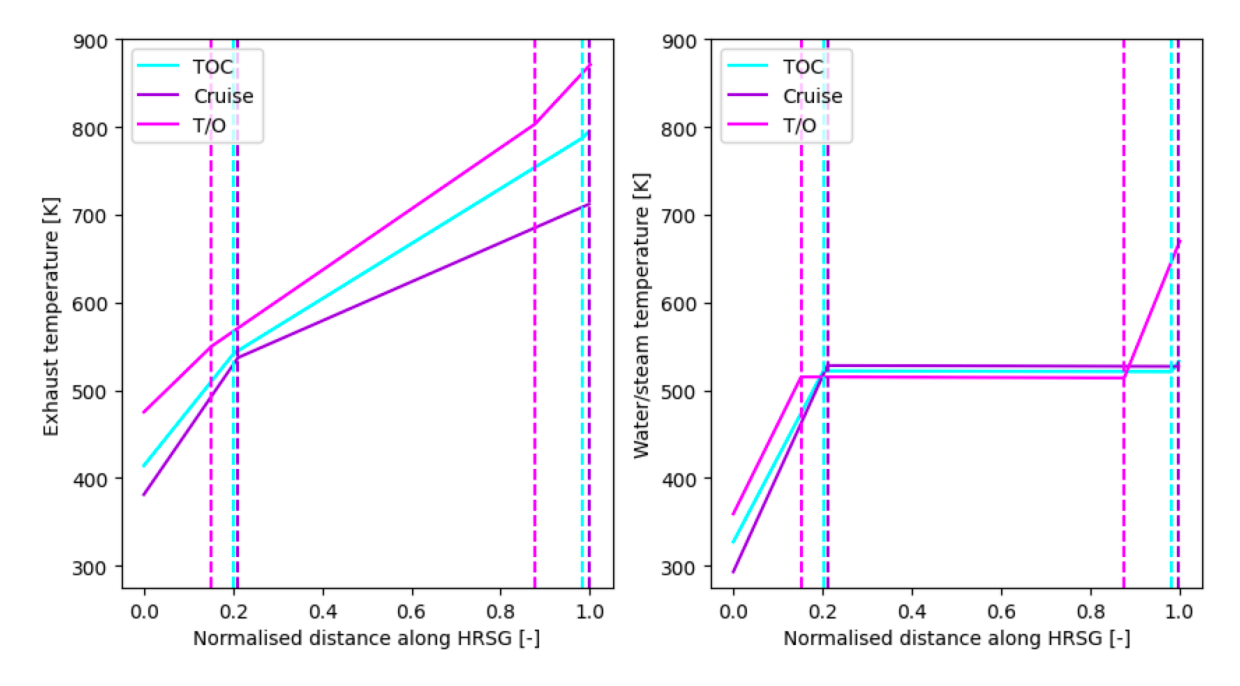


Figure 5.12: Temperature distribution of the exhaust and water/steam flow across the HRSG

In Figure 5.12, the temperatures across the HRSG are illustrated for both the exhaust and water/steam streams. Dotted lines are used to indicate the different sections (economiser, evaporator, superheater) of the HRSG and the horizontal axis shows the normalised distance along the component. This is calculated by assuming the distance distribution of the three sectors to be equal to the total heat transfer area distribution.

The exhaust temperatures follow the expected trend, being cooler in mid-cruise compared to top of climb due to reduced engine throttle. In take-off, temperatures are similarly expected to be higher as the engine is at high throttle and the atmospheric temperature is high. Similarly, the bypass flow is hotter at take-off than both cruise and top of climb, and lower in cruise than top of climb. The evaporator inlet temperature shows an increase in saturation temperature from top of climb to cruise, and a reduction from top of climb to take-off. The relative sizes of the economiser, evaporator and superheater are once again shown to be similar for cruise and top of climb, while the superheater increases in size and the economiser decreases in size for take off. The reduction in economiser size can be explained by an increase in engine temperatures and thus the incoming water temperature, which brings the flow closer to its boiling temperature. This is aided further by the boiling temperature also decreasing as seen in the evaporator temperatures. The superheater also grows as the high temperature of the exhaust flow allows for a greater total heat transfer rate.

In Figure 5.13, the exhaust temperature is shown along the two condensers, the ACEC and HCEC. Once again, the dotted lines show the sections of the three condensers: the ACEC dry cooling section, the ACEC condenser section and the HCEC condenser section. The HCEC is relatively small and equal in size for all operating points as discussed in Section 4.6. The overall exhaust temperatures are higher at top of climb compared to thrust due to the higher engine throttle level, while for take off the increase in ambient temperature leads to even higher temperatures.

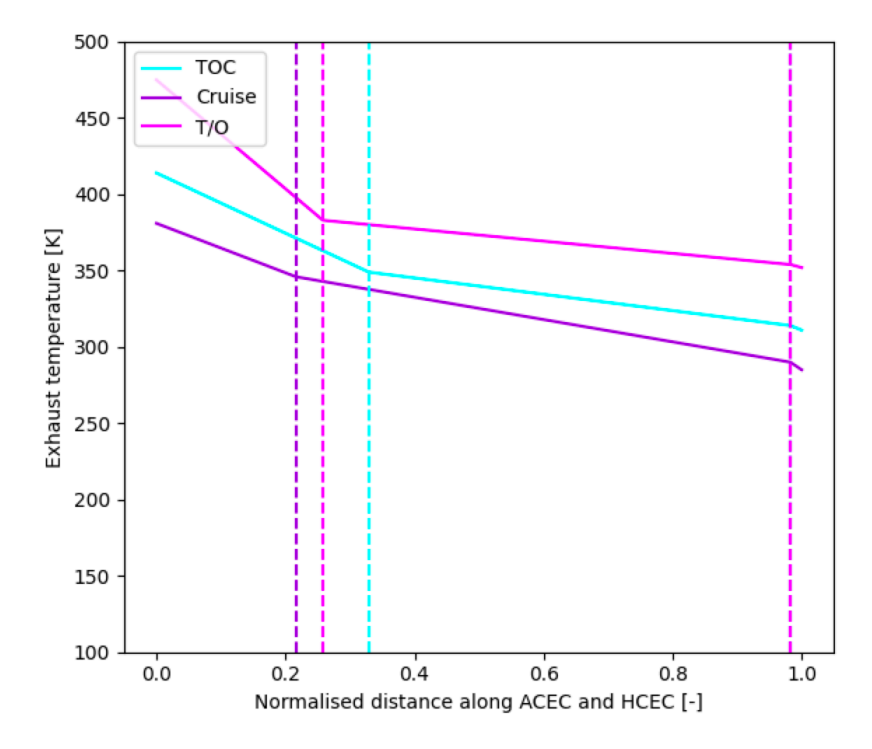


Figure 5.13: Temperature distribution of the exhaust flow across the ACEC and HCEC

Figure 5.14 shows the temperatures of the two cooling streams - the bypass flow and the hydrogen flow. The hydrogen flow experiences a much higher and temperature change for all operating points and also enters the condenser at the same temperature. The hydrogen outlet temperature drops from top of climb to cruise as the heat transfer rate as the exhaust temperature entering the HCEC drops, limiting the total temperature change.

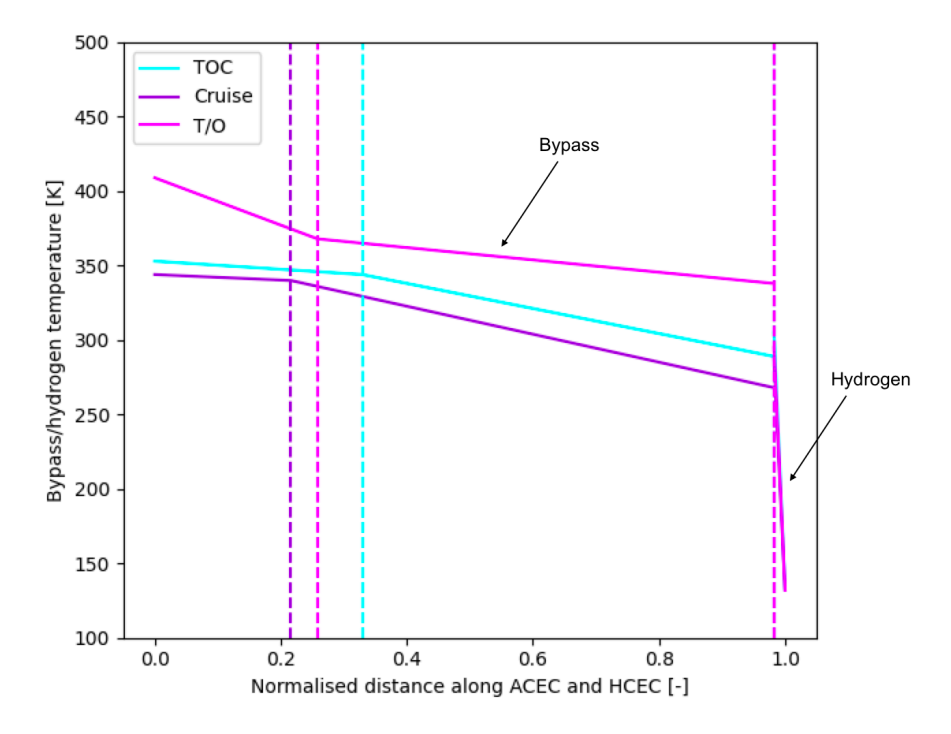


Figure 5.14: Temperature distribution of the bypass and hydrogen flow across the ACEC and HCEC

5.5. Recommendations for future work

Due to the limited scope of this project, there were multiple points where further detailed study was neglected but could be of interest. Below, some of these are summarised as recommendations for further work.

Detailed heat exchanger design

The heat exchangers are shown to be a crucial part of the steam injection and water recovery cycle as they are integral to supplying the steam for injection, while imposing a considerable weight and volume penalty on the engine as a whole. With the benefits of the cycle dependent on a feasible design of the heat exchangers, a detailed geometric design study is recommended in order to show that such a cycle is feasible, as well as to quantify the impact of adding the HRSG, ACEC and HCEC. This holds especially the ACEC which has been shown to require a significant total area of heat transfer, which currently too high to guarantee a feasible engine.

Mission analysis

The current engine has been designed for top of climb and is shown to be fully water self-sufficient at the design point as well as at cruise, while failing at take-off. A detailed analysis of the required tank size for take-off and likely most of climb could be completed to estimate the weight penalty and perhaps require a re-design to ensure water self-sufficiency already at take-off or climb. On the other hand, designing the heat exchangers for cruise instead might reduce their weight enough to counteract the weight added by an additional water tank for take-off and climb, which can motivate allowing water non-self-sufficiency at some points in the mission.

Engine weight estimation

An overall estimate of the engine weight is recommended to be able to better compare its performance to other engines. While simulations show promising results for the SFC of the hydrogen-fuelled steam injection and water recovery cycle, a number of added components in the form of heat exchangers and additional hydrogen fuel systems are expected to reduce the calculated improvement.

Engine emission estimation

Emissions are not estimated for this engine, but an analysis is recommended to verify the environmental advantages provided by this engine. While hydrogen will predictably produce less carbon emissions, a detailed study of contrails could be of interest considering the level of humidity in a hydrogen engine's exhaust. Furthermore, NO_X emissions, which are often high for hydrogen combustion, might be reduced considerably by steam injection. As emissions are a large motivator in choosing both hydrogen and steam injection as novel technologies, a quantitative study can verify the expected benefits.

6

Conclusion

Owing to the main driver of operating cost as well as rising fear of future regulation and penalties, the aircraft industry is driven to improve fuel consumption and reduce the environmental impact of the engine. Two promising technologies to tackle these are introduced in this work: the steam injection cycle, and the use of hydrogen as a fuel. The combination of these two technologies in the hydrogen-fuelled steam injection cycle is shown to have a strong synergy due to the high humidity of hydrogen exhaust, the strong heat sink capabilities of cryogenic hydrogen and the effect of steam injection offsetting the potentially higher energy consumption and NO_X emissions of hydrogen aircraft. Neither technology has passed the demonstration stage and their combination is highly novel, identifying a research gap. However, a high degree of risk and complexity is recognised for the considered cycle, with the condenser and evaporator highlighted as the most challenging and important components to model.

The research objective is to determine the performance of a hydrogen-fuelled engine with steam injection and water recovery. Two research questions are posed: investigating how to build an accurate model for the cycle, and determining the engine's performance in terms of thrust-specific fuel consumption and the ability to reach water self-sufficiency at both on- and off-design points. The first question is answered by developing a general cycle model in NPSS which is supplemented by a detailed heat exchanger model which determines a more accurate performance of the heat exchangers, notably the rate of condensation of water. The second question is answered with water self-sufficiency being reached at the design point (top of climb) and one of the off-design points (mid-cruise), while the third (take off) off-design point does not reach the required rate of condensed water. Performance evaluation at design and off-design is also successfully completed, with a reduction in SFC seen compared to the baseline engine.

Modelling is accomplished using the *Numerical Propulsion System Simulation* (NPSS) software, building upon a previously developed kerosene-fuelled engine cycle model utilising steam injection and water recovery. Custom elements are developed to model the heat exchangers in the cycle, and the solver setup and design parameters are outlined in detail. An overview of the cycle model is presented in Figure 1.

The critical components to the steam injection and water recovery cycle are the *heat recovery steam generator* HRSG, the *air-cooled exhaust condenser* ACEC and the *hydrogen-cooled exhaust condenser* HCEC. The core exhaust flow passes through the HRSG where its energy is harnessed to generate steam. After the HRSG, the exhaust passes through the ACEC and HCEC, where water from the humid exhaust is condensed. The ACEC is cooled by a fraction of the bypass flow, while the HCEC is cooled by the hydrogen flow, functioning also as a fuel pre-heater. The condensed water is separated from the flow and pumped through the HRSG, evaporating before injection into the combustor. The steam is also expanded through a turbine to provide additional shaft power.

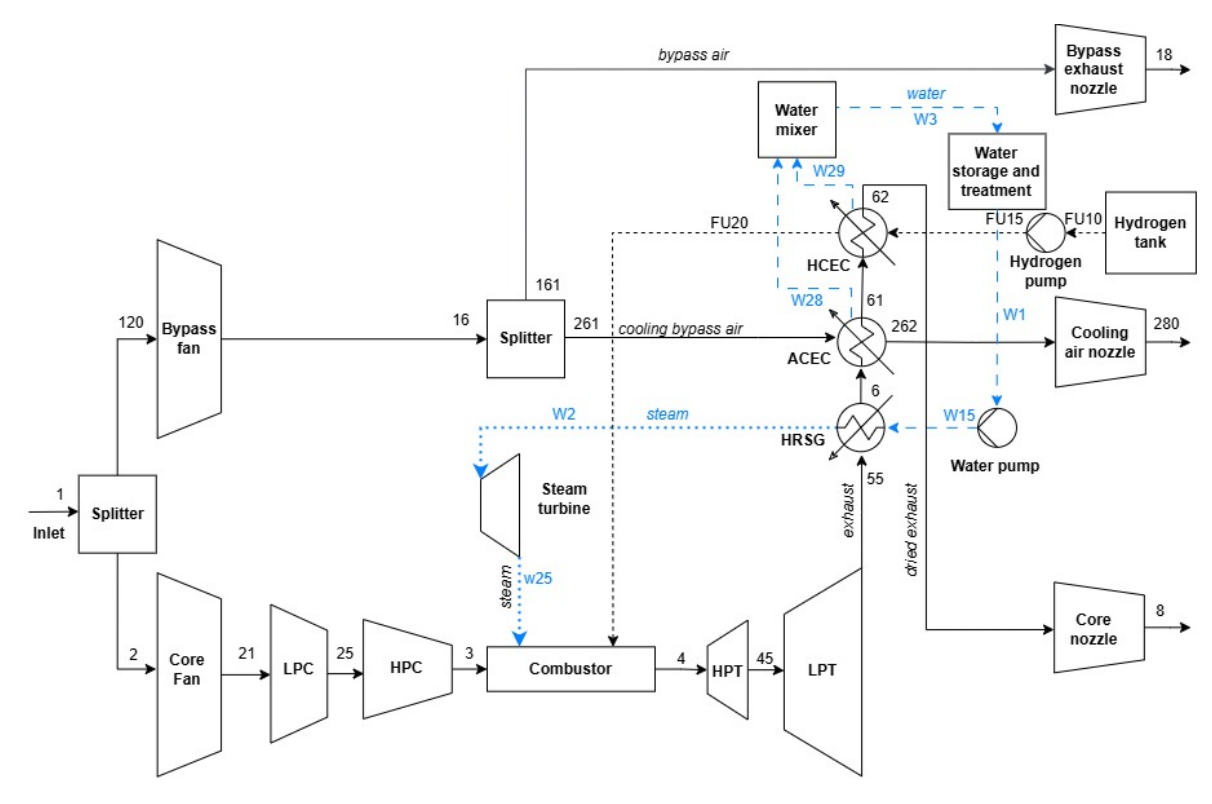


Figure 6.1: Overview of the steam injection and water recovery cycle model with station numbering

A number of design parameters are investigated to reach a design point which is water self-sufficient and minimises SFC at the top of climb operating point, summarized in Table 6.1.

Water-to-air ratio WAR [-]	0.33
Cooling flow ratio W_{cool}/W_{core} [-]	11.3
Ideal exhaust jet velocity ratio ζ [-]	1.3
Overall pressure ratio OPR [-]	40
Steam pressure [MPa]	4

Table 6.1: Final values of parameters for the top of climb design point determined in the study

In addition to the cycle model, a detailed heat exchanger model is developed to model the HRSG, ACEC and HCEC in detail, allowing for sizing estimation to be completed at the design point. Various configurations are explored, after which the design of heat exchangers is fixed and off-design conditions simulated. The detailed heat exchanger model is used to augment the overall cycle model by correcting the assumed effectiveness values by more accurately estimated ones, as well as fixing the cooling flow rate to ensure water self-sufficiency at the design point.

Parameter	Value
F_n [kN]	38.178
SFC [g/(kNs)]	5.215

Table 6.2: Overview of baseline hydrogen engine performance at top of climb

In Table 6.2, the performance of the baseline hydrogen engine without steam injection are presented. The results of simulating the steam injection and water recovery hydrogen cycle, integrating the overall model with the detailed heat exchanger model, are provided in Table 6.3.

Point	Top of climb (Design)	Mid-cruise	Take off
F_n [kN]	38.178	28.686	138.194
SFC [g/(kNs)]	4.645 (-18%)	4.269	2.974
Injected steam \dot{m}_{inj} [kg/s]	2.94	2.48	6.95
Total condensed water \dot{m}_{cond} [kg/s]	3.09	3.43	2.26
ACEC condensed water [kg/s]	2.92 (94.4%)	3.43 (97.9%)	1.92 (84.7%)
HCEC condensed water [kg/s]	0.17 (5.5%)	0.070 (2.1%)	0.35 (15.3%)
Condensation margin [%]	+5%	+38%	-67.5%
Steam turbine power [kW]	134	0	4156
Turbine power fraction [%]	1.2%	0%	9.8%

Table 6.3: Overview of engine performance

Water self-sufficiency is reached for both the top of climb design point and the cruise off-design point. At top of climb, a condensation margin of 5% excess of the required flow for steam injection is achieved, which accounts for an assumed 95% separation efficiency of condensed water from the flow. In cruise, a significantly higher excess of 38% is condensed. while a significant deficit in condensed water is seen for take-off, necessitating the inclusion of a water tank to provide additional water during take-off and part of the climb. The inclusion of a water tank together with the high rate of condensation in cruise could allow for solutions such as condensing and storing water at cruise during one mission for use during the descent and even the take off and climb segment of the following mission. Alternatively, redesigning the ACEC completely would be necessary to ensure water sufficiency at all operating points.

The ACEC provides nearly all of the condensed water flow for both top of climb and cruise, which is due to the small relative size of the HCEC. While hydrogen has a high heat capacity and provides a high maximum temperature difference due to its low storage temperature, the small fuel flow rate compared to the core mass flow rate limits the heat transfer by the total stream capacity of the hydrogen flow. In take off, the HCEC provides a notably larger fraction of total condensation at 15%, but this is a result of the drop in heat transfer and signficant reduction of condensation in the ACEC for this operating point.

Conversely to condensation, water evaporation is not successful in cruise, with the HRSG unable to raise pure steam. This impacts the steam turbine included in the cycle model, which must be bypassed at this operating point. The inclusion of a steam turbine is shown to generate nearly 10% of the total engine shaft power in take off while having a small impact at top of climb. With the expanded power largely limited by the quality of steam at the turbine exit, removing the turbine from the cycle entirely relaxes that design constraint and also slightly reduces the complexity of the engine. With steam injection not strictly requiring saturated steam, a cycle without a steam turbine can be a wiser choice to avoid redesign or heat transfer enhancements in the HRSG.

A significant 18% improvement in thrust-specific fuel consumption is achieved compared to the baseline hydrogen engine, but this is with the caveat of weight estimation missing from detailed analysis. The heat exchangers, specifically the ACEC, will add a significant amount of weight, complexity and maintenance cost to the engine, the effect of which has not been quantified and may outweigh the improvement in SFC.

Results of the detailed heat exchanger areas and effectivness are given in Table 6.4. The ACEC is infeasibly large for all operating points and significant redesign is required to reduce the required heat transfer area and the resulting engine weight. This could be achieved by adding fins on tubes in order to increase the total heat transfer area or by considering other configurations such as a plate heat exchanger. The HRSG and HCEC sizes are reasonable and show promise for the steam injection and water recovery cycle if the ACEC design is resolved.

Point	Top of climb (Design)	Mid-cruise	Take-off
Total HRSG $(A_h)_{HRSG}$ [m ²]	287		
HRSG effectiveness [%]	82.1%	79.7%	84.7%
Total ACEC $(A_h)_{ACEC}$ [m ²]	2956		
ACEC effectiveness [%]	93.5%	98.9%	72.3%
$HCEC\ (A_h)_{HCEC}\ [m^2]$	52.7		
HCEC effectiveness [%]	95%	95%	95%

Table 6.4: Overview of total heat transfer areas and effectiveness in design and off-design

The cycle benefit of steam injection and water recovery is shown to be large, improving the specific fuel consumption from 5.215 g/s.kN without steam injection to 4.645 g/s.kN with steam injection, as shown in Table 5.1 and Table 5.3. The cycle has a smaller core than a conventional engine, with a high BPR. Despite the improvements in fuel consumption, uncertainties remain about the weight of the added heat exchangers, the pressure drop across them and the design of the exhaust condenser, which is identified as a critical point for the success of this engine. If a suitable configuration is found for the ACEC to reduce its size to feasible limits, the cycle shows an interesting possibility for harnessing two complex and novel technologies in order to improve fuel consumption and reduce emissions. The specific synergy with hydrogen is notable as steam injection has not proven as successful in kerosene engines [14], whereas it can help alleviate some of the problems faced by hydrogen-fuelled engines and encourage a transition to the carbon-free fuel.

- [1] European Commission, Reducing emissions from aviation: Aviation emissions, Accessed on 11.11.2024. [Online]. Available: https://climate.ec.europa.eu/eu-action/transport/reducing-emissions-aviation_en#aviation-emissions.
- [2] International Civil Aviation Organization (ICAO), *Economic impacts of covid-19 on civil aviation*, Accessed on 08.11.2024, 2022. [Online]. Available: https://www.icao.int/sustainability/Pages/Economic-Impacts-of-COVID-19.aspx.
- [3] R. Singh, G. Ameyugo, and F. Noppel, "4 jet engine design drivers: Past, present and future," in *Innovation in Aeronautics*. Woodhead Publishing, 2012, pp. 56–82.
- [4] F. Yin and A. G. Rao, "A review of gas turbine engine with inter-stage turbine burner," *Progress in Aerospace Sciences*, vol. 121, Dec. 2020. DOI: https://doi.org/10.1016/j.paerosci.2020.100695.
- [5] Airbus, *Airbus reveals new zero-emission concept aircraft*, Toulouse, France, Sep. 2020. [Online]. Available: https://www.airbus.com/en/newsroom/press-releases/2020-09-airbus-reveals-new-zero-emission-concept-aircraft.
- [6] Clean Aviation, *Programme overview and structure*, Accessed on 27.11.2024. [Online]. Available: https://www.clean-aviation.eu/programme-overview-and-structure.
- [7] S. Jagtap, P. Childs, and M. Stettler, "Energy performance evaluation of alternative energy vectors for subsonic long-range tube-wing aircraft," *Transportation Research Part D: Transport and Environment*, vol. 115, Jan. 2023. DOI: https://doi.org/10.1016/j.trd.2022.103588.
- [8] J. Brand, S. Sampath, R. B. F. Shum, and J. Cohen, "Potential use of hydrogen in air propulsion," in *AIAA international air and space symposium and exposition: the next 100 years*, Dayton, Ohio, USA, Jul. 2003. DOI: https://doi.org/10.2514/6.2003-2879.
- [9] H. Webberm and S. Job, "Realising zero-carbon emission flight: Primary energy source comparison and selection," *FlyZero Open Source Reports*, 2021, Accessed on 26.11.2024. [Online]. Available: https://www.ati.org.uk/wp-content/uploads/2021/10/FZ_0_6.1-Primary-Energy-Source-Comparison-and-Selection-FINAL-230921.pdf.
- [10] A. Görtz and D. Silberhorn, *Thermodynamic potential of turbofan engines with direct combustion of hydrogen*, 2022.
- [11] G. Norris, *Pratt outlines hydrogen steam-injection engine concept*, A. Week, Ed., Accessed on 08.11.2024, 2022. [Online]. Available: https://aviationweek.com/special-topics/sustainability/pratt-outlines-hydrogen-steam-injection-engine-concept.
- [12] R. K. Shah and D. Sekulić, *Fundamentals of Heat Exchanger Design*, 8th ed. Hoboken, New Jersey, USA: John Wiley & Sons, Inc, 2003.
- [13] Southwest Research Institute®, Mechanical Engineering Division Machinery Department, *Npss user's guide v3.2*, San Antonio, TX, USA, Aug. 2020.
- [14] A. Feim, "Master thesis: Modeling the performance and emissions of a steam injected water recovering turbofan engine," 2025.
- [15] O. Schmitz, H. Klingels, and P. Kufner, "Aero engine concepts beyond 2030: Part 1 the steam injecting and recovering aero engine," in *Proceedings of ASME Turbo Expo 2020*, Virtual: ASME, Sep. 2020.
- [16] A. Görtz, J. Häßy, M. Schmelcher, and M. El-Soueidan, "Water enhanced turbofan: Improved thermodynamic cycle using hydrogen as fuel," in *Proceedings of ASME Turbo Expo 2023, GT2023-100807*, Massachussetts, USA: ASME, Jun. 2023.
- [17] M. Kuropatwa, J. Kozuba, and N. Wegrzyn, "Turbofan engines efficiency, historical trends, and future prediction a review," *Safety & Defense*, vol. 8, no. 2, Dec. 2022. DOI: https://doi.org/10.37105/sd.186.

[18] International Civil Aviation Organization (ICAO), *Declaration: International aviation climate ambition coalition*, Accessed on 11.11.2024, 2021. [Online]. Available: https://www.gov.uk/government/publications/declaration-international-aviation-climate-ambition-coalition/declaration-international-aviation-climate-ambition-coalition#declaration.

- [19] International Civil Aviation Organization (ICAO), *Trends in emissions that affect climate change*, Accessed on 11.11.2024. [Online]. Available: https://www.icao.int/environmental-protection/Pages/ClimateChange_Trends.aspx.
- [20] J. Kurzke, "Aeroengine design: From state of the art of turbofans towards innovative architectures," in von Karman Institute for FLuid Dynamics Lecture Series 2013- 2014, 2013.
- [21] J. P. van Buijtenen, W. Visser, and A. G. Rao, Aero engine technology, ae4238, 2021.
- [22] C. Soares, "10 performance, performance testing, and performance optimization," in *Gas Turbines*, Second edition. Butterworth-Heinemann, 2008.
- [23] D. L. Daggett, L. Fucke, R. C. Hendricks, and D. J. H. Earnes, "Water injection on commercial aircraft to reduce airport nitrogen oxides," *NASA/TM*—2010-213179, Mar. 2010.
- [24] E. D. Larson and R. Williams, "Steam-injected gas turbines," *Journal of Engineering for Gas Turbines and Power*, vol. 109, p. 55, 1987.
- [25] D. Y. Cheng and A. L. C. Nelson, "An analysis of example," in *The Chronological Development of the Cheng Cycle Steam Injected Gas Turbine During the Past 25 Years*, Amsterdam, The Netherlands: ASME Turbo Expo, Jun. 2002.
- [26] B. T. Kelleher and M. Haselgrüber, "Nox control for the cheng cycle cogeneration system," *International Power Technology*, Nov. 1988.
- [27] D. Y. Cheng, Regenerative parallel compound dual-fluid heat engine, 1976.
- [28] M. D. Paepe and E. Dick, "Industrial application of water recovery in steam injected gas turbines," in *Proceedings of ASME-IGTI TURBO, 97-GT-435*, Orlando, USA: ASME, Sep. 1997.
- [29] W. Xueyou, Z. Jigou, F. Zheng, Y. Shikang, and L. Lingbo, "A test rig for the realisation of water recovery in a steam-injected gas turbine," in *Proceedings of ASME-IGTI TURBO, 96-GT-9*, Birmingham, UK: ASME, 1996.
- [30] H. B. Nguyen and A. den Otter, "Development of gas turbine steam-injection water recovery (siwr) system," in *International Gas Turbine and Aeroengine Congress and Exposition*, Cologne, Germany: ASME, Jun. 1992.
- [31] H. Abedi, C. Xisto, I. Jonsson, T. Grönstedt, and A. Rolt, "Preliminary analysis of compression system integrated heat management concepts using lh2-based parametric gas turbine model," *Aerospace*, vol. 9, p. 216, Apr. 2022. DOI: https://doi.org/10.3390/aerospace9040216.
- [32] W. M. Rohsenow, J. P. Hartnett, and Y. I. Cho, *Handbook of Heat Transfer*, Third. McGraw-Hill, 1998.
- [33] D. G. Wilson, "10 convective heat transfer in blade cooling and heat-exchanger design," in *The Design of High-Efficiency Turbomachinery and Gas Turbines*. Cambridge, Massachusetts, USA: The MIT Press, 1984.
- [34] J. H. L. V and J. H. L. IV, *A Heat Transfer Book*, Sixth. Boston, Massachusetts, USA: Pholigston Press, 2024.
- [35] H. Müller-Steinhagen, "Fouling of cryogenic liquids," in *Fouling Science and Technology*. Dordrecht, The Netherlands: Springer, 1988. DOI: https://doi.org/10.1007/978-94-009-2813-8_21.
- [36] S. Corneliussen, J. Couput, K. F. E. Dahl, et al., Handbook of Multiphase Flow Metering, Revision 2. Oslo, Norway: The Norwegian Society for Oil et al., 2005.
- [37] G. F. Hewitt, "Gas-liquid flow," in *Fouling of Cryogenic Liquids*. Thermopedia, 2010. DOI: https://doi.org/10.1615/AtoZ.g.gas-liquid flow. [Online]. Available: https://www.thermopedia.com/.
- [38] M. Schmelcher, J. Häßy, A. Görtz, and M. El-Soueidan, "Methods for the preliminary design of heat exchangers in aircraft engines," in *Proceedings of ASME Turbo Expo 2023*, GT2023-102959, Massachussetts, USA: ASME, Jun. 2023.

[39] P. Stephan, S. Kabelac, M. Kind, D. Mewes, K. Schaber, and T. Wetzel, *VDI Heat Atlas*. Berlin, Heidelberg: Springer, 2019. DOI: https://doi.org/10.1007/978-3-662-52989-8.

- [40] E. S. Gaddis and V. Gnielinski, "Pressure drop in cross flow across tube bundles," *International Chemical Engineering*, vol. 25, no. 1, 1985. [Online]. Available: https://www.osti.gov/biblio/6503251.
- [41] J. R. Thome, *Encyclopedia of two-phase heat transfer and flow I: Fundamentals and methods; a 4 volume set.* New Jersey, United States: World Scientific, 2015.
- [42] D. Chisholm, "Two-phase flow in bends," *International Journal of Multiphase Flow*, vol. 6, pp. 363–367, 1980. DOI: https://doi.org/10.1016/0301-9322(80)90028-2.
- [43] M. Nitulescu, S. Andersson, J. Bergh, and I. Jonsson, "Early results from the design of an integrated steam vaporizer for hybrid aero engine applications," in *Proceedings of 26th Conference of the International Society for Air Breathing Engines, ISABE-2024-023*, Toulouse, France: ISABE, Sep. 2024.
- [44] CFM International, *Cfm56-3 time on wing upgrade performing well in service*, Accessed on 18.11.2024. [Online]. Available: https://www.cfmaeroengines.com/press-articles/cfm56-3-time-on-wing-upgrade-performing-well-in-service/.
- [45] A. Poggio and A. Strasser, Cheng cycle cogeneration system, application and experience of exhaust gas condensing unit, 1995.
- [46] M. D. Paepe and E. Dick, "Technological and economical analysis of water recovery in steam injected gas turbines," *Applied Thermal Engineering*, vol. 21, no. 2, pp. 135–156, 2001.
- [47] E. Watson, "The first hydrogen balloon," *Engineering Science*, vol. 9, no. 11, pp. 12–16, 1946.
- [48] G. D. Syon, Zeppelin!: Germany and the airship, 1900-1939. JHU Press, 2002.
- [49] J. Zeitlin, "Flexibility and mass production at war: Aircraft manufacture in britain, the united states, and germany, 1939-1945," *Technology and Culture*, vol. 36, no. 1, pp. 46–79, 1995.
- [50] J. L. Sloop, *Liquid Hydrogen as a propulsion fuel, 1945-1959*. Washington, DC, USA: National Aeronautics and Space Administration, 1978.
- [51] ICAO Secretariat, "Electric, hybrid, and hydrogen aircraft-state of play," in *Climate Change Mitigation: Technology and Operations*, 2019, pp. 124–130.
- [52] Airbus Deutschland GmbH, *Cryoplane: Final technical report*, May 2002. [Online]. Available: https://www.fzt.haw-hamburg.de/pers/Scholz/dglr/hh/text_2004_02_26_Cryoplane.pdf.
- [53] Boeing, Fact sheet: Hydrogen and sustainable aviation, Mar. 2024. [Online]. Available: https://www.boeing.com/content/dam/boeing/boeingdotcom/principles/sustainability/assets/pdf/Hydrogen_Factsheet.pdf.
- [54] International Continental Scientific Drilling Program (ICDP), *Kola superdeep borehole (ksdb)*, Archived from the original on 07.05.2014. Accessed on 26.11.2024.
- [55] M. Hermesmann and T. E. Müller, "Green, turquoise, blue, or grey? environmentally friendly hydrogen production in transforming energy systems," *Prog. Energy Combust. Sci*, vol. 90, 2022. DOI: https://doi.org/10.1016/j.pecs.2022.100996.
- [56] S. T. Wismann, J. S. Engbæk, S. B. Vendelbo, *et al.*, "Electrified methane reforming: A compact approach to greener industrial hydrogen production," *Science*, vol. 364, pp. 756–759, 2019. DOI: https://doi.org/10.1126/science.aaw8775.
- [57] G. Squadrito, G. Maggio, and A. Nicita, "The green hydrogen revolution," *Renewable Energy*, vol. 216, pp. 756–759, Jul. 2023. DOI: https://doi.org/10.1016/j.renene.2023.119041.
- [58] M. Petrova, *Green hydrogen is gaining traction, but still has massive hurdles to overcome*, CNBC, Ed., Accessed on 26.11.2024, Dec. 2020. [Online]. Available: https://www.cnbc.com/2020/12/04/green-hydrogen-is-gaining-traction-but-it-must-overcome-big-hurdles.html.
- [59] J. M. Pfofenhauer and S. W. V. Sciver, Lecture 1.3 properties of cryogenic fluids, Accessed on 10.12.2024, Boston, MA, USA, Jun. 2010. [Online]. Available: https://uspas.fnal.gov/materials/ 10MIT/Lecture_1.3.pdf.

[60] E. W. Lemmon, I. H. Bell, M. L. Huber, and M. O. McLinden, *Nist standard reference database 23: Reference fluid thermodynamic and transport properties-refprop, version 10.0, national institute of standards and technology*, 2018. DOI: https://doi.org/10.18434/T4/1502528. [Online]. Available: https://www.nist.gov/srd/refprop.

- [61] G. D. Brewer, *Hydrogen aircraft technology*. Boca Raton, Florida, USA: CRC press, 1991.
- [62] A. J. B. Jackson, "Optimisation of aero and industrial gas turbine design for the environment," *Cranfield University School of Engineering*, Feb. 2009.
- [63] H. G. Klug, S. Bakan, and V. Gaylor, "Cryoplane-quantitative comparison of contribution to anthropogenic greenhouse effect of liquid hydrogen aircraft versus conventional kerosene aircraft," in *European Geophysical Society, XXI General Assembly*, The Hague, The Netherlands, May 1996.
- [64] P. Minnis, "Clouds and fog: Contrails," in *Encyclopedia of Atmospheric Sciences*, Second. Hampton, VA, USA: Science Directorate, NASA Langley Research Center, 2015, pp. 121–132.
- [65] U. Schumann, "Review-article: On conditions for contrail formation from aircraft exhausts," *Meteorol*, vol. 5, pp. 4–23, Feb. 1996.
- [66] C. Marek, T. Smith, and K. Kundu, "Low emission hydrogen combustors for gas turbines using lean direct injection," in *41st AIAA/ASME/SAE/ASEE Joint Propulsion Conference & Exhibit*, Tucson, Arizona, USA, Jun. 2012. DOI: https://doi.org/10.2514/6.2005-3776.
- [67] Kawasaki, *Hydrogen gas turbine combustion technology*, Accessed on 05.12.2024. [Online]. Available: https://global.kawasaki.com/en/corp/rd/technologies/energyb.html.
- [68] S. Tiwari, M. J. Pekris, and J. J. Doherty, "A review of liquid hydrogen aircraft and propulsion technologies," *International Journal of Hydrogen Energy*, vol. 57, pp. 1174–1196, 2024, ISSN: 0360-3199. DOI: https://doi.org/10.1016/j.ijhydene.2023.12.263.
- [69] E. J. Adler and J. R. Martins, "Hydrogen-powered aircraft: Fundamental concepts, key technologies, and environmental impacts," *Progress in Aerospace Sciences*, vol. 141, p. 100 922, 2023, Special Issue on Green Aviation, ISSN: 0376-0421. DOI: https://doi.org/10.1016/j.paerosci. 2023 100922
- [70] D. Silberhorn, G. Atanasov, J. Walther, and T. Zill, "Assessment of hydrogen fuel tank integration at aircraft level," in *Proceedings of the Deutscher Luft-und Raumfahrtkongress*, 2019, pp. 1–14.
- [71] D. Verstraete, "The potential for liquid hydrogen for long range aircraft propulsion," Apr. 2009. [Online]. Available: https://dspace.lib.cranfield.ac.uk/handle/1826/4089.
- [72] GKN Aerospace Sweden, RISE Research Institutes of Sweden, Chalmers University, Royal Institute of Technology (KTH), and Lund University, *H2jet research project*. [Online]. Available: https://research.chalmers.se/en/project/10388.
- [73] Wikipedia contributors, *Airbus a320 family Wikipedia, the free encyclopedia*, [Online; accessed 26-May-2025], 2025. [Online]. Available: https://en.wikipedia.org/w/index.php?title=Airbus_A320_family&oldid=1292256933.
- [74] N. J. Terwilliger and A. A. Alahyari, *Water separator for hydrogen steam injected turbine engine*, Mar. 2024.
- [75] A. Rolt, V. Sethi, F. Jacob, *et al.*, "Scale effects on conventional and intercooled turbofan engine performance," *The Aeronautical Journal*, vol. 121, no. 1242, pp. 1162–1185, Jun. 2017, ISSN: 2059-6464. DOI: 10.1017/aer.2017.38. [Online]. Available: http://dx.doi.org/10.1017/aer.2017.38.
- [76] O. Sjögren, C. Xisto, and T. Grönstedt, "Estimation of design parameters and performance for a state-of-the-art turbofan," *Proceedings of the ASME Turbo Expo*, vol. 1, 2021. DOI: https://doi. org/10.1115/GT2021-59489.
- [77] A. Guha, "Estimation of design parameters and performance for a state-of-the-art turbofan," *Journal of Propulsion and Power*, vol. 17, no. 5, 2001. DOI: https://doi.org/10.2514/2.5852.
- [78] M. Ebrahim and Al-Kawari, "Pinch technology: An efficient tool for chemical-plant energy and capital-cost saving," *Applied Energy*, vol. 65, no. 1, pp. 45–49, 2000, ISSN: 0306-2619. DOI: https://doi.org/10.1016/S0306-2619(99)00057-4. [Online]. Available: https://www.sciencedirect.com/science/article/pii/S0306261999000574.

[79] R. Sinnott, *Coulson & Richardson's Chemical Engineering Design*, 3rd. Butterworth-Heinemann, 1999, vol. 6.